Volcanic risk assessment at Irazú volcano, Costa Rica

Daniela Campos Durán

VOLCANIC RISK ASSESSMENT AT IRAZÚ VOLCANO, COSTA RICA

Daniela Campos Durán

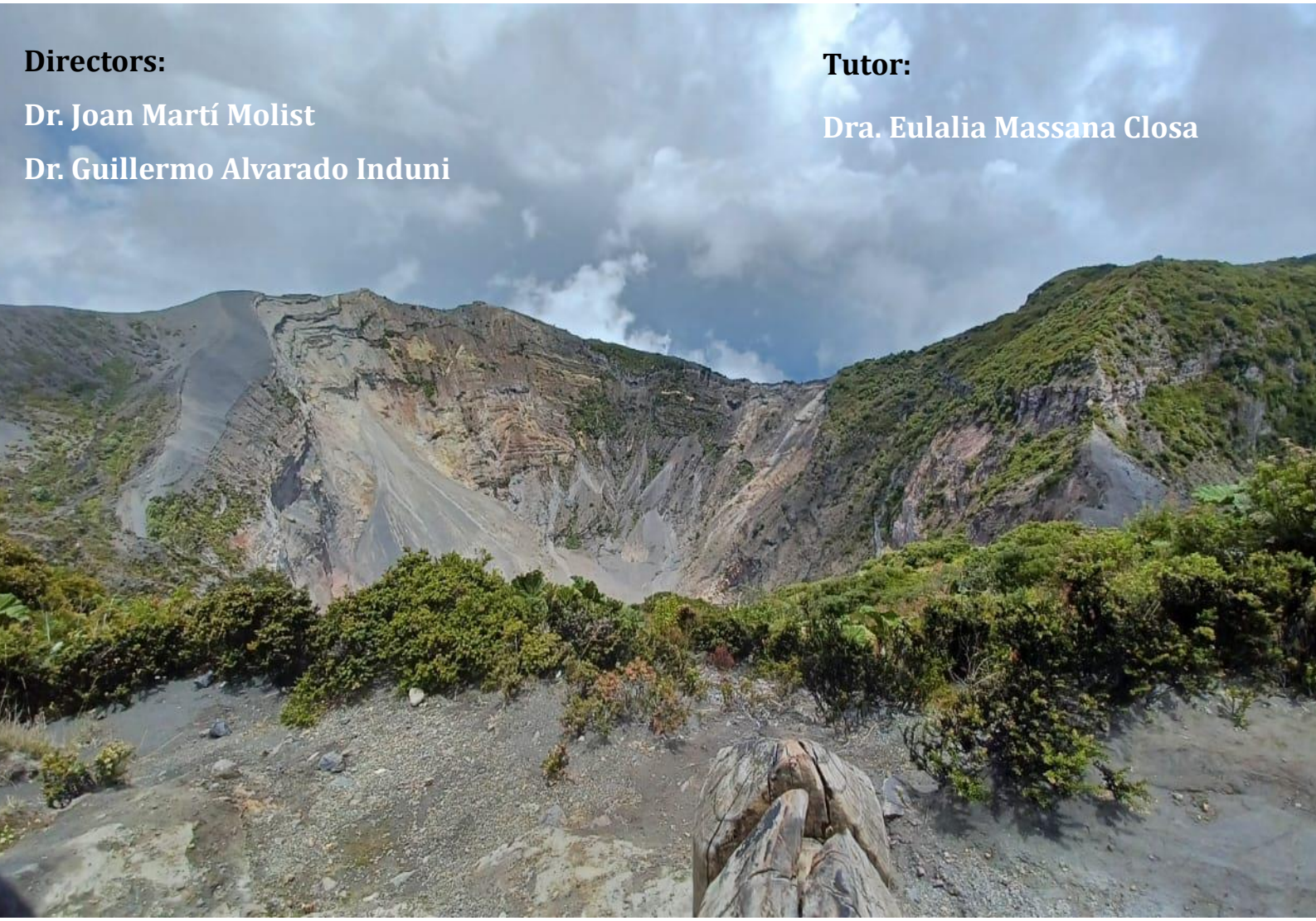

Directors:

Dr. Joan Martí Molist

Dr. Guillermo Alvarado Induni

Tutor:

Dra. Eulalia Massana Closa

PHD THESIS – EARTH SCIENCES
2023

UNIVERSITAT DE BARCELONA
Facultat de Ciències de la Terra

UNIVERSITAT DE BARCELONA

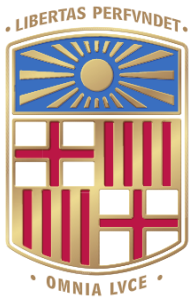

UNIVERSITAT DE BARCELONA

VOLCANIC RISK ASSESSMENT AT IRAZÚ VOLCANO, COSTA RICA

A dissertation submitted to

Doctorate Program in Earth Sciences

Universitat de Barcelona

for the degree of

Doctor of Earth Sciences

Presented by

Daniela Campos Durán

Director: Dr. Joan Martí Molist

Co-Director: Dr. Guillermo Alvarado Induni

Tutor: Dra. Eulalia Massana Closa

Barcelona, November 2023

UNIVERSITAT DE BARCELONA

PHD THESIS

VOLCANIC RISK ASSESSMENT AT IRAZÚ VOLCANO, COSTA RICA

Daniela Campos Durán

DOCTORATE PROGRAM IN EARTH SCIENCES

UNIVERSITAT DE BARCELONA

Daniela Campos Durán	**Joan Martí Molist**	**Guillermo Alvarado Induni**	**Eulalia Masana Closa**
Phd. student	Director	Co-director	Tutor

Barcelona, November 2023

….. Con esfuerzo titánico creció convirtiéndose en túmulo, lentamente de túmulo en duna, despaciosamente de duna en loma, de loma en montaña, de montaña en el imponente Irazú. Irazú, centinela gallardo de aquella llanura. El juramento estaba cumplido…

En las mañanas frías, la nube blanca, vaporosa y femenina, cariñosamente envuelve al gigantesco Irazú, guerrero viril, disfrutando eternamente de su amor, el cual ni el omnipotente Dios del viejo cacique logró romper….

La leyenda del Irazú
Castro, G. (1957)

Acknowledgements

A Dios por permitirme culminar este largo proceso que inició como un sueño más en mi vida profesional y a mi familia por su apoyo incondicional.

A mis directores Joan Martí y Guillermo Alvarado por su paciencia y todas sus enseñanzas en este largo camino.

ABSTRACT

Irazu is the highest volcano in Costa Rica (3427 m.a.s.l.); it constitutes an andesitic shield, with two main craters at the top and several pyroclastic cones cuspidal, and adventitial on the South Flank. The first historical eruption was registered in 1723, and other eruptive episodes took place in 1917-1921, 1924, 1928-1930, 1933, 1939-1940 and 1963-1965. These eruptive events were characterized by phreatomagmatic, strombolian and phreatic phases that generated pyroclastic fall deposits, pyroclastic density current (PDC) deposits and lahars. The 1963-1965 eruptions had considerable effects on the population, crops, and pastures, as well as on civil works (collapse of roofs and bridges). The most considerable economic losses occurred in the Greater Metropolitan Area (GAM), mainly due to ash and lahars.

We have reconstructed the tephro-chronostratigraphy of the last 2.6 ka of the Irazu volcano, these data allowed us to estimate that this volcano has had an eruptive frequency that ranges between 23 and 100 years, with a major event every 85 years (VEI between 1 and 3). Furthermore, this eruptive reconstruction was the basis for carrying out a long-term hazard assessment, which has been conducted by us in two steps a) a spatial analysis (susceptibility) and b) a temporal analysis.

Regarding susceptibility, we determined that the highest values correspond to the Main Crater area, from where all historical eruptions have been vented. On the southern flank we identified an area with medium susceptibility values due to the presence of fissures and scoria cones that were active during the Holocene, therefore, we cannot rule out a possible future eruptive foci on this flank.

In the case of the temporal analysis, we could expect for a five-year window a magmatic unrest that results in a magmatic eruption in the Main Crater with VEI ≥1 (that is, VEI between 1 and 3), with pyroclastic falls, short PDCs, ballistics and lahars (mainly on the south and southwest flanks), similar to the eruptions of 1723-1724, 1939-1940, or 1963-1965. A geothermal unrest (the least likely) culminating in a phreatic explosion is also conceivable. In the case of a three-years forecasting window, we obtained a significant probability of an eruption of VEI=3 with ashfall,

lahars, PDCd and ballistics, all of an extension similar to the eruptive episode of 1963- 1965.

The other probable scenarios (VEI between 1 and 3) could range between ashfall and lahars of medium to large extent, in lower ballistic grades and low magnitude earthquakes (between 3.1-5.0 Mw). It is important to highlight that, for all possible scenarios, the ashfall would mainly affect the southwest flank, while in the case of lahars it would affect the south and southwest flank, and for the PDCd and ballistics, they would be restricted to the Main crater area.

The inputs generated with the spatial and temporal analysis were the basis for determining that the 1963-1965 eruptive scenario (VEI=3) is the one that represents the greatest hazard, so we reconstructed and simulated all the hazards that were registered in that episode, which allowed us to define three hazard areas: high, medium, and low. This information was the basis for carrying out an analysis of population, land use and critical infrastructure exposure.

Among the most relevant results we have that currently more than 2.5 million people live in the GAM, mainly at urban areas in the cities of San Jose and Alajuela, where the development of the industrial sector is concentrated. On the other hand, in the surroundings of Irazú, rural communities base their economy on agricultural activities. Likewise, there are more than 150 informal settlements exposed to the lahar hazard. Regarding educational and health centers, the majority are located in sectors of the GAM exposed mainly to the impact of ashfall.

Finally, we provide an essential contribution to territorial planning, which must consider hazards of volcanic origin within the planning processes for updating and improving emergency plans to face future volcanic crises.

RESUMEN

El Irazú es el volcán más elevado de Costa Rica (3427 m.s.n.m.), constituye un escudo andesítico, con dos cráteres principales en la cima y varios conos piroclásticos cuspidales y adventicios en el flanco sur; su primera erupción histórica se registró en 1723 y otros episodios eruptivos tuvieron lugar en 1917-1921, 1924, 1928-1930, 1933, 1939-1940 y 1963-1965, los cuales se caracterizaron por presentar erupciones freatomagmáticas, estrombolianas y freáticas que generaron depósitos de caída de piroclastos, PDCd y lahares. Las erupciones de 1963-1965 tuvieron efectos considerables sobre la población, los cultivos y los pastos, así como en las obras civiles (colapso de tejados y puentes). Las pérdidas económicas más considerables se produjeron en la Gran Área Metropolitana (GAM), principalmente a causa de la ceniza y los lahares.

Ante este complejo escenario, se reconstruyó la tefrocronostratigrafía de los últimos 2600 años del Irazú, datos que permitieron estimar que la frecuencia eruptiva de este volcán oscila entre 23 y 100 años, con un evento importante cada 85 años (VEI entre 1 y 3). Además, esta información fue la base para llevar a cabo una evaluación de peligro a largo plazo, la cual se realizó en dos líneas a) un análisis espacial (susceptibilidad) y b) un análisis temporal.

En cuanto a la susceptibilidad, se determinó que los valores más altos corresponden al área del Cráter Principal, donde se han registrado todas las erupciones históricas; en el flanco sur se identificó una susceptibilidad media debido a la presencia de fisuras y conos de escoria que estuvieron activos durante el Holoceno, por lo tanto, no es posible descartar posibles futuros focos eruptivos en este flanco. Referente al análisis temporal se esperaría para una ventana de cinco años un unrest magmático que dé como resultado una erupción magmática en el Cráter Principal con VEI ≥1 (es decir, VEI entre 1 y 3) con caída de piroclastos, PDCd cortos, balística y lahares (principalmente en los flancos sur y suroeste); similar a las erupciones de 1723-1724, 1939-1940 o 1963-1965. También es concebible un unrest geotérmico (el menos probable) que culmine en una explosión freática. En el caso de una ventana de tres años, se obtuvo una importante probabilidad para una

erupción de VEI=3 con caída de ceniza, lahares, PDCd y balística, todos de una extensión similar al periodo eruptivo de 1963-1965. Los otros escenarios probables (VEI entre 1 y 3) podrían oscilar entre caída de ceniza y lahares de extensión media a grande, en menor grado balística y sismos de baja magnitud (entre 3,1- 5,0 Mw). Es importante destacar que, para todos los escenarios posibles, la caída de ceniza afectaría principalmente al flanco suroeste, en el caso de los lahares afectaría al flanco sur y suroeste; en cuanto a los PDCd y balística, se restringirían a la zona del cráter principal.

Los insumos generados con el análisis espacial y temporal fueron la base para determinar que el escenario eruptivo de 1963-1965 (VEI=3) es el que representa una mayor amenaza, por lo que se llevó a cabo una reconstrucción y simulación de todos los peligros que se registraron en este periodo (caída de ceniza, balística, lahares y PDC), lo que pemitió, definir tres áreas de amenaza: alta, media y baja. Esta información fue base para realizar un análisis de exposición de la población, de los usos del suelo y de la infraestructura crítica.

Entre los resultados más relevantes destacan que actualmente más de 2,5 millones de personas viven en la GAM, principalmente en áreas urbanas en las ciudades de San José y Alajuela, donde se concentra el desarrollo industrial; por otra parte, en los alrededores del Irazú, las comunidades rurales basan su economía en las actividades agropecuarias. Asimismo, se determinó que hay más de 150 asentamientos informales expuestos a amenaza por lahar, principalmente en los ríos del flanco sur y suroeste. En cuanto a los centros educativos y de salud, la mayoría se ubica en sectores de la GAM expuestos principalmente a la afectación por caída de ceniza.

Con lo anterior, se brinda un aporte esencial para la planificación territorial, la cual debe considerar las amenazas de origen volcánico dentro de los procesos de ordenación; así como para la actualización y mejoras de los planes de emergencia para hacer frente a futuras crisis volcánicas.

CONTENTS

LIST OF FIGURES

CHAPTER 1: INTRODUCTION

CHAPTER 2: **METHODOLOGY**

CHAPTER 3: RESULTS

CHAPTER 4: DISCUSSION

LIST OF TABLES

CHAPTER 1: INTRODUCTION

CHAPTER 2: METHODOLOGY

CHAPTER 3: RESULTS

CHAPTER 1: INTRODUCTION

1.1 Motivation

Volcanoes are complex geological systems, and the study of their eruptions and deposits has allowed us to understand how they work. In the case of Latin America, most of volcanoes are located where there is the influence of subduction zones. Costa Rica is not an exception, because of the subduction of tectonic plates (Cocos plate beneath the Panama microplate), which have generated the formation of important volcanoes in the interior of the country. One of these volcanoes is Irazú, which corresponds to an andesitic shield volcano, with an altitude of 3427 m a.s.l., located 25 km NE of the Great Metropolitan Area (GAM) of the country, from where due to its altitude it seems to be the guardian of this region. It was between 1963 and 1965 when the Irazú registered its last and most important eruptive period in historical times (VEI=3), where for more than 30 months ashfall produced important economic losses (especially in the agricultural and livestock activity) in cities of the GAM, such as San José, Heredia, Alajuela, and Cartago. During this last eruptive episode also important lahars destroyed bridges, roads, and houses, as well as caused the loss of human lives in the sub-basin of the Reventado river.

More than 60 years have passed since this eruptive period, time in which cities have grown, the economy has diversified, and more people live in areas that were once affected, especially by ashfall and lahars. In this new socio-economic context, it is important to ask a) Do we have enough knowledge of Irazú's eruptive past to be able to forecast where and how the next eruption could be? and b) what would happen in the GAM if Irazú erupts again in an equal or similar to that of 1963-1965?

To answer these questions, has been the main motivation to conduct the present research. In order to achieve such ambitious but necessary objective, this PhD thesis: 1) presents a tephrostratigraphic reconstruction of Irazú and its eruptive recurrence in the last 2.6 ka; 2) based on these data, conducts a long-term temporal analysis, including spatial and temporal analysis and hazard scenarios based on numerical

simulations: and 3) describes an exposure analysis for the main hazard scenarios considering relevant information, such as population distribution, economic activities, and the distribution of the main infrastructures. It is expected that this work will constitute the basis for future, more detailed studies on the vulnerability and estimation of the potential costs of damage caused by volcanic processes, and that the resulting volcanic hazard maps will be considered in land-use planning politics and emergency plans.

1.2 Specific objectives of the PhD Thesis

In order to achieve the main goal outlined before, this PhD Thesis included the following specific objectives: **a)** to estimate the eruptive frequency of the Irazú volcano by a reconstruction of the tephro-chronostratigraphy supported by radiometric dating (14C method), **b)** to analyze the volcanic susceptibility of the Irazú volcano to identify the areas with the highest probability of eruption, **c)** to conduct a long-term temporal analysis of future eruptive scenarios by implementing the corresponding event tree using Bayesian Inference, **d)** to evaluate the long-term volcanic hazard at Irazú volcano by simulation of the different volcanic hazard processes, and **e)** to estimate the degree of exposure of critical infrastructure, economic systems, and the population to long-term volcanic hazard at Irazú volcano.

1.3 Thesis outline

This thesis is structured in chapters. They are: 1) the introduction, where the motivation of this research, the state of the art and the objectives developed are presented, 2) the methodology, 3) the results, this one is divided in five sections, and chapters four and five correspond to the discussion and conclusions, respectively. All chapters are formulated following a logical structure defined in the objectives.

1.4 State of the art

1.4.1 Disaster risk management and systematic risk

Initially, the term risk was understood under the approach of the natural sciences, which pointed out that a natural event represented a disaster. As a result, research on disasters focused on the spatio-temporal distribution and the magnitude and intensity-characteristics of geological, meteorological, and hydrological processes. In the decade of the 1970s, social scientists questioned this approach and new research on the causes of vulnerability emerged, suggesting that vulnerability was the product of social, economic, and political processes that do not allow a population to absorb and recover from the impact of a hazard event. This allowed a change in the perception and approach to the problem of disasters, where the problem was focused on risk, which is before the occurrence of a disaster (Maskrey, 1998; Guellert, 2012). In this sense risk is a complex concept, since it is composed of other concepts such as hazard, vulnerability, and, more recently, the exposure. Therefore, it is important to review the basic terms related to this topic.

Firstly, hazard is the probability of occurrence of a potentially damaging natural phenomenon within a specific period of time in a given area. This phenomenon may cause loss of life, injury or other health impacts, property damage, loss of livelihoods and services, social and economic disruption, or environmental damage (UNDRO, 1991; United Nations Office for Disaster Risk Reduction, 2009). On the other hand, the vulnerability corresponds to the conditions determined by physical, social, economic, and environmental factors or processes, which increase the susceptibility of a community to the impact of hazards and the exposure is defined as the people, property, systems, or other elements present in hazard zones that are thereby subject to potential losses (United Nations Office for Disaster Risk Reduction, 2009).

The potential disaster losses, in lives, health status, livelihoods, assets and services, which could occur to a particular community or a society over some specified future period corresponding to the risk. In this sense, the disaster risk management is a systematic process of using administrative directives, organizations, and operational skills and capacities to implement strategies, policies

and improved coping capacities in order to lessen the adverse impacts of hazards and the possibility of disaster (United Nations Office for Disaster Risk Reduction, 2009).

A new concept has gained relevance in recent years. This corresponds to systemic risk, which is associated with cascading impacts that spread within and across systems and sectors (e.g., ecosystems, health, infrastructure, and the food sector) via the movements of people, goods, capital, and information within and across boundaries (e.g., regions, countries, and continents). The spread of these impacts can lead to potentially existential consequences and system collapse across a range of time horizons (Sillmann et al. 2022). Systemic risk is different from conventional risk and thus challenges well-established approaches to risk analysis and risk governance that seek to analyze and manage by addressing individual elements of a system or sub-systems as though they are or act in isolation (Cutter et al., 2015).

1.4.2 Volcanic hazard and its relationship with the territory

Volcanism has been fundamental in the planet's geological past, bringing important benefits to society, such as fertile land and scenic landscapes; however, eruptive processes that have occurred in inhabited or cultivated territories have had a social, economic, and environmental impact. More than 1300 volcanoes have erupted during the last 10.000 years; approximately half of these have erupted in historical times, on average about 50 volcanoes erupt annually, and this average has not varied in historical times (Simkin et al., 1981).

Historically, the science of volcanology has been associated with volcanic hazards and disasters. Fournier d'Albe (1979) defines volcanic hazard as the probability of a particular area being affected by a destructive volcanic process in a given period of time. Essential data for an adequate hazard assessment should include the following: 1) complete records of historical eruptions; 2) prehistoric eruptive activity inferred from the geologic record; 3) geologic (especially stratigraphic), petrologic, and geochemical data regarding the nature, distribution, and volume of eruptive products; and 4) dating of volcanic products and events

interpreted from them. Combined, these data allow the reconstruction of the past eruptive behavior of the volcano, which provides the basis for assessing the potential hazards of future eruptions (Crandell et al. 1984). In this sense, Blong (2000) emphasizes that volcanic hazard assessment is divided into long-term and short-term assessment.

Long-term hazard assessment is based on historical and geological data, simulation models, and refers to the available time window before an unrest episode occurs (Marzocchi et al., 2010; Sobradelo et al., 2014; Marti, 2017). On the other hand, short-term hazard assessments focus on the unrest phase, using real-time monitoring data in combination with the long-term analysis to update the status of the volcanic hazard (Blong, 2000; Marzocchi et al., 2008; Sobradelo and Martí, 2010; Bartolini et al., 2014; Martí, 2017). To estimate the long-term hazard assessment is necessary to evaluate the spatial probability (volcanic susceptibility), which aims at determining the potential position of future vents based on knowledge of past eruptions, the existence of structural controls (fissures, dikes, faults) on vent distribution (cones and craters), the characterization of products from previous eruptions, and their spatial interrelations (Felpeto et al., 2007; Martí and Felpeto, 2010; Bartolini et al., 2013).

Nowadays, there are many big cities and megacities growing close to highly dangerous volcanoes, and more than 600 million people live near active volcanoes, thus increasing vulnerability (Sparks, et al. 2013). For this reason, these advances in volcanology help with the provision of early warning systems and improving the management of volcanic emergencies. Also, volcanic risk assessment is pertinent for designing emergency plans and territorial planning, and to evaluate potential costs and planning and executing mitigation decisions, during crises or preventing crises from arising (Rougier, et al. 2013; Marti, 2017).

Recent disasters associated with volcanic eruptions such as Eyjafjallajökull, Iceland (2010); Puyehue-Cordón Caulle, Chile (2011); Mount Sinabung, Indonesia (2014); Volcán de Fuego, Guatemala (2018); Whakaari, New Zealand (2019); La Palma, Spain (2021), Hunga Tonga, Tonga (2021) and Nyiragongo, Democratic Republic of Congo (2021), are just a few examples of the relevance that volcanic hazard assessment (long term and short term) has within risk management

processes, as it contributes to the reduction and mitigation of human and economic losses. Therefore, risk management around active volcanoes in periods of inactivity should allow for the development of activities such as hazard assessment, improved monitoring, and implementation of early warning systems, as well as land use planning mechanisms (Rougier, et al. 2011).

1.4.3 Geological Background of Irazú volcano

The Central American Volcanic Arc (CAVA) extends from Panama to Guatemala and runs roughly parallel to, and 150–200 km away from, the deep-sea trench (Kutterolf et al., 2008), the Mesoamerican Trench results from the subduction of the Cocos plate beneath the Caribbean plate, the Cocos plate has a convergence rate between 60-80 mm/yr (DeMets et al., 1990). The complex tectonic framework of Costa Rica is defined by the interaction of three plates and one microplate: Cocos, Caribbean, and Nazca plates and the Panama microplate (Barckhausen et al., 2001) (Fig. 1a).

The interaction between Cocos and Caribbean plates has resulted in the Costa Rican Volcanic Front (CRVF) where the Quaternary stratovolcanoes of the CRVF from north to south are: The Cordillera de Guanacaste (Orosí-Cacao, Rincon de la Vieja-Santa Maria, Miravalles-Paleo-Miravalles, Tenorio-Montezuma), an isolated volcanic group (Arenal-Chato), and the Cordillera Central (Platanar-Porvenir, Poás, Barva, Irazu and Turrialba) (Alvarado, 1993) (Fig. 1b).

Irazú is an andesitic shield volcano located to the east of the Great Metropolitan Area (GMA) when the main cities of the country are located, included the capital city of San José (Fig. 1b), which reaches an altitude of 3427 m a.s.l. The volcanic edifice covers an area of approximately 700 km^2, with a volume of 359 km^3. Krushensky (1972) points out that the volcanic edifice consists of basalts to andesites that overlie dacitic ignimbrites, Pleistocene lavas, mudflows, landslides, and ash-flow tuffs of the Irazú Group. Recent geochronological studies (Alvarado et al., 2006; Carr et al., 2007; Ruiz et al., 2010; Alvarado and Gans, 2012), and the detailed work around Paraíso de Cartago (Sojo, 2018), notoriously changed the

concepts, boundaries, predominant lithological composition, and position of many of the units included in Krushensky (1972).

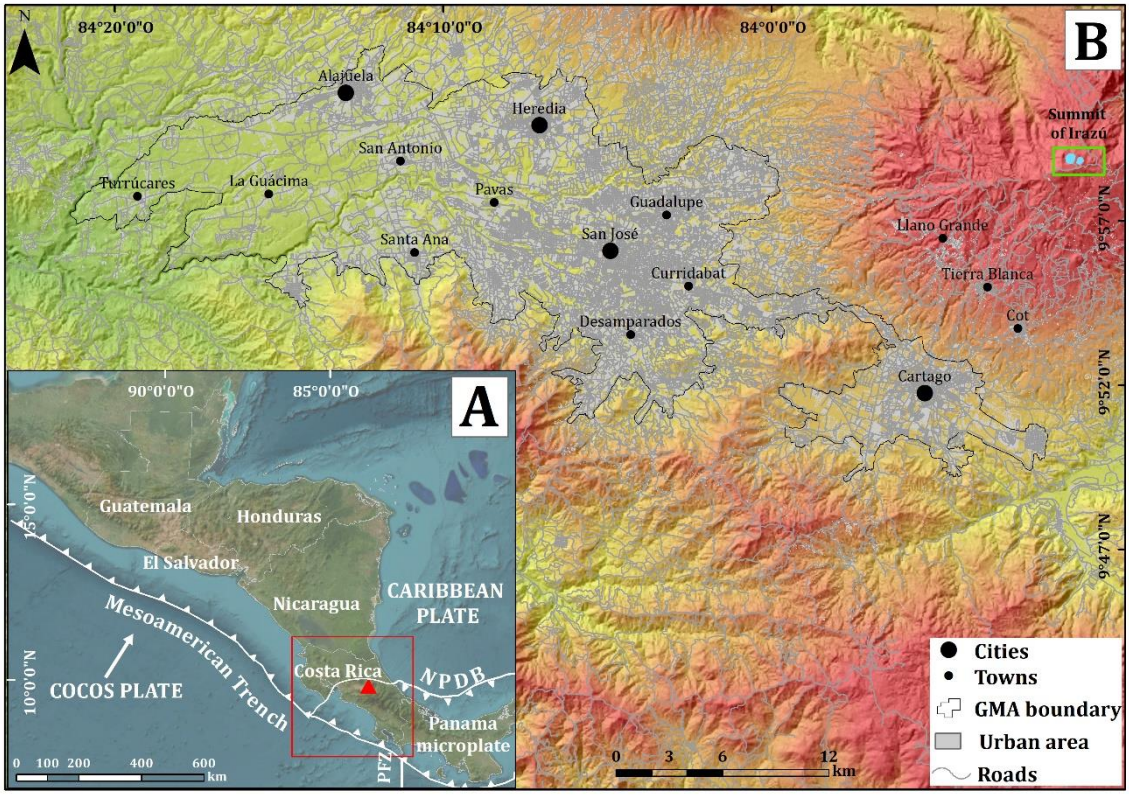

Figure 1. A) Location of Irazú volcano in the Central Volcanic Cordillera of Costa Rica and its position respect to Great Metropolitan Area (GAM) when the cities of San José, Alajuela, Cartago, and Heredia are located. B) Geodynamic setting of Costa Rica. NPDB: North Panama Deformed Belt, PFZ: Panama Fracture Zone.

The birth of the Irazú volcano could possibly be traced back to less than a million years ago (Alvarado and Gans, 2012), although most of the rocks of that phase are covered by later products and can only be identified in the deepest parts of the canyons eroding the volcano flanks (Virilla, Durazno, Tiribí, Birrís, Honda, Blanco, Cajón, Sucio, Corinto, Blanquito and Toro Amarillo rivers). A few dated lavas flow from there are younger than 600,000 years (= 600 ka or 0.6 Ma). The 40Ar/39Ar and 38U/230Th radiometric dates available to date (Allegre and Condomines, 1976; Alvarado et al., 2006; Carr et al., 2007; Alvarado and Gans, 2012) related to Irazú, group the eruptive products into three large age groups (Alvarado and Gans, 2012): the Proto-Irazú at 0.85 Ma, followed by the construction phase proper of the Paleo-Irazú at 0.6-0.25 Ma, and the Neo-Irazú formed mainly of lava flows and volcanic products younger than 0.2 Ma (Fig. 2).

From the geological record it is not easy to identify how many volcanic edifices have intervened in the construction of the final Irazú volcano, but there is evidence that several of them joined and collapsed until the bases were widened and the height of the Irazú increased (Alvarado, 1993). However, most of what can be distinguished today forming the Irazú volcano has been built less in less than 0.2 Ma and mostly during the last 0.1 Ma (Alvarado et al., 2006; Alvarado and Gans, 2012).

The Proto-Irazú proposed by Alvarado and Gans (2012) corresponds to what Krushensky (1972) defined as the ignimbrites of the Aguacaliente and San Jerónimo, which lie on pre-Irazú rocks (volcanic rocks not belonging to the Irazú massif, with an age other than 1 Ma) in a stratigraphic position that was not very well defined. They outcrop as isolated patches unconformably overlaid by the Irazú units. In general, they correspond to welded to partially welded ignimbrites of andesitic composition, with abundant plagioclase, traces of pyroxene, glass and fiammes and, in the case of the San Jerónimo, with biotite. The San Jerónimo ignimbrites were recently dated by Alvarado et al. (2006) at 847 ± 11 ka, 855 ± 6 ka, and 862 ± 9 ka with the 40Ar/39Ar method, which suggest a correlation with the Paleo- and Proto-Cordillera Central of Alvarado and Gans (2012).

The Paleo-Irazú can be distinguished to the W of the top of Irazú, where some ancient cones associated with the Irazú massif can be recognized, such as for example the eroded "crater" of the Las Nubes "volcano" (Pico Piedra hill, 2661 m a.s.l.) and two more, unnamed, located to the NE of the Las Nubes volcanic relict, as well as the Cerro Cabeza de Vaca (2,960 m a.s.l.) (Bergoeing, 1979), has two large amphitheaters (avalanche scars; Hidalgo et al., 2004) (Fig. 2). These volcanic relics are in the continental watershed between the Caribbean and the Pacific, on the border between the provinces of San José, to the S, and Cartago to the N. The Paleo-Irazú is mostly formed of porphyritic andesitic lavas composed of plagioclase, clinopyroxene, orthopyroxene, floating in glassy groundmass (56% to 67%). Almost 4 km to the NE of the Irazú Main Crater, there are the remains of the flank of an ancient cone, which was part of the Paleo-Irazú, represented by the prominent Alto Grande hill (2803 m a.s.l.), about 200 m high, composed of basaltic andesitic lava flows, limited by faults (Fig. 2). Altered (intense silicification and pyritization) pyroclastic rocks are also abundant in the Paleo-Irazú (Ulloa et al., 2016).

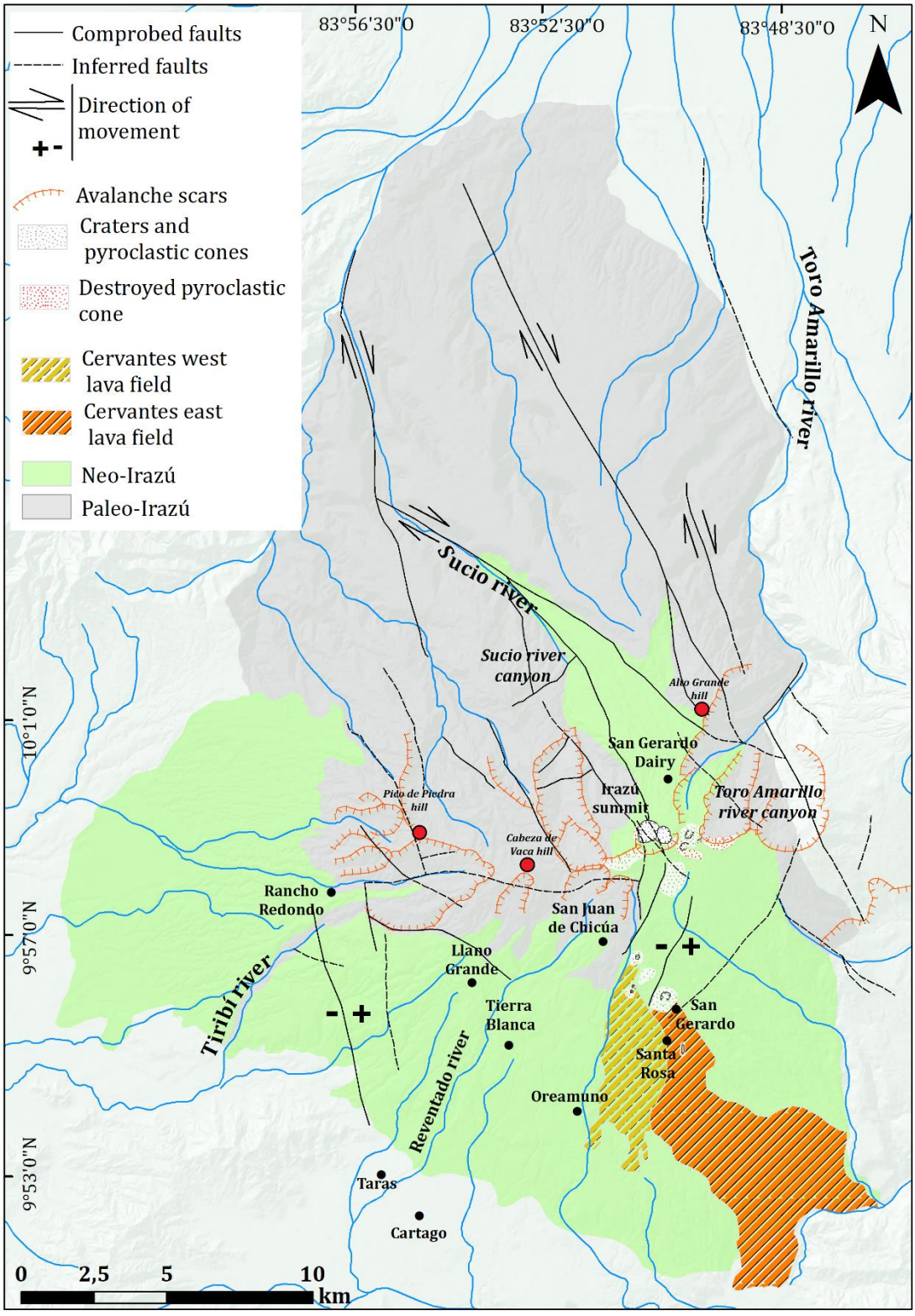

Figure 2. Main pyroclastic cones on the southern flank of the summit and the main avalanche scarps both north and south of the summit. Also, it shows the Irazú constructive units (proto-Irazú and Paleo-Irazú) and the two large lava fields Cervantes West and Cervantes East (57 ka and 17 ka, respectively) and finally the main faults.

The Neo-Irazú group is the most recent deposits of Irazú volcano (< 0.2 Ma), which form most of the current volcanic edifice. The stratigraphy of Neo-Irazú comprises four different units (Alvarado et al., 2006): 1) The Cot Unit comprises several lavas, mainly basaltic andesites with clinopyroxenes to andesites with hornblende, interbedded with lahars and tephras, covering most of the volcanic edifice in all sectors, but particularly in the southern sector. 2) The Diego de la Haya Unit, which appears on the northern inner wall of the Diego de la Haya crater, as a 100 m thick succession of thin (1 m to 2 m thick) basaltic lava flows. These lava flows have interbedded breccias and scoria fallout layers of basaltic compositions. 3) The Sapper Unit of tephras with interbedded lava flows, about 200 m thick, which in the Diego de la Haya crater locally overlies the Diego de la Haya Unit, but which in the northern sector may also be laterally interdigitated. and 4) The Birrís Unit, exposed on the top of Irazú, from the collapsed La Torre cone and La Laguna cone to the Sapper tower (the Torres Garden to the west of the top) and consisting of agglutinates and lavas with tephras and breccias, occasionally showing evidence of magma mingling and mixing. All these units are intersected by numerous dykes, some of which show evidence of having been feeder dykes (Fig. 3). Geophysical studies (Bonilla, 2020) of the summit of Irazú show the complex internal structure of this most recent part of the volcano, with different dense bodies (dikes? agglutinates) overlapping with scoria cones or their remains (Fig. 4).

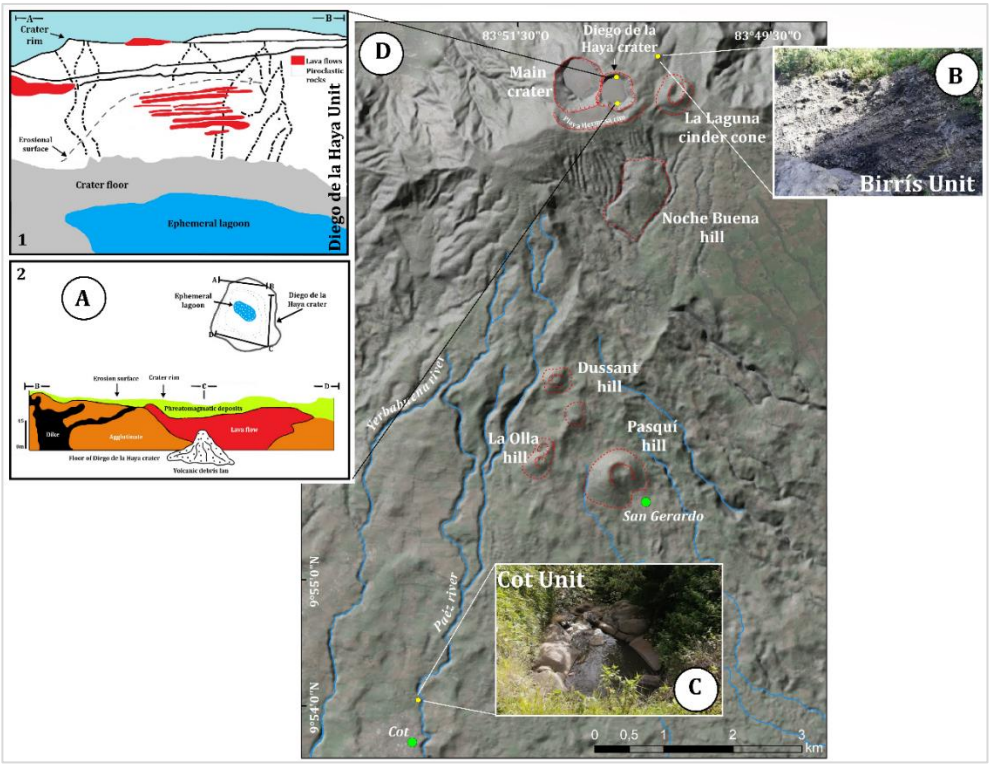

Figure 3. A) Section and generalized stratigraphic column of the most recent part of the Irazú. In the upper part, the detail of the Diego de la Haya crater, while in the lower part, the south wall of the same crater (Alvarado et al., 2006). B) Crudely stratified scoria of the La Laguna cinder cone, typical of the Birrís unit. C) Lava flow outcropping north of the town of Cot in the Paéz River, a typical example of the Cot Unit. D) Main scoria cones on the southern flank of the summit of Irazú volcano, which follow a pattern associated with a fissure.

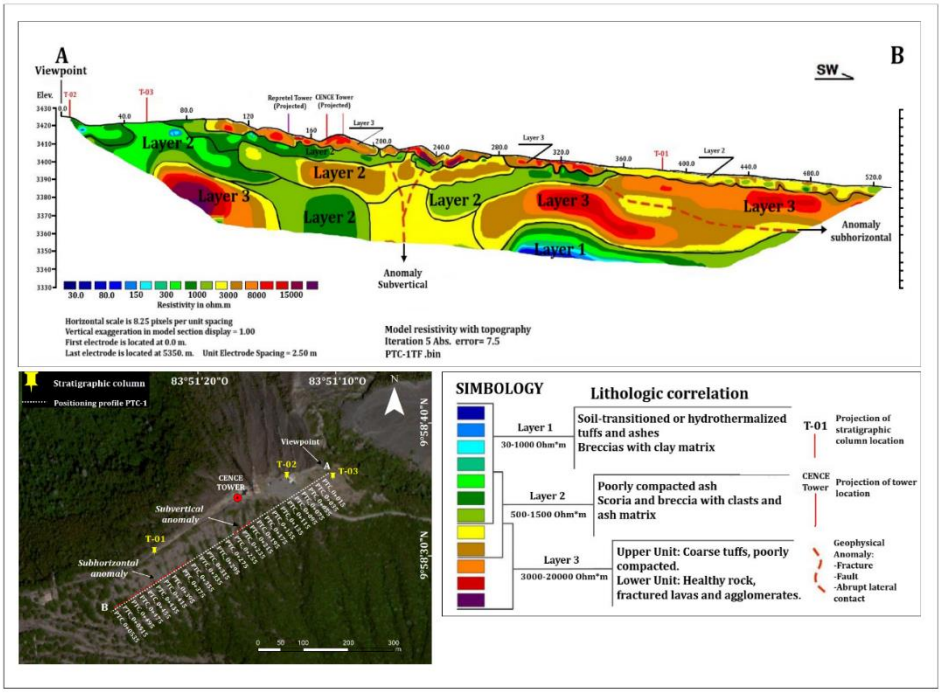

Figure 4. Above, location of the electrical tomography profiles and their results at the bottom (Bonilla, 2020). Towards B (SW) it is observed how layer 3 seems to correspond to the agglutination of the Birrís unit.

1.4.3.1. Tectonics and seismicity

Tectonic activity in the area is very relevant, with several seismic events registered during the historical period and evidence of tectonic movements during the Holocene and upper Pleistocene. From a geotectonic point of view, the depth of the Cocos plate subducted under the Caribbean, at the height of Irazú, seems to be about 110 km below the volcano (Lücke and Arroyo, 2015). The Moho (limit of the upper mantle with the lower crust) has been seismically delimited between 35 km and 45 km, while with gravimetry it is located at about 38 km (Dzierma et al., 2010; Lücke, 2012; Hayes et al., 2013). From a more regional tectonic point of view, it is well established that, in the central part of Costa Rica, the maximum compressive horizontal stress has a strike of N10-22°E (Montero, 1994; López, 1999) and is associated with reverse faults oriented close to E-W, normal faults with orientation close to N-S, and dextral (mainly NW-oriented) and sinistral (mainly NE-oriented) strike-slip faults. This system of compound faults follows a theoretical shear model as originally proposed by Montero (1994, 2001) for the country. The volcano is influenced by various faults trending NE-SW, E-W and NW-SE (Fig. 5) on its various slopes and flanks (Montero, 1994; Montero and Alvarado, 1995; Linkimer, 2003; Linkimer et al., 2018).

The distribution of volcanic vents and craters at Irazú is mainly controlled by the tectonic system mentioned before, with cone lineations and eruptive fractures-oriented NW-SE, E-W and N-S (Figs. 3 and 5) (Elizondo et al., 2019). Similarly, the thermal anomalies detected in the field as thermal springs and fumaroles and by means of infrared images also follow the same main structural trends (Gawarecki et al., 1980; Rouwet et al., 2021) (Fig. 5). Finally, several dykes are exposed at the interior of the some of the Irazú craters and show the same structural controls than vents and thermal anomalies.

Historical and current seismicity in Costa Rica, including volcano-tectonic events, is greater in Irazú than in the other volcanoes. This may reflect the higher proportion of active tectonic faults around Irazú and Poás-Chocosuela with respect to the rest of the volcanoes. In Irazú, scattered earthquakes and tremor swarms are frequent, but surface earthquakes have also occurred, both on its NW flank (e.g.,

Patillos earthquake, 12-30-1952, Mw 6.0), and on its SE flank, between Irazú and Turrialba (e.g., Capellades earthquake, 11-30-2016, Mw 5.4), associated with the same NW-SE faulting system (Montero and Alvarado, 1995; Campos-Durán and Quintero-Quintero, 2020).

The fault called Irazú (OVSICORI, 1997), which seems to correspond to the Lara fault (Montero and Alvarado, 1995) (Fig. 5), has been active at various times between 1991 and 1997 and in 2015 (BGVN, 1993-1994a; Muller et al., 2020; Pacheco et al., 2015). From 2006 to 2016, a total of 320 seismic events were recorded under the Irazú volcano, located mainly on the western flank, and dispersed towards the eastern flank, with depths less than 6 km (Cascante-Matamoros and Porras-Espinoza, 2017). Currently, the area with the highest seismicity corresponds to Prusia, to the NW of the Main Crater, to the N of Llano Grande and by the Alto Pizote, and coincides with sectors with hydrothermal alteration, fumarolic activity and known thermal springs, covered by thick layers of ashes. In summary, seismicity at Irazú volcano is almost continuous with different ups and downs, at least since 1978, with seismic swarms separated between 1 to 5 years, on average one about every 3 years (See Table 1).

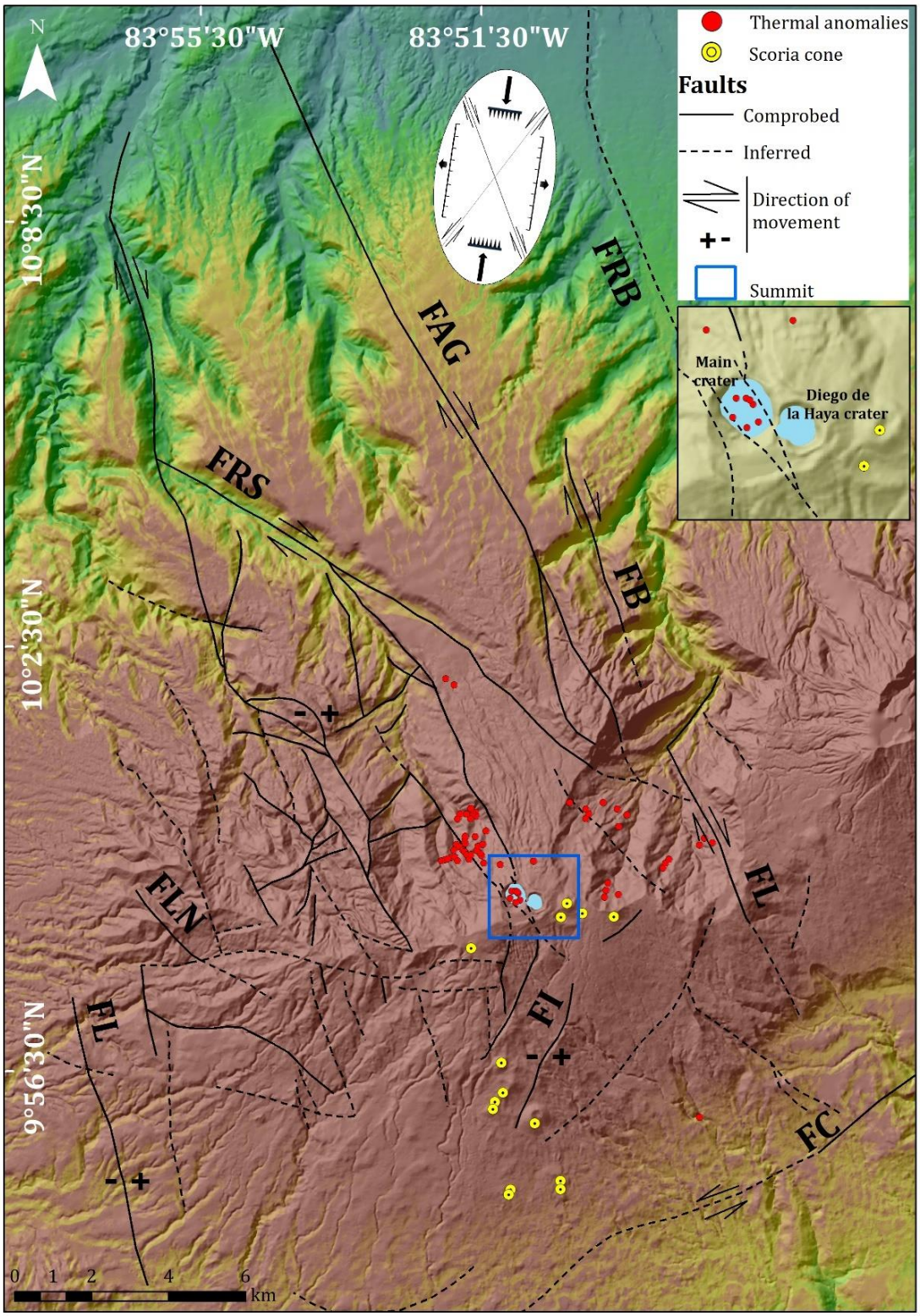

Figure 5. Main faults identified in the Irazú massif (Montero and Alvarado, 1995; Linkimer, 2003; Linkimer et al., 2018) associated with the distribution of scoria cones, craters, and thermal anomalies. FI: Irazú Fault, FC: Capellades Fault, FL: Liebres Fault, FRB: Río Blanco Fault, FB: Blanquito Fault, FRS: Río Sucio Fault, FL: Lara Fault, FLN: Las Nubes Fault, FRD: Rancho Redondo Fault.

Table 1. Main historical records of seismic events around Irazú volcano between 1933 and 2016

Earthquake Name	Date	Location	Maximum Magnitude	Source
Santa Cruz de Turrialba	1933	Between the Irazú and Turrialba massifs	IMM V	1,2
Patillos	1952	8 km WNW of the Irazú Main crater	IMM VIII	2
Cascajal de Coronado Seismic swarm	1978-1979	Cascajal (11 km NW of the main crater of Irazú)	IMM IV	3
Seismic swarm between Irazú and Turrialba	June 1982	Flank SW of Turrialba and SE of Irazú	IMM VI	3,4,5,6,7
	September 1982	SW flank of Turrialba volcano	M_W 4.0	
Seismic swarm of 1987	January 1987	NW flank of Irazú	M_L 3.4-3.7	7,8,9
	August, 1987			
Seismic swarm of 1990	March 1990	Summit of Irazú	Mw 4.4 IMM IV	10
Irazú Seismic swarm of 1991-1992	January-November 1991 January- September 1992	5 km around the summit of Irazú	MC 3.9	11
Seismic swarm of 1994	November 1994	Between Irazú and Turrialba	M 3.4	12
Seismic swarm of 1996	February-March,1996	Around the summit of Irazú	----	13,14
Seismic swarm of 1997	April-June 1997	Around the summit of Irazú	M 3.9	15,16
Seismic swarm of 2010	January-March 2010 June-July 2010	Around the summit of Irazú 5 km al NW de Pacayas	M_L 3.2	17
Seismic swarm of 2012	January, July and September 2012	Around the summit of Irazú	MC 4.5	18
Seismic swarm of 2014-2015	December 2014-February/May 2015	Summit of Irazú and SW of the Main crater	ML 4.0	17
Capellades	November 2016	~4 km north of Capellades	Mw 5.4	19

1. Schaufelberger and Jiménez (1933)
2. Montero and Alvarado (1995)
3. Montero and Dewey (1982)
4. Morales and Montero (1984)
5. Güendel (1985)
6. Fernández et al., (1998)
7. Barquero and Alvarado (1989)
8. Güendel (1987)
9. Boschini (1988)
10. Barquero et al., (1991)
11. Barquero et al., (1995)
12. BGVN (1994b)
13. BGVN (1996a)
14. BGVN (1996b)
15. BGVN (1997a)
16. BGVN (1997b)
17. Quintero-Quintero and Porras-Hernández (2018)
18. Mora et al., (2012)
19. Campos-Durán and Quintero-Quintero (2020)

1.4.3.2. Volcano inestability

A particular characteristic of the Irazú volcano is the large number of avalanches and sectoral collapses of smaller volumes (< 30 x 10^6 m^3) that have affected its main flanks and craters, as evidenced by the historical and prehistoric records (Alvarado et al., 2021).

These destructive events have been facilitated by the combined effect of the meteorological conditions of the area (the average annual precipitation is 2387 mm, SINAC, 2008), the steep slopes of the volcano flanks, the presence of abundant clay soils, recurrent seismicity, and volcanism (Alvarado 1993; Alvarado et al., 2004, 2006, 2013; Hidalgo et al., 2004, Pavanelli et al., 2004; Floris et al., 2005, Fallas et al., 2018; Muller et al., 2020). These avalanches and sector collapses have occurred along the whole recent evolution of the volcano, including the historical time, and have deeply modified the relieve created by the accumulation of volcanic materials (Table 2, Fig. 6).

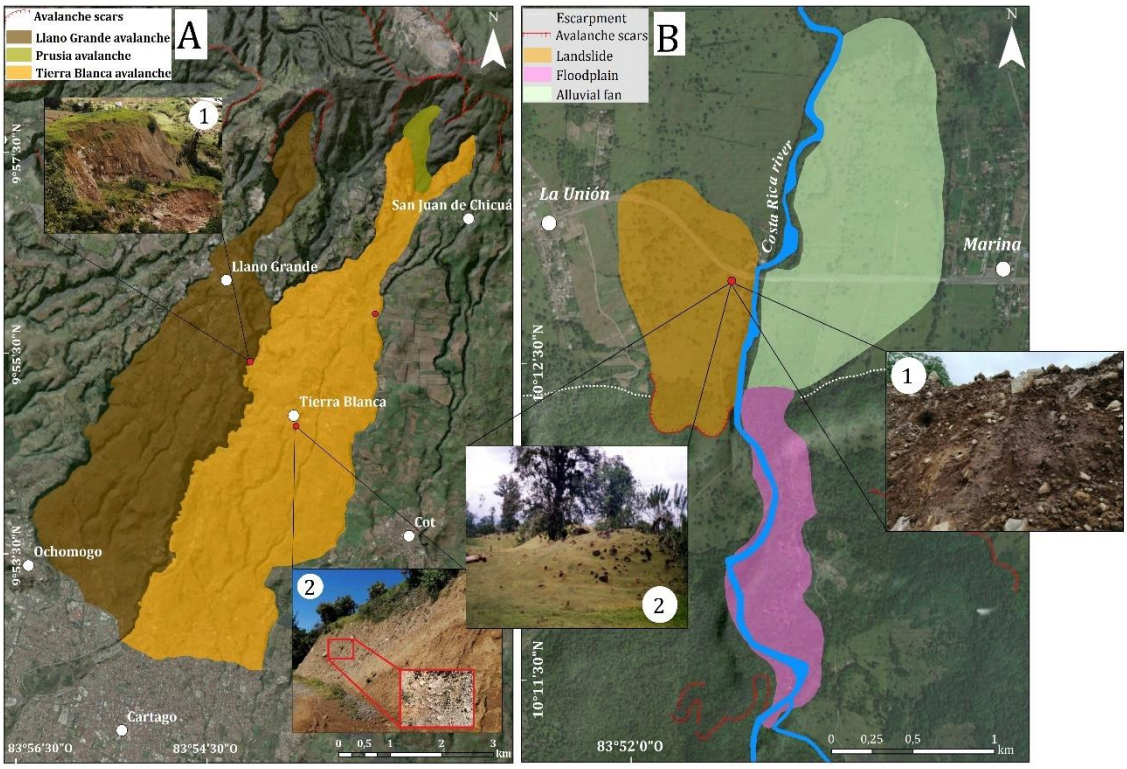

Figure 6. Field map of main avalanche deposits at north and south flanks of Irazú volcano.

Table 2. Compilation of prehistorical and historical avalanches and sector collapses at Irazú volcano

Avalanche	Date	Sector	Extent	Source
La Lavina del Valle Central	150 ka -250 ka	WSW of the Irazú summit	~30 km	1
Angostura	~17 ka	SE flank between Irazú and Turrialba	18 km	2
Reventado-Tierra Blanca	~4100 B.C.	SW flank of Irazú	15 km	2, 3
Río Costa Rica	~800 A.C.	N flank of the Irazú summit	~2 km	2,4
Río Sucio	1821	NW flank of the Irazú summit	?	5
	1994		~2 km	5, 6
	2014		4 km	7
	2020		4 km	8

1. Hidalgo et al., (2004)
2. Alvarado et al., (2004)
3. Pavanelli et al., (2004)
4. Alvarado et al., (2021)
5. Alvarado et al., (2013)
6. Fallas et al., (2018)
7. Pacheco et al., (2015)
8. Muller et al., (2020)

1.4.3.3. Geomorphology

The geomorphological aspects shown by the Irazú volcano are relevant in a hazard assessment study as they may extend a strong control on the emplacement of several of their potential volcanic and associated hazards. The Irazú volcano (3427 m a.s.l.) is a composite stratovolcano with slopes between 6° and 22° and with a dozen summit and adventitious pyroclastic cones and several avalanche scars, located NE of the city of Cartago. It is the highest volcano in Costa Rica, 2,000 m higher than the city of Cartago, 2,200 m above the Central Valley, and 3,200 m higher than the San Carlos plain. Bergoeing (1978, 1979, 1998, 2007, 2009), Alvarado (1989), Soto and Sjöbohm (2015) and Alvarado et al. (2021) make general geomorphological descriptions of the most outstanding features of the Irazú massif (Fig. 7).

The drainage patterns are predominantly of the subdendritic type, subparallel to angular on its western flank (Vargas, 2001), a pattern that is repeated throughout the Irazú massif, although from a more macro point of view, the general pattern is radial with valleys consequent and subsequent to the regional slope. However, there are also some minor valleys that depart for this general pattern, as can be observed at the Tiribí River through Corralillo, next to Rancho Redondo.

The Toro Amarillo River canyon (formerly called only Toro) stands out for being one of the deepest in the country, with a depth of 1,100 m and one of the highest erosion rates in the world (Galve et al., 2016). This river divides the massif of the Turrialba volcano from that of the Irazú (Fig. 7). Other less spectacular ones are the canyons of the Sucio and Corinto rivers, which are about 500 m deep. In most of these rivers and streams there are waterfalls, some of them of great height. Galve et al. (2022) indicate that the Santa Clara mega-fan (located in the northern piedmont of the Cordillera Central) is formed by the coalescence of the alluvial depositional systems of the Sucio, Chirripó, Toro Amarillo and Tortuguero rivers (Fig. 7).

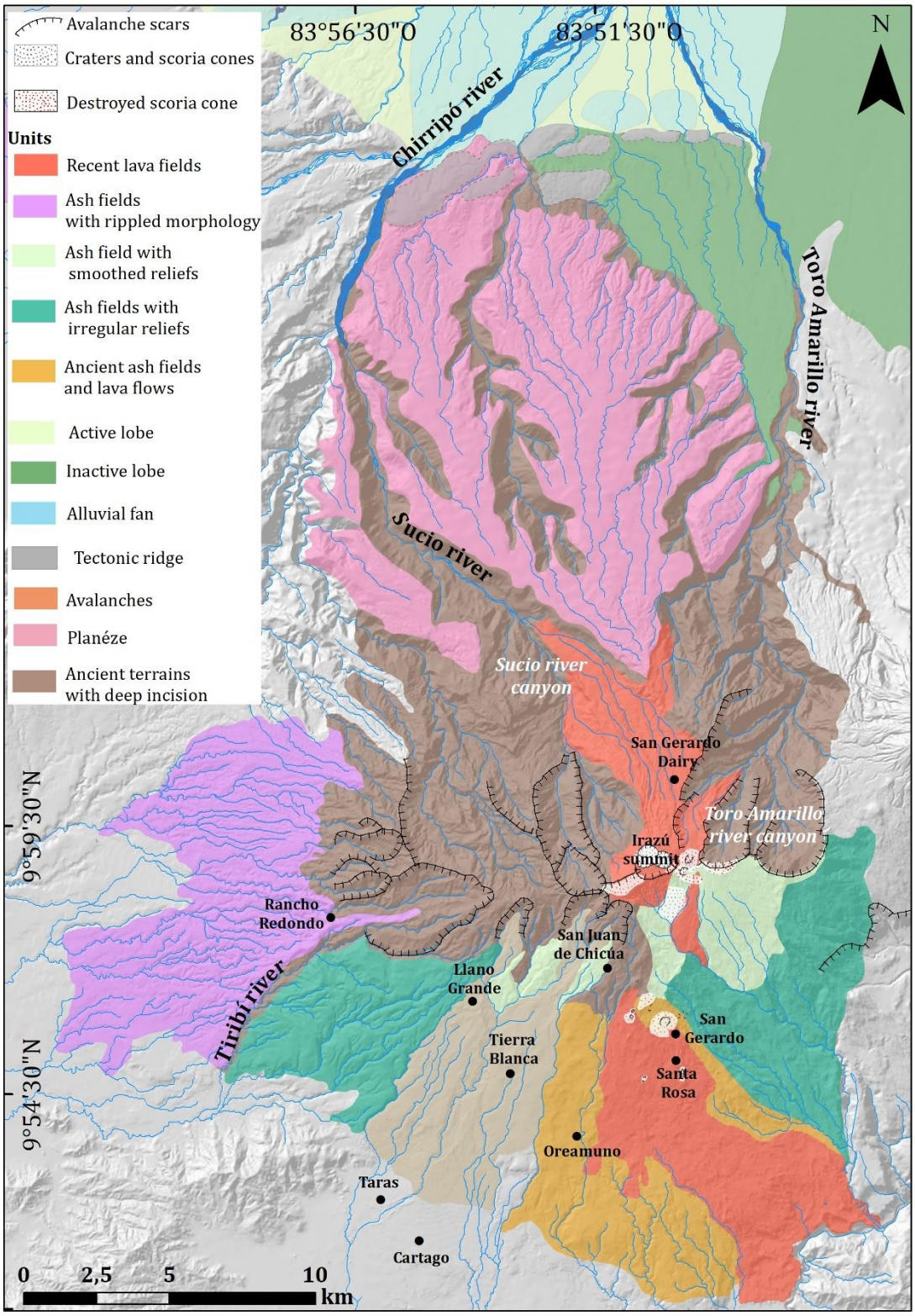

Figure 7. Simplified geomorphological map of a part of the Irazú volcano.

1.4.3.4 Recent and historical eruptive activity in the Irazú volcano

The first historical eruption was registered in 1723-1724 and other eruptive episodes were recorded in 1917-1921, 1924, 1928,1930, 1933, 1939-1940 and 1963-1965 (Table 3). The most important historical explosive events occurred in 1723-1724, 1917-1921 and 1963-1965. The eruptive period of 1723-1724 (VEI = 3) started on February 16, 1723, and produced violent Strombolian phases followed by phreatomagmatic explosions, all accompanied by the largest volcanic-tectonic earthquakes recorded (Ml ~5.5) (De la Haya, 1852; Alvarado, 1993; Alvarado et al., 2006). Ashfall was reported in Barva, 30 km ONO from the volcano summit, as well as the emplacement of lahars up to 14 km long in the Reventado basin (south flank). Also, small dilute PDC deposits have been recognized near the summit (Alvarado, 1993; Alvarado and Schmincke, 2013).

The activity in 1917-1921 (VEI ≥ 2) was characterized for the ash fall, which was reported in the Golfo de Nicoya, 120 km OSO from the summit, and ballistics and small dilute PDCs near the summit (Tristán, 1922; Tristán, 1923; Alvarado, 1993). The 1963-1965 eruption (VEI =3) started on March 13, 1963, with a series of great explosions that hurled out much ash, blocks, and bombs >30 cm diameter, which fell within 4 km of the crater. Small pumice fragments reached San Isidro de Coronado, 18 km W of the summit (Murata et al., 1966; Paniagua and Soto, 1988; Alvarado, 1993). Ashfall was recorded in Matapalo, Guanacaste, 220 km NW from the summit; however, most of the ash fell 30 SW km from de crater, mainly in San Jose city. By early April 1963, dairy pastures, and vegetable farms on the W slopes within 15 km of the summit were buried under several centimeters of ash, and the economic losses in potato, corn, and tomato harvest were estimated by Banco Nacional in $200 000 (Armbrister, 1964; Murata et al., 1966). Approximately 90 lahars were recorded between May 1963 and December 1964, 40 of them in the Reventado basin. The most destructive occurred on December 9, 1963, which resulted in the death of at least 20 people in the western suburbs of Cartago (Taras and San Nicolas towns), destroying or damaging approximately 400 houses, roads, bridges, the railroad to the Atlantic coast, and several factories. The economic losses caused by this event were estimated to be more than $ 3.5 million and about $ 15 million corresponding to the impact of lahars (Murata et al., 1966; Waldron, 1967;

Alvarado, 1993). Similar disastrous lahars of the Reventado river impacted the area of Cartago in 1861,1891, 1928, and 1951 when Irazu was not erupting (Murata et al., 1966; Waldron, 1967; Alvarado, 1993; Alvarado and Schmincke, 2013).

Table 3. Principal characteristics of the historical eruptions between 1723 and 1963-1965

Year	Type of eruption	Duration	Maximum height of eruptive column above crater level (km)	VEI (max.)	Hazards
1723-1724	Strombolian, phreatomagmatic and phreatic	≥ 12 months	> 2 km	3	Fallout, ballistic, PDCd, lahars and seismicity.
1917-1921	Phreatomagmatic	≥ 44 months	~5.5	2	Fallout and PDCd.
1924	Phreatomagmatic	~2 months	¿?	~1	Fallout
1928-1930	Phreatomagmatic	~6.5 months	> 2 km	2	Fallout and lahars
1933	Phreatomagmatic	4 months	~5.5?	2	Fallout
1939-1940	Phreatomagmatic	9 months	~4.5	2	Fallout
1963 -1965	Phreatomagmatic	30 months	8	3	Fallout, ballistic, PDCd, and lahars

On December 8, 1994, a debris avalanche was recorded in Sucio river (north flank), which had its origin from a major landslide near summit (Alvarado et al., 2013; Fallas et al., 2018). Similar events have occurred in the Sucio river on December 17, 2014, and August 26, 2020, both debris avalanches having extensions approximately 4 km from the summit. In these cases, it is assumed that the avalanches were triggered by terrain instability and heavy rainfall rather than by eruptive events (Pacheco et al., 2015; Muller et al., 2020).

Regarding the eruptive activity in the XIX century, most of the existing records are inaccurate, corresponding in many cases to reports from explorers who confused the usual intense fumarolic activity or steam columns with ash columns. In general, the written records agree in considering that after the eruptions of 1723, the activity was fumarolic and gradually decreased until it disappeared, possibly in 1889. In 1825 at least 7 small craters were observed inside a larger crater, one of them with intense vapor activity with sulfur incrustations on the crater walls, a fact that was repeated in 1844 and 1859, these data was documented by Hale, Dunlop and

Trollope respectively (Montessus de Ballore, 1888; Tristan, 1923), and in 1870, according to a letter and a croquis of the Main crater provided by Father Garita to Don Jose Fidel Tristan (Barquero, 1976). In 1888, a strong gaseous activity was reported by Pittier (Barquero, 1976). In 1910, fumarolic activity was observed in the north bottom of the Main crater. In fact, there are no geological records (volcanic deposits) to prove the supposed eruptive activity of the 19th and early 20th centuries, unless they were eroded (Alvarado, 1993) but still some texts continue to repeatedly mention the eruptive activity of the 19th century (Siebert et al., 2010).

CHAPTER 2: METHODOLOGY

2.1 Tephro-chronostratigraphy and eruptive frequency of the Irazú volcano

Volcanic terrains in tropical areas are heavily affected by weathering, which covers most of them in thick soils that allow the growth of a dense vegetation cover. Irazú volcano is not an exception and most of it is covered by a dense forest, mainly toward the N flank where a dense rain forest exists. In particular, it is important to emphasize that at Irazú field work in 2020 to 2022 was hampered by: a) the conditions of the few existing access roads, sometimes impracticable even with a four wheel drive car, b) the outcrops on the road were usually covered by vegetation, so most of them had to be cleaned with a shovel, thus limiting its lateral observation, c) on some occasions the rainy conditions made it difficult to clean the outcrops and to describe them , and d) most of the outcrops visited where in private properties, so we had to obtain permits to access them. Nevertheless, fourteen detailed stratigraphic columns were established in the proximal areas of Irazú (< 6 km), where the deposits are exposed and accessible, mainly on its NE and SW flanks, while most of other areas are highly urbanized or completely covered by vegetation (Fig. 8).

Correlation between outcrops was established using volcanic-stratigraphic criteria (e.g., Martí et al., 2018) and comparison of the lithological and sedimentological characteristics of the deposits. Thickness measurements, as well as lithological characteristics were obtained for all volcanic deposits from these stratigraphic sections. These new stratigraphic sections were combined with the existing ones from Clark (1993), which we revised in the field (Fig. 8 for location). Also, we included four fallout deposit units (González, Dóndoli, Tristán, and Alfaro) previously identified by Alvarado (1993) and Alvarado et al. (2006). Another important and distinctive tephra layer from the Turrialba volcano (10 km NE of Irazú), dated by Reagan et al. (2006) to 2010±60 yr B.P., and which is identifiable on the NE and SW flanks of Irazú, was used as a marker horizon in that area to refine the stratigraphic correlation of the overlying deposits from the Irazú volcano. All

this stratigraphic information was plus the available and new dates was combined to construct.

Eleven samples from six outcrops (Fig. 8) corresponding to paleosoils underlying or overlying primarily pyroclastic deposits (fallout or pyroclastic density current (PDC), deposits) that contain sufficient organic matter were sampled for being radiocarbon dating. The outcrops were carefully cleaned and then the dating material was taken, without touching it, into the soil matrix. Radiometric dating was carried out at Beta Analytic Laboratories (USA) using the accelerator mass spectrometry (AMS) dating. The Beta Analytic's BetaCal 4.2 calibration program, used the international IntCal20 database. A more detailed explanation of the analytical procedure is available at the company's website (https://www.radiocarbon.com/espanol/datacion-laboratorio.html). The new dates were combined with the existing ones (Clark, 1993; Clark et al., 2006), giving a total of 18 radiometric ages for paleosoils intercalated with the Irazú tephras for the last 2,600 years. All ages were calibrated with the Calib Rev 8.1.0 calibration program (http://calib.org/calib/), used the international IntCal20 database.

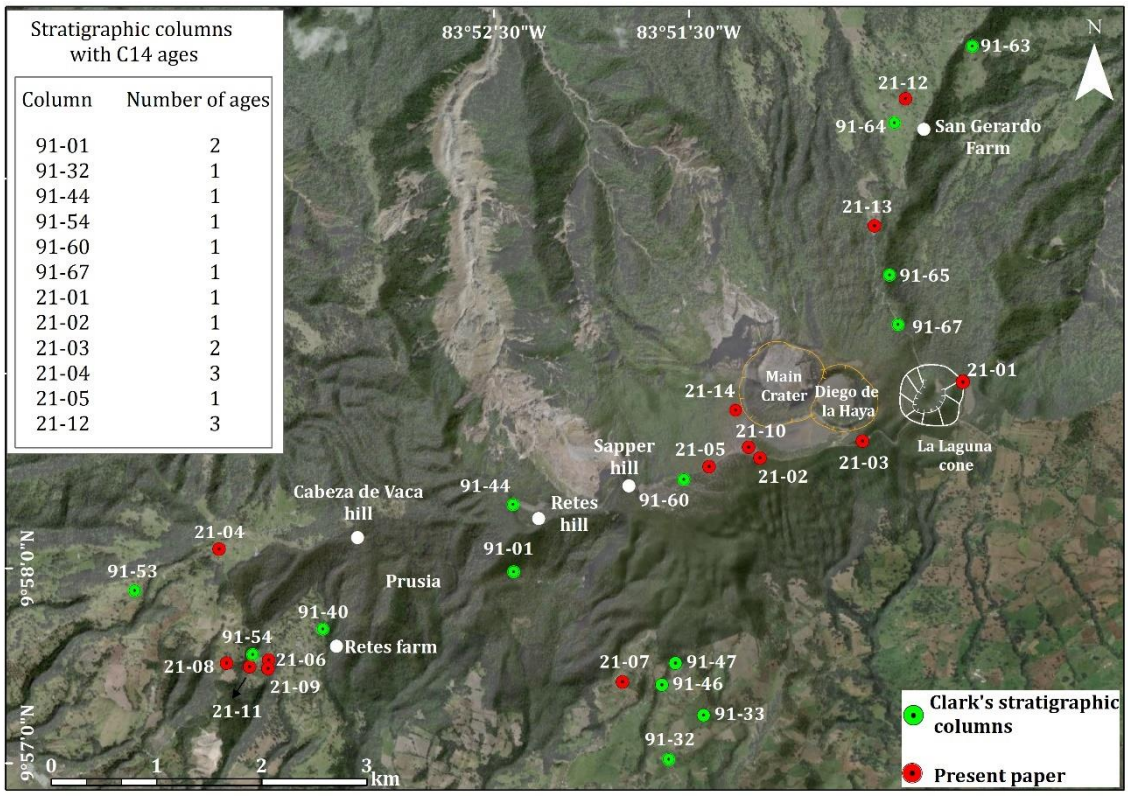

Figure 8. Location of the previous (Clark, 1993) and new stratigraphic columns on the summit and SW and NE flanks of Irazú volcano.

The existing historical records (e.g., Tristan, 1923) (the first eruption was reported in 1723) were reviewed and revised in order to complete the stratigraphy. From all those mentioned in the available historical records, only four of them are recognizable in the stratigraphic record, i.e., produced deposits that can be identified in the field (1723-1724, 1917-1921, 1939-1940 and 1963-1965). So, only those events represented by specific tephra units were incorporated into the final stratigraphy of the last 2.6 ka of Irazú volcano.

To determine the ages of the tephra units, the paleosol samples were taken just at the lower and in several cases also at upper contact of the primary tephra layer of interest, trying to apply the sandwich method, which allowed us to enclose the pyroclastic unit between two age ranges and to establish an intermediate age based on the ranges of variation of the paleosol ages. In those cases where a tephra unit was not dated, but there are ages in upper and lower tephra layers, an age was estimate based on the grade of paleosoils development (thickness, color, relative content of clay). Therefore, the 18 ages by C14 for the last 2.6 ka allow us to assert that there is a good precision to assign ages to the studied units.

To evaluate the past eruptive frequency and estimate the possible occurrence of future eruptions we have followed the methodology proposed and applied by Montero (1986), Ryan et al. (2022) and Benito et al. (2023). This methodology allowed us to diagram each event according to its date of occurrence, allowing us to estimate the eruptive frequency of each event and the periods of quiescence.

2.2 Spatial (volcanic susceptibility) analysis

The spatial analysis is aimed at obtaining the spatial probability of hosting a new vent (volcanic susceptibility, Martí and Felpeto, (2010) of the study area. This is important because the position of vents, together with topography, conditions the resulting eruptive scenarios, as it controls the direction of emplacement of some volcanic hazards (e.g., PDCs, lava flows). For this, we followed the approach proposed by Martí and Felpeto (2010) and considered all the structural elements that could inform on the current stress field of the area and, consequently, on where the next eruptive vent could be located. In this case, these were the location of vents (scoria cones and craters), eruptive fissures, dykes, fumaroles, and faults, which

were mapped in previous studies (Bergoeing, 1978; Hudnut, 1983; Alvarado, 1989; Alvarado, 1993; Montero and Alvarado, 1995; Elizondo et al., 2019) and the ones identified in this investigation. The different structural elements considered were grouped according to their relative age, distinguishing those of Holocene age from the older ones (Fig. 9). In the case of the vents (scoria cones) located on the western and the southern flanks of the volcano, we obtained seven radiocarbon dates (14C method), which allowed us to group them by age and to identify possible eruptive fissures. Radiometric ages were obtained at three laboratories, two of them at Beta Analytic Laboratories (USA), four at International Chemical Analysis Inc (USA), and the last one at Czech Radiocarbon Laboratory (Czech Republic). All of them used accelerator mass spectrometry (AMS) dating and the international IntCal20 database calibration. A more detailed explanation of the analytical procedure can be found at https://www.radiocdating.com/, https://www.radiocarbon.com/espanol/datacion-laboratorio.html. All ages were calibrated with the Calib Rev 8.1.0 calibration program (http://calib.org/calib/), using the international IntCal20 database. These vents are clearly older than the ones corresponding to the central craters, located at the summit of the volcano, and from which all the historical eruptions have been vented.

To calculate spatial susceptibility, we used the probabilistic tool QVAST (Bartolini et al., 2013) that allows to obtain a probability density functions (PDFs) for each of the volcano-structural data set considered. This tool also allows to apply the most appropriate smoothing factor (h) to model the Kernel function used to obtain the PDFs. The smoothness of the spatial density is determined by the bandwidth (parameter h), which controls how the probabilities spread from the considered volcanic structures (Silverman, 1986; Connor and Hill, 1995; Cappello et al., 2012). In other words, this smoothing factor determines how probabilities are distributed depending on the clustering behavior of the volcanic structures considered and varies proportionally with the volcanic field size and density distribution of such structures. For the case of Irazú and based on how the structural features considered are distributed in the study area, we used the Least Square Cross-Validation (LSCV) method (Capello et al., 2012; Becerril et al., 2013) (see Bartolini et al., 2013 for more details).

The total volcanic susceptibility map was obtained through a non-homogeneous Poisson process (NHPP), where the PDFs and their relative weights were combined using a weighted sum. The relative weights (relevance) we applied to the different PDF were: 0.01 for faults and dikes, 0.05 for fissures, 0.08 for fumaroles, 0.2 for scoria cone (≥2 ka B.C), 0.25 for scoria cone (≤ 2 ka B.C) and 0.4 for historical crater (Fig. 9). These values were established following an expert judgment elicitation (see Aspinall, 2006; Neri et al., 2008) process among 8 experts belonging to the Universidad Nacional de Costa Rica (UNA), 2 Instituto Costarricense de Electricidad (ICE), and 2 CSIC Group. Reliability was considered high in all the datasets (value of 20-50) since all of them come from previously published volcano-structural studies and direct field observations. The mesh dimension used was 50 m x 50 m, from a Digital Elevation Model (DEM) at a 1:25000 scale.

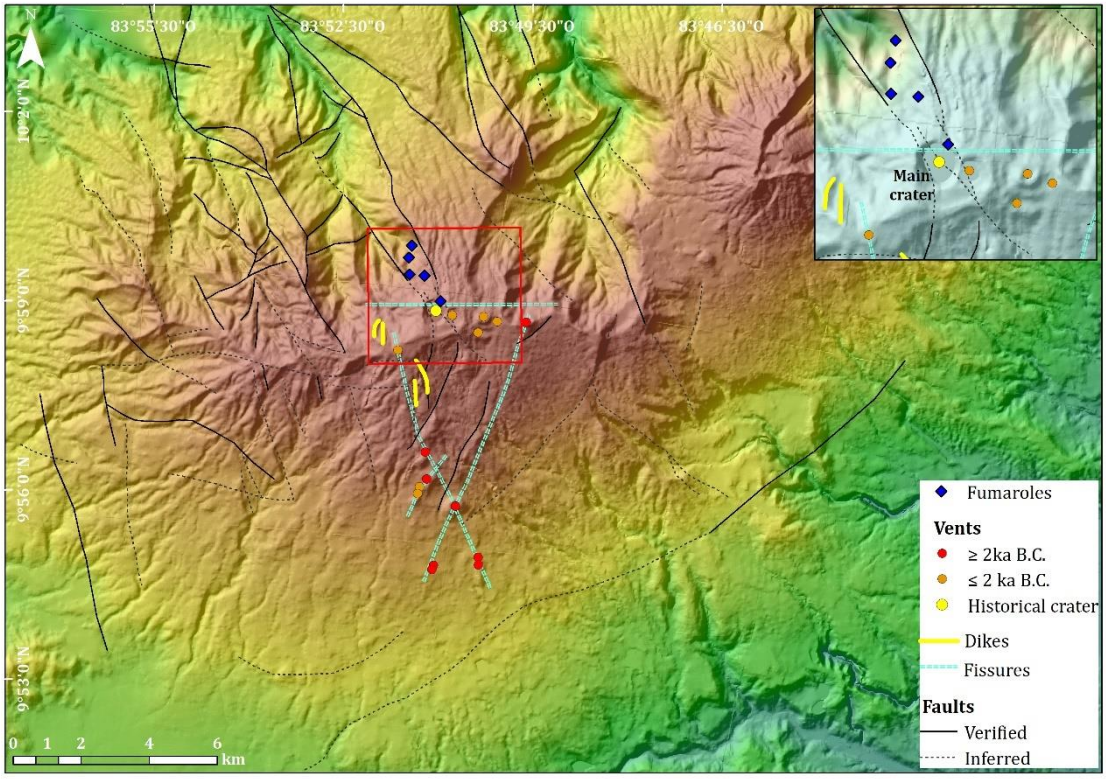

Figure 9. Volcano-structural map of Irazú showing vents (craters and scoria cones), eruptive fissures, faults, dikes, and fumaroles.

2.3 Temporal probability analysis

Temporal analysis was performed using HASSET (Sobradelo et al., 2014), a Bayesian event tree structure with seven nodes (unrest, origin, outcome, location, composition, Volcanic Explosion Index (VEI), and hazard group). They represent different steps to evaluate the temporal probability and evolve from a more general node of unrest to the more specific node of the type and extent of the hazard (Sobradelo and Martí, 2010). The nodes were completed from previous information on the eruptive historical record of Irazú (De La Haya, 1852; Tristán, 1922; Sapper, 1925; Schaufelberger y Jiménez, 1933; Gutiérrez, 1963; Miller, 1966; Murata et al., 1966; Krushensky, 1972; Alvarado, 1993; Alvarado and Schmincke,1994; Montero and Alvarado, 1995; Alvarado et al., 2004; Hidalgo et al., 2004; Pavanelli et al., 2004; Alvarado et al., 2006; Alvarado et al., 2013; Pacheco et al., 2015; Muller et al., 2020) and new stratigraphic data and estimated ages of the eruptions of the last 2.6 ka obtained in this research. Compared to the original version of the HASSET event tree proposed by Sobradelo and Martí (2010) the version used here presents a modification in the last nodes.

Nodes Hazards type (node 7) and Extend (node 8) from the former version have been substituted by a Hazards Group node, which includes different combinations of hazards and of their extend, according to what can be deduced from the products of each eruption, as this ensures keeping the conditions of exhaustivity and exclusivity imposed by the Bayesian inference (see Sobradelo and Martí, 2010). Therefore, to build node 7 (hazard group), we conducted a comprehensive review of the different hazards documented at Irazú from the late Upper Pleistocene to the present. For each particular eruption, we identified the hazards (e.g., fallout deposits, PDC, debris avalanches, lahars, ballistics, and seismicity) produced and the relative extent (long, medium, and short) shown by the different hazards (Table 6). The combination of hazard types and extent provided different hazard groups that were exclusive among them and represented in total all the different hazard combinations generated by the Irazú volcano in the period considered. Therefore, each event identified at Irazú may show the same or a different hazards group compared to the others (Tables 4 and 5).

Table 4. Extension of hazards in the Irazú volcano

Hazard	Extension (km)		
	Short (S)	Medium (M)	Large (L)
Lava flow	3	7	10
Ballistic	2	4	6
Fallout	10	30	200
PDC (Pyroclastic Density Current)	1	3	10
Lahar	8	14	30
Debris flow	2	4	18
Earthquake	≤3.0 (Mw)	3.1- 5.0 (Mw)	≥5.1 (Mw)

The combination of hazard types and extent provided different hazard groups that were exclusive among them and represented in total all the different hazard combinations generated by Irazú volcano in the period considered. Therefore, each event identified at Irazú may show the same or different hazards group compared to the others (Table 5).

Table 5. Hazard groups for events registered between 2600 B.C and 1991 A.D.

Eruption	Hazards	Extension	Assigned group	Hazard groups
~900 B.C. – 1561 A.D.	Fallout	?	2	**Group for geological and historical events** Group 1: Fallout (L), Lahar (M), Ballistic (S), PDC (S), earthquake (M). Group 2: Fallout (?). Group 3: Fallout (S), PDC (S), Lahar (L). Group 4: Fallout (M) Group 5: Fallout (L), Lahar (L), Ballistic (L), PDC (L). **Group for historical events** Group 1: Fallout (L), Lahar (M), Ballistic (S), PDC (S), earthquake (M). Group 2: Fumaroles (?). Group 3: Fallout (S), PDC (S), Lahar (L). Group 4: Fallout (M) Group 5: Fallout (L), Lahar (L), Ballistic (L), PDC (L). Group 6: Fumaroles (?), Earthquake (S)
1723-1724	Fallout	L	1	
	Lahar	M		
	Ballistic	S		
1825, 1844, 1859, 1870, 1888, 1910	Fumaroles	S	2	
1917-1921	PDC	S	1	
	Fallout	L		
	Ballistic	S		
1924	Fallout	S	3	
1928-1930	Fallout	S	3	
	Lahar	L		
1933	Fallout	M	4	
1939-1940	Fallout	S	3	
	PDC	S		
1963-1965	Fallout	L	5	
	Lahar	L		
	Ballistic	L		
	PDC	L		
1984	Fumaroles	?	2	
1991	Fumaroles	?	6	
	Earthquake	S		

HASSET estimates the probability of occurrence of a future volcanic or related scenario and evaluates the most relevant sources of uncertainty in the

corresponding volcanic system. HASSET assesses the hazards group of each scenario by estimating its probability of occurrence within a future time interval. The probabilistic event tree exposes all types of events (possibilities) that have occurred and could occur in a specific volcano or volcanic area and, according to the input data that it receives, calculates the corresponding probabilities for those events that have a higher probability to occur among all the possibilities considered. This is why the resulting probabilities appear lower than one would expect, as they refer not only to the most probable scenarios but to all possible ones.

Moreover, it is important to emphasize that once the information has been included in the event tree, we must consider the uncertainty of the data. First, we must consider the aleatoric (stochastic) uncertainty, which is a consequence of the intrinsic complexity of a system, hence a limitation to our ability to predict the evolution of the system in a deterministic way. Second, we must consider the epistemic uncertainty that is directly related to our knowledge of the system and the quality of the data we have or the degree of confidence we have on our data. These uncertainties are expressed in HASSET as prior and data weight values, respectively. Prior weights are assigned between all the branches of the same node with the condition that the total must be 1. In the case of data weights values may go from 1 (total ignorance) to 50 (or more) (total confidence) (Sobradelo and Martí, 2010; Martí et al., 2022).

HASSET estimates the probability that a volcanic or related (e.g., seismic swarm, landslide, etc.) episode will occur within a given forecasting time interval. For the Irazú volcano, we considered two-time intervals, one that corresponds to the last 2600 years, and another that only includes the historical time (i.e., since 1723). The first case included geological and historical records, while the second case only included the historical ones. The reason to choose these two different periods was to emphasize the importance in the type of data considered when identifying possible future scenarios and calculating their corresponding probabilities. When considering only historical records the total time length considered is much shorter but the occurred scenarios are more than when extending the observational period 2600 years ago, as in this second case it requires to incorporate also what is observed in the geological record.

For this reason, scenarios of activity observed and described in the historical period, such as seismic swarms or volcanic unrest not ending with an eruption, cannot be considered when taking into account a longer period that requires to incorporate geological data, as there is no way to demonstrate that such scenarios also occurred, as there are no deposits associated with them. So, those scenarios that are recorded in the historical period but cannot be identified before, have to be removed from the list of events considered when assuming an observational time window than the historical period. Otherwise, it would cause a biased assignment of probabilities to the resulting scenarios.

Therefore, to conduct our temporal analysis, we considered the tephrochronological reconstruction of the past 2600 years and a catalog of historical eruptive and associated activity on Irazú (1723 A.D.- 1991A.D.). This resulted in two analyses, the first for the entire time interval of 2923 years (~900 B.C. - 2023 A.D.), including the historical activity, and another only covering the historical period (1723 A.D.- 2023 A.D.). Despite being much shorter, there is more precise information for this latter period, also including records of unrest episodes that have not led to an eruption and seismic swarms.

In the first case, a time window of a total of 2923 years (geological and historical time) and a forecasting time interval of 5 years were chosen, resulting in a total number of time window of 585 for the entire study period. The forecasting time interval must correspond to the maximum time window that ensures having only one event in it (see Sobradelo and Martí, 2010). In this period, we identified 26 eruptive events in the stratigraphic record (2600 B.C – 1561 A.D.), and 7 events in the historical time (1723 A.D -1963 A.D) having assumed magmatic unrest for each of them. This gives a total of no event windows of 552, as the number of time windows has to be the same as the sum of the unrest and no-unrest episodes (see Sobradelo et al., 2014). Obviously, the stratigraphic record may not be complete, as part of the deposits may have had completely eroded out or buried by the deposits of younger eruptions, but it offers a minimum approach to the volcanic activity that occurred in Irazú for that period, which provides an order of magnitude for its frequency and size.

For the historical period only, the total time length is 300 years, and assuming a forecasting time window of 3 years, it gives a total number of time windows of 100. From these time windows, 15 of them have event and the remaining 85 have not event. In this case, the observation time is much shorter, but the completeness of the data set is much better than in the previous case, so the comparison between the two cases offers a good idea of how important the number and type of data is when making this kind of hazard analysis.

2.4 Eruptive scenarios and total qualitative hazard map

In this section, we reproduced the 1963-1965 eruptive scenario, as it corresponds to the best historically documented event, also based on the geological (2.6 ka) and historical data it corresponds to the most hazardous scenario expected (VEI = 3). For the simulation/ reconstruction of the volcanic hazard (ashfall, lahars, PDC and ballistic) registered is this period we generated a series of maps, one for each hazard, which were combined and subsequently considered to represent the total qualitative volcanic hazard map of Irazú.

In volcanological literature, the is a wide variety of hazard maps (see Calder et al., 2015 for a review). However, in this case, as in previous studies (e.g., Jimenez et al., 2018; Martí et al., 2022), we assumed the simplest concept of hazard map that was to consider the total number of hazards that may impact on a particular location during the same eruptive or non-eruptive event, regardless of nature of this impact or the relative frequency each hazard may impact on a particular point. Therefore, we define three hazard areas a) high hazard (impacted by three hazards or more), b) medium hazard (impacted by two hazards) and c) low hazard (impacted by one hazard), this was done by applying a map algebra which consider the number and type of hazards affecting each point (pixel) of the map.

To simulate lahars, we use the tool LaharZ (Schilling, 1998) a semi-empirical code for creating hazard-zonation maps that depict estimates of the location and extent of areas inundated by lahars. The input parameters for this model are the Digital Elevation Model (1:25000 scale) and the lahar volume, which provide an automated method for mapping areas of potential lahar inundation. Concerning the volumes and extent of the lahars we have taken as a basis (to calibrate the model)

the 1963-1965 eruption, where the volume of the 9 December event was estimated at 4 x 10^6 m^3, while the total sediment volume (between 1963-165) was around 10 x 10^6 m^3 (Alvarado and Schmincke,1994). Therefore, we have assumed three volumes: 1 000 000, 3 000 000 000 and 5 000 000 000. Relating to the distances, we used the historical record of destroyed bridges (S. A., 1964) as an extension parameter.

Regarding the ashfall the proximal facies of the 1963-1965 tephra deposits (their characteristics and thicknesses) were studied during field season in 2019 and 2020 in outcrops in the Irazú volcano National Park and at medial distances along roads and artificial cuts for construction (SW flank of Irazú and Great Metropolitan Area (GMA)) (Fig. 10). Unfortunately, in most places in the GMA, most of 1963-1965 tephra deposits were reworked quickly and later removed for coffee plantations, urban and industrial development. Thus, we have supplemented our own fieldwork by reviews of historical documents (Gutiérrez, 1963; Coen, 1964; Miller, 1966; Murata et al., 1966; Krushensky and Escalante, 1967; Barquero, 1976; Gawarecki et al., 1980; Alvarado, 1993; Clark, 1993; Clark et al., 2006) to understand deposition and transport mechanisms. With this information we have reconstructed the thicknesses in cm (isopachs)of this eruption, which corresponds to perhaps the best documented eruptive event of Irazú, therefore, we have considered this scenario as the basis for the assessment of the ashfall hazard.

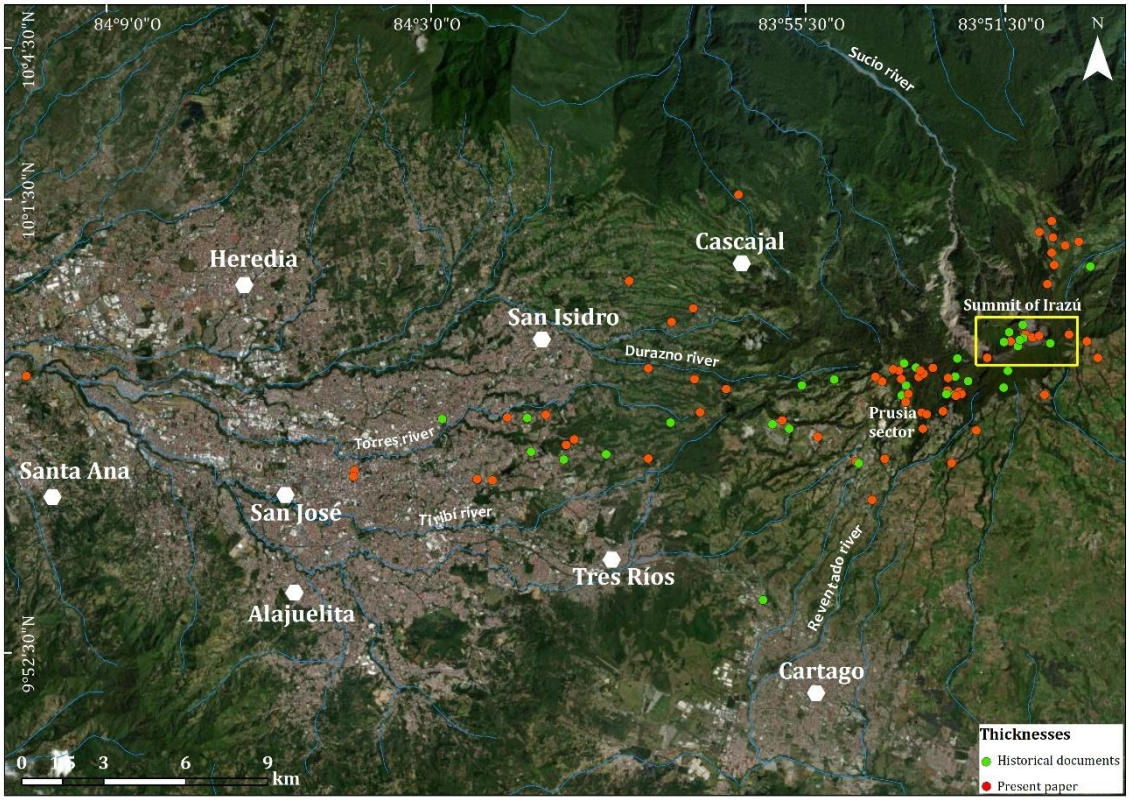

Figure 10. Localities of the principal stratigraphic sections of the 1963-65 tephra deposits.

The emplacement of ballistic clasts is a phenomenon common in Irazú explosive eruptions, we conducted a review of the historical documents (see Miller, 1966; Murata et al., 1966; Soto and Sjöbohm, 2015 for more details) about the diameters of the clasts and their distribution; this data was supplemented with a field trip in 2020 when we registered 11 additional ballistic clasts that were measured up to 1.7 km from the Main crater and two juvenile blocks with dimensions of 1.0 x1.3 x1.8 m and 1.5 x1.5 x1.7 m preserved to the west of the Main crater were included (Figure 11). With this information, we established the hazard ballistic map, considering a circular area around the Main crater, the diameter of which was inferred from reports and the statistical clasts distribution in different past eruptions (mainly 1963-1965).

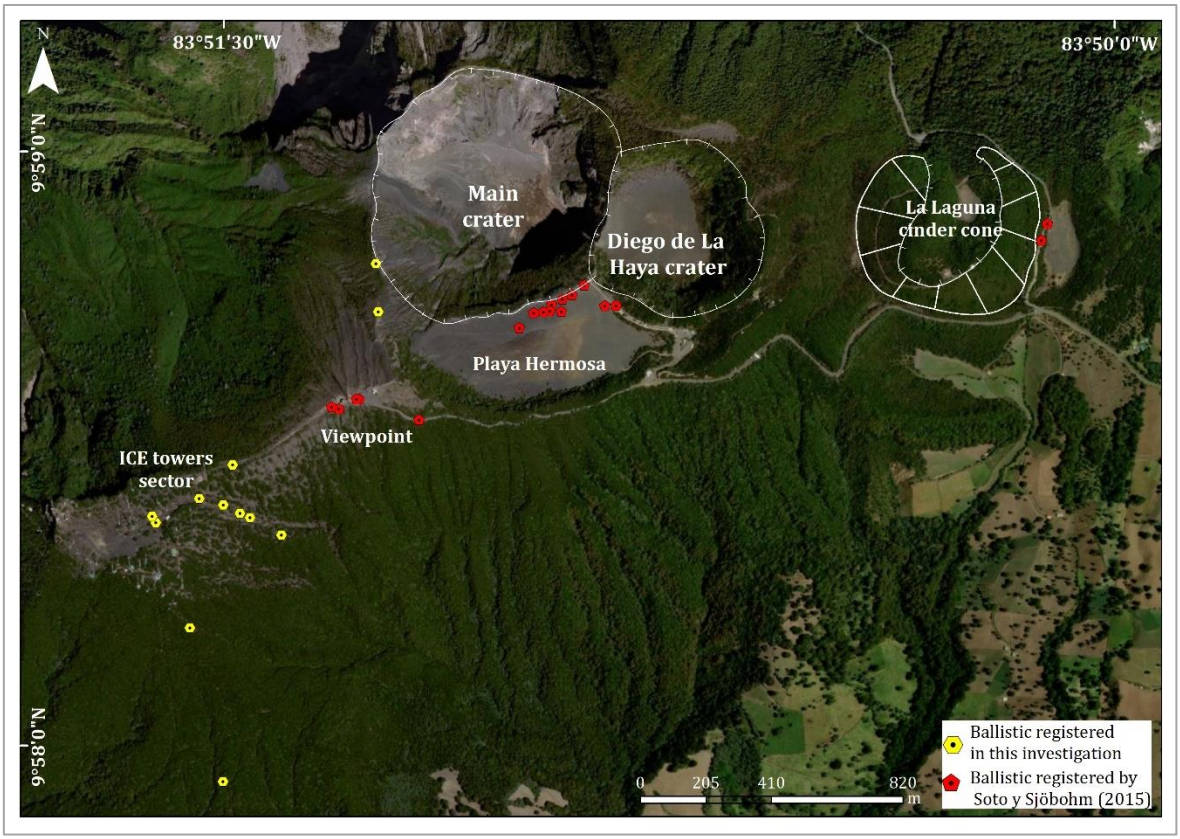

Figure 11. Location of ballistic documented by Soto and Sjöbohm (2015) and registered in this investigation.

Pyroclastic density currents (PDC) were simulating using VORIS 2.0.1 (Felpeto et al., 2007), a simulations model based on the energy cone model proposed by Sheridan and Malin (1983). The input parameters are the topography, the collapse equivalent height (H) of the eruption columns, and the collapse equivalent angle (h). The intersection of the energy cone, originating at the eruptive source, with the ground surface defines the distal limits of the flow. For the PDC scenario, we considered previous investigation where PDC deposits have been documented in the field (Clark, 1993; Alvarado,1993; Young et al.,1998), in the same way, we located several ash deposits with rippled structures, lateral thinning or wedging and inclined lamination in distant sectors toward SW such as Laguna (between Rancho Redondo and Llano Grande), Hacienda Retes and toward NE in San Gerardo (10, 5 and 3 km from the Main crater, respectively). The extension of the PDC deposits found in the literature and the geological record were considered in order to determine the input parameters for a specific scenario that could simulate a PDC hazard.

2.5 Exposure of critical infrastructure, economic systems, and the population to volcanic hazards

We combine the total qualitative volcanic hazard map of Irazú volcano with socio-economic and infrastructure data (population, land use, critical infrastructure, and informal settlements). This information allowed us to construct the exposure maps and to identify the exposed elements. Based on this information, we carry out an exposure analysis method, for which we proposed four categories a) population and villages by canton, b) land use and c) critical infrastructure and d) informal settlements.

Population data was taken from the National Population Census for the year 2022, carried out by the Instituto Nacional de Estadística y Censos (INEC,2022). The data about villages, cantons, roads, educative centers, and land use (pastures, crops, and urban area) were taken from the Sistema Nacional de Información Territorial (SNIT, 2022) (https://www.snitcr.go.cr/ico_servicios_ogc). About the land use the information corresponds to the 2019, so we conducted some field trips during 2023 to update the different land uses in the areas of interest. The informal settlements were taken from the Ministerio de Vivienda y Asentamientos Humanos (MIVAH, 2022) (https://www.mivah.go.cr/Informacion_Geo_Espacial_General.shtml); the Caja Costarricense de Seguro Social (CCSS) provided the information about the distribution of the health centers. All these information was obtained in vector layers (shapefiles).

For the first category (population and villages by canton), we consider the total population per canton and the number of villages located in each hazard volcanic area (high, medium, and low) and that would potentially be affected by hazards. For the land use category, we proposed three subcategories: a) crops, b) pasture and c) urban area. In each volcanic hazard area, we estimated the percentage (area in km^2) of each of the uses that could be affected, this was done by an overlay of layers.

In the case of critical infrastructure (road networks, educative centers, and health centers), we count the elements located within the volcanic hazard areas. Roads networks were divided into three categories (primary road, secondary road, and tertiary road) according with the legal classification from *Ley General de*

Caminos Públicos (Ley 5060) de Costa Rica; health centers were grouped (according with the *Decreto Ejecutivo 38536-MP-PLAN)* in three categories: hospitals, specialized centers, and Equipos Básicos de Atención Integral en Salud (EBAIS); in the case of the educative centers, we defined two categories (schools and high school) (See Table 6 for details). Regarding informal settlements, we identified the number of these exposed at the hazard areas.

Table 6. Description of the sets included in the critical infrastructure

Category	Subcategory	Description
Roads	Primary road	Network of routes serving as corridors, characterized by relatively high traffic volumes, with a high proportion of international, interprovincial, or long-distance trips.
	Secondary road	Routes connecting important cantonal centers (not served by primary roads), as well as other centers of population, production, or tourism, which generate a considerable volume of inter-regional or inter-cantonal traffic.
	Tertiary road	Routes that serve as traffic collectors for primary and secondary roads and are the main routes for travel within a region, or between districts.
Health centers	Hospitals	An establishment designed to carry out all or some of the activities of recuperation, rehabilitation, promotion, and protection of health. They are also teaching and research units.
	Specialized centers	Establishment that attends to a group of patients with certain pathologies that are not attended to in the ordinary treatment.
	EBAIS	Basic integrated health care team consisting of a general medical doctor, a nursing assistant, a network assistant and may include a pharmacy health technician.
Educative centers	School	Educational centers where the first and second cycles of General Basic Education (EGB) are offered to students between the ages of 6 and 12.
	High school	Educational centers where the first and second cycles of General Basic Education (EGB) are offered to students between the ages of 6 and 12.

CHAPTER 3: RESULTS

3.1 Reconstruction tephro-chronostratigraphic and eruptive frequency

3.1.1 Main characteristics of the Upper Holocene tephra deposits

The lithological (grain size, composition of components, and their morphology and texture) and sedimentological (internal grading, stratification, thickness variations, and facies changes) description of the tephra deposits are summarized in Table 7. These characteristics were used to identify the nature of tephra layers (Figs. 12 and 13). They mostly correspond to fallout deposits, originated either by magmatic, phreatomagmatic, and/or phreatic processes, as can be deduced from the lithological and sedimentological characteristics of the deposits. Their components mainly correspond to juvenile (fragments of erupting magma) scoria fragments of basaltic and andesitic composition (Alvarado, 1993) and of variable sizes (ash, lapilli, bombs) and lithic fragments (fragments of host rock) of older volcanic rocks, often hydrothermally altered. The poor preservation of most of the studied tephra deposits and their high degree of weathering do not allow to establish isopach maps. However, variations in thickness of the deposits, as well as their spatial distributions and stratigraphic correlations were used to infer the source of some deposits. Most of these tephras are non-consolidated but locally they may appear partially lithified and endured. Fallout deposits may correspond to intermediate to distal (3->6 km) ashfall deposits (massive or stratified) (Figs. 12 b and d), proximal to intermediate (< 0.5-2 km) stratified scoria lapilli deposits (Figs. 13 b and d), or proximal (0-< 1 km) agglomerates and agglutinates deposits (Fig. 13 c).

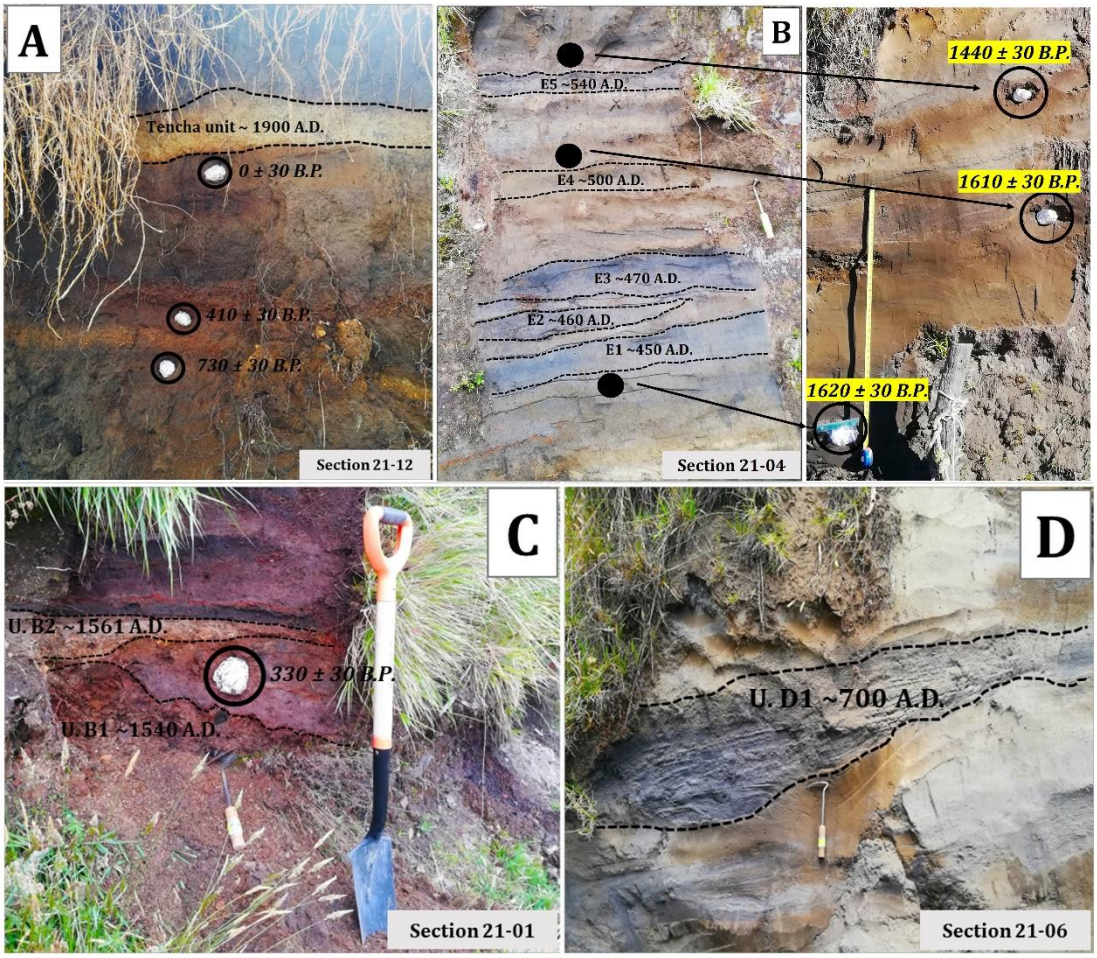

Figure 12. A) A paleosol dated at 0±30 yr B.P. under Tencha unit (avalanche deposit), easily recognizable in Units 21-12 and 21-13, both NE of the summit. The age indicates that this event took place around 1900 A.D. The black circles indicate the points where paleosol samples were taken. B) Units E1 until E5 represent one of the most important explosive events at Irazú of the last thousand years and are recognizable and separated by thin paleosols. These units are restricted by two relatively close ages, 1620±30 and 1440±30 yr B.P. The black circles indicate the points where paleosol samples were taken. C) Deposits associated with units B1 (~1540 A.D.) and B2 (~1561 A.D.), separated by a paleosol dated at 330±30 yr B.P. (it is showed with a black circle) in the section 21-01. D) Unit D1 (informally called the Shining layer in the field, due to its freshness) is recognized as resembling in color, texture, and grain size at the gray ash layers of the 1963–1965 eruption and is easily observed in sections 21-06, 21-07, and 21-08.

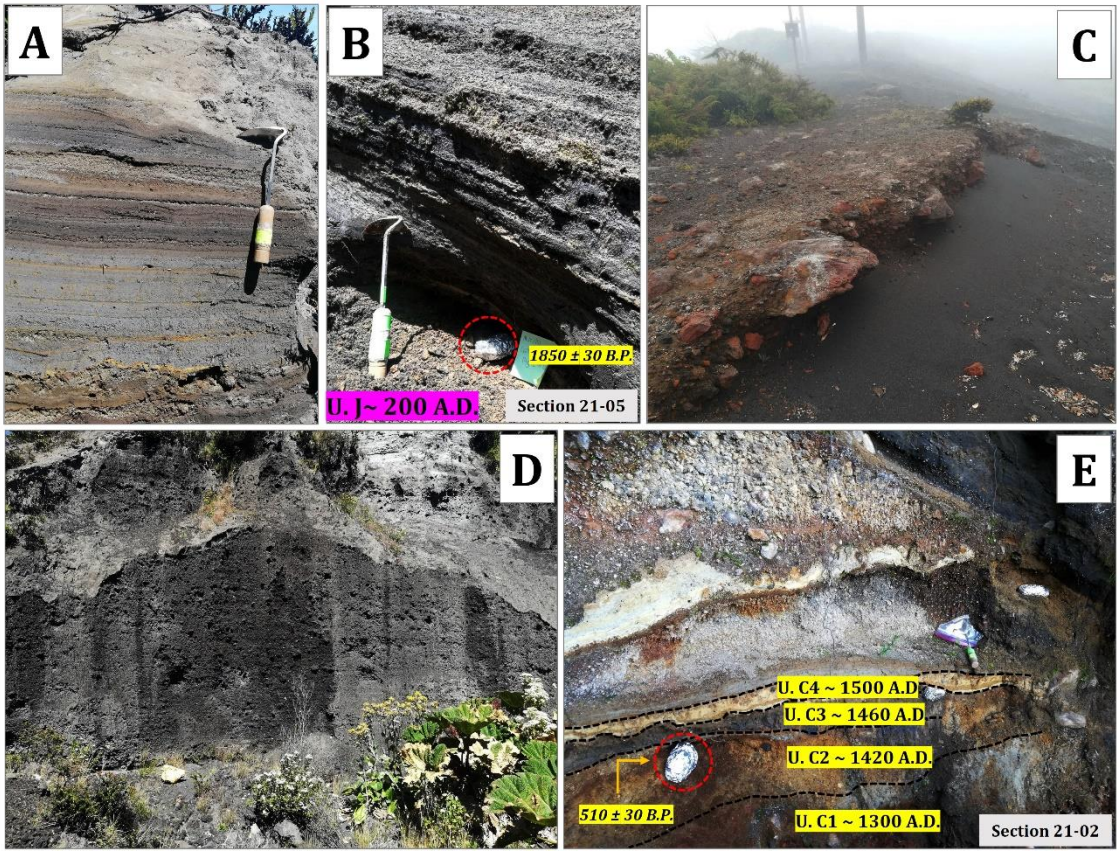

Figure 13. A) Phreatomagmatic deposits associated with the 1963-1965 eruption. Deposits are located on the summit near section 21-14. B). Paleosol dated at 1850±30 yr B.P. on the agglutinated outcropping at the summit of Irazú (section 21-05). The estimated age of this Unit (J or Tristán) is ~200 A.D. The red circle indicates the point where paleosol sample was taken. C). Agglutinated deposit (level of welded bombs), which outcrops throughout the Las Torres sector on the western summit of Irazú. D) Scoria deposit associated with the 1723 eruption, near the Main crater. E) Outcrop 21-02, where a paleosol was dated at 510±30 yr B.P. and on which four units (C1 to C4) were identified, with ages chosen between 1300 and 1500 A.D. The red circle indicates the point where paleosol sample was taken.

Some deposits formed by accumulation of ballistic blocks, probably ejected during phreatic explosions, are also present (sections 21-05 and 91-01 in Fig.13). The thickest (up to 2 m) fallout deposits (unit C1, sections 21-02 in Fig. 13e and Fig.8 for location) are located at the top and on the SW flank of the volcano (proximal area: < 1 km of the Main crater), which suggests a dominant wind towards that direction at the time of these eruptions. In addition to the large variety of fallout deposits, some small pyroclastic density current (PDC) deposits have also been identified, all corresponding to dilute PDCs, reaching a few kilometers from the main crater. These deposits are fine grained, well-stratified, sometimes thinly laminated or showing crossbedding, and containing mostly juvenile ash fragments with occasional scoria lapilli and lithic fragments of variable lithologies of the same sizes

(Table 7). Thicknesses of the studied pyroclastic deposits may vary from one centimeter to several tens of meters in the proximal area (Figs. 13a, b, and c). The gradation can be normal, inverse, non-graded, or combinations of both. Granulometric selection is usually good in fallout layers and dilute PDC deposits, while being poor in agglomerates, agglutinates, and proximal explosion breccias (Figs. 12 and 13). Bioturbation is frequent (animal holes, trunks, and root effects), and remobilization structures (erosion, slumps, landslides) may be locally present. In addition, desiccation crack structures can be observed in the vicinity of the Main crater.

Table 7. General lithological and sedimentological characteristics of studied deposits

Type of deposit	**Lithology** and **petrography**	**Sedimentary structures**	**Location**
Proximal fallout	Compositionally and texturally discrete stratigraphic packets of coarse to medium size ash, well sorting and layered deposits, mantle the topography, including non-gradedd escoriaceous bombs and lapilli layers, and impact bombs and blocks. The dominant color is dark to hell gray, to brown color. Some deposits are rich in hydrothermally altered ash and lithics, with variable colored (orange, red, with, brown). Petrographically, the rocks are basaltic to andesite.	Symmetric to asymmetric grading (normal or reverse to normal), but also non-graded and coarse-grained character in layers in some deposits implying short transport distance, and the orientation of asymmetric ballistic impact sags showing the source.	Summit and near vents
Distal fallout	Widespread fine to medium size ash and lapilli deposits, well sorting, massive to layered sequence. The dominant color is dark to light gray, to brown color, with very thin layers of yellow to strong orange or pale red color. Petrographically, the juvenile components are basaltic andesite to andesite.	Massive, laminated or stratified parallel layering and mantling the topography, well selection and normal gradding.	SW flank NE flank
Dilute Pyroclastic Density Currents (PDCd)	Fine grain, thinly laminated, well sorted, fine to medium ash beds deposits, including massive layers. The dominant color is dark to light gray, orange, or brown color. Petrographically, the juvenile components are basaltic andesite to andesite in composition.	Flat upper surface and an irregular lower surface with low-angle, cross to dune lamination (sand wave), pinch and swell structure to truncation structures, erosive channel filled. Passage between cohesive to non-cohesive deposits is sharp but normally without any erosional surface. Some shows plastic bedding-deformation (contorned stratification) and slide blocks. Plasted ash deposits against trees and vertical walls.	Summit NE flank
Agglomerate	Massive bomb deposits with juvenile block and scoria lapilli layers, and rare hydrothermally altered lithic deposits. Petrographically, the deposits show characteristic magma mixing, present as spatter fragments and scorias with black and white banded texture, of basaltic to andesite with dacites as banded tephra.	Distinctive poorly structureless horizons of welded bombs, with little or no internal layering.	Summit and near vents
Agglutinated	Massive welding deformed bombs and spatter fragments, crudely layered with angular to subangular glassy clast to highly vesicular bombs and lapilli, and rare hydrothermal altered lithics. Petrographically, the deposits are of basaltic to andesite composition. There are also small thin scoria lapilli and bomb lenses, or thin layer formed by deformed and welded bombs which constructed a clastogenic lava flows without roofs.	Distinctive poorly structureless horizons of welded and flattened bombs, with little or no internal layering.	Summit and near vents

The stratigraphic relationships between the analyzed deposits are mainly of three types (Figs. 12, 13 and 14): a) conformity, when there is no erosion or any significant hiatus between deposits; that is, there is stratigraphic concordance and continuity; b) local erosive discordance or disconformity, where there is an irregular surface with an erosive character separating two consecutive deposits, and c) progressive discordance, when the discordances between consecutive deposits are presented gradually over time and space, mainly in the proximal area. Near the summit and towards the Cabeza de Vaca, Retes, and Prusia hills (Fig. 8), local erosional discordances and hiatuses between the pyroclastic sediments are frequent, either because of the steep slopes that favor erosion, the shadow effect of cliffs slopes, the directionality of most of the events, or the continuous occurrence of landslides that modify and cover the original stratigraphy and interbed with the pyroclastic deposits.

The presence of paleosols between pyroclastic units is common. The thickness of the paleosols can range from < 2 cm to > 6 m depending on the volcano flank and the distance from the source region (vent) of each deposit. The edaphological development varies from dark soils (rich in organic matter contents) to brown soils (with more edaphic development or with a certain degree of weathering).

3.1.2 Tephrostratigraphic units of the Upper Holocene

The tephrostratigraphy of uppermost part of Irazú volcano was established combining the new stratigraphy, all the available radiocarbon data, and the existing historical records from which there is a geological correspondence (i.e., presence of tephra units in the field). The stratigraphic order from base to top and the name of the different stratigraphic units, was elaborated considering the original stratigraphy nomenclature from Clark (1993), named, in an aging order, with letters A (historical tephras) and from B to S (pre-historical tephras). In order to preserve this nomenclature when new layers were added, we used numbers (e.g., A1, A2, C1, C2, etc.) following the main unit identified by Clark (1993).

Some of these former stratigraphic units were revised and adapted to the new stratigraphy when their position disagreed with the new data. The new and

former radiocarbon dates (18 in total) (Table 8) were associated with the corresponding stratigraphic units. The result obtained is shown in Table 9, where 30 tephra units, names from P to A4 in stratigraphic order, are identified in the last 2,6 ka of the Irazú volcanological history.

Table 8. ^{14}C ages of the Irazú volcano

Stratigraphic section	Coordinates	Site Description	Conventional age (yr B.P.)	Calibrated age	Source
21-12-03	10°00'23"N 83°50'23"W	~250 m E of the San Gerardo farm	0±30	1876-1916 A.D.	1
91-01-10	9°57'58"N 83°52'28"W	Prusia, ~440 m SW of Retes hill, El Roble Trail	315±20	1521-1577 A.D.	2,3
21-01	9°58'56"N 83°50'05"W	~~400 m N of the main entrance of Irazú Volcano National Park. La Laguna cone	330±30	1549-1598 A.D.	1
21-12-02	10°00'23"N 83°50'23"W	250 m E of the San Gerardo farm	410±30	1432-1520 A.D.	1
21-02	9°58'32"N 83°51'08"W	~200 m SE of Irazú Volcano National Park Viewpoint	510±30	1409-1435 A.D.	1
21-12-01	10°00'23"N 83°50'23"W	250 m E of the San Gerardo farm	730±30	1254-1302 A.D.	1
91-44-09	9°58'18"N 83°52'28"W	Top of Retes hill	920±60	1040-1175 A.D.	2,3
21-03-01	9°58'38"N 83°50'36"W	50 m W of the new Irazú Volcano National Park payment station, on the way to the crater.	1110±30	895-990 A.D.	1
91-67-05	9°59'14"N 83°50'30"W	~800 m N of the La Laguna cone, from Route 219.	1230±70	780-883 A.D.	2,3
21-03-02	9°58'38"N 83°50'36"W	50 m W of the new Irazú Volcano National Park payment station, on the way to the crater.	1300±30	740-773 A.D.	1
91-01-05	9°57'58"N 83°52'28"W	Prusia, ~440 m SW of Retes hill, El Roble Trail	1325±35	657-687 A.D.	2,3
21-04-01	9°58'04"N 83°53'54"W	Road cut at Cabeza de Vaca farm	1440±30	604-643 A.D.	1
21-04-02	9°58'04"N 83°53'54"W	Road cut at Cabeza de Vaca farm	1610±30	496-534 A.D.	1
21-04-03	9°58'04"N 83°53'54"W	Road cut at Cabeza de Vaca farm	1620±30	415-533 A. D.	1
91-54-02	9°57'29"N 83°53'51"W	SW boundary of the Irazú Volcano National Park, near Retes hill.	1600±180	321-611 A.D.	2,3
21-05-02	9°58'30"N 83°51'23"W	~400 m W of the Irazú Volcano National Park viewpoint. Carcava, to the right, after the ICE tower.	1850±30	158-236 A. D.	1
T-109-7	10° 0' 24"N 83°50' 23"W	350 m E San Gerardo dairy	2010 ± 60	53 B.C.-81 A.D.	
91-32-01	9°57'00"N 83°51'40"W	Route 219, 400 m NE from San Juan de Chicuá	2530±170	807-451 B.C.	2,3

1. This work
2. Clark (1993)
3. Clark et al., (2006)
4. Reagan (1987)

The stratigraphic unit P (Fig. 14 c., sections 91-54 and 91-40), with a frequent thickness of 21 cm (distal area: 5 km SW from the Main crater), corresponds to gray ash, fine to coarse, with orange and pinkish levels with discontinuous wavy layers, and its age is ~900 B.C. being the oldest layer identified in the last 2.6 ka. Unit O (Fig. 8., section 91-53), with age of ~800 B.C. corresponds to a very fine gray ash deposit, and their thicknesses varies from 25 to 52 cm (distal area: 6 km SW from the Main crater). Units N, M and L (Figs. 8 and 14a, b, and c., sections 91-32, 91-40 and 91-54), corresponding to deposits rich in ash and lapilli juvenile fragments are underlain by the Subplinian deposit of the Turrialba volcano (guide layer, T. U4), which can be identified in the whole study area (Fig. 14a, b, and c., sections 9-54, 21-04, and 21-12). According with the C^{14} ages these eruptions occurred between ~300 and ~100 B.C. Unit K (Fig. 8., sections 91-46 and 91-47) is a thin ash layer (maximum thickness is 10 cm in the distal area: ~3 km SW from the Main crater), poorly defined and that towards the base presents discontinuous layers of brown to orange coloration; its age is ~100 A.D.

In the stratigraphic section 21–05 (Fig. 14a) (see Fig. 8 for location), we identified an important layer with thicknesses between 1.0 and 1.4 m (proximal area: < 1 km of the Main crater), which corresponds to a scoriaceous agglutinate, locally showing features of a lava-like flow. It shows vertical fractures that resemble a poorly developed columnar jointing and seems to thin towards the Main crater. Radiocarbon dating on the paleosol overlying this layer provided an age of 1850±30 yr B.P. (calibrated age 120–248 A.D.) (Figs. 13b and c; 14a), so we have named this deposit unit J (Figs. 14a and c, sections 21-05, 91-40 and Table 9) assigning to it an age of 200 A.D. This same unit was identified as the Tristán unit by Alvarado et al., (2006). At the site where the dating was obtained, the agglutinate has at least three levels of overlying paleosols, with intercalated tephras, culminating at the top with the historical tephra deposits of 1723–1724 and 1963–1965 (Figs. 14a, b and c). In other sectors where it corresponds to stratified scoria lapilli, and which were subjected to rain, and particularly, strong wind erosion, generating an erosional unconformity, the 1723-1724 historical tephras directly overlie it (Fig. 14a, section 21-05), which gives the false appearance that it must have formed around the age of La Conquista.

In stratigraphic section 21-04 (see Figs. 8 and 14b) we dated three paleosols with organic matter (thicknesses between 5 and 20 cm) the paleosol under unit E1 gave an age of 1620±30 yr B.P, the second paleosol (between units E4 and E5) was dated in 1610±30 yr B.P., and finally, the paleosol above unit E5 gave an age of 1440±30 yr B.P. (Fig. 12b).

Unit E1 (lower) (Figs. 12 b and 14b, section 21-04) is a layer of dark gray, medium-grained ash interbedded with a soil (4 cm thick) overlain by a poorly defined brown paleosol (5 cm thick). This is followed by a level of gray ash, massive, medium to fine-grained, with a level of occasional white lapilli fragments (6 cm thick), overlain by a paleosol rich in ash and fragments of organic matter (Unit E2). This is overlain by a poorly defined level of gray, massive, medium to fine-grained ash (10 cm thick, Unit E3), on which a poorly defined brown to gray soil developed, with occasional charcoal fragments (15 cm thick). Next, there are gray, fine, and massive ash layers (Units E4 and E5), with an intermediate hydrothermally altered level of ash and a thin paleosol in the middle (5 cm thick). According with the data these units (from E1 to E5) have ages between ~450 A.D. and ~540 A.D., i.e., approximately 90 years of relatively sustained activity in time. These units are located in the distal area: ~5.5 km SW from the Main crater.

Unit D1 (Figs. 14b and c, sections 91-54, 91-01, 91-44, 21-03), corresponds to a stratified deposit rich in lapilli and coarse gray ash juvenile fragments; its thickness varies between 8 and 55 cm (maximum distance: ~5.5 km SW from the Main crater). It presents lateral thinning, an eroded upper surface with filling structures, and oxidized levels towards the top. Its bright gray color, stratification, and presence of internal parallel and cross lamination and absence of cohesion, makes it resembling to the 1963-1965 deposits, although it is notoriously thicker, a distinctive feature to recognize it in the field, as observed in the stratigraphic sections (21-03, 21-06, 21-09, 21-08) (see Figs. 8 for location and Fig. 12d). This unit is overlying a paleosol dated in 1300±30 yr B.P. (Figs. 14b and c., section 21-03, calibrated age 740-773 A.D.); Clark (1993) obtained an age of 1325±35 yr B.P. (section 91-01), similar to ours. Therefore, we can say that both ages are associated with unit D1. These calibrated ages provide maximum ages between 740-773 A.D.

and 657-687 A.D., respectively (Table 9). Therefore, 700 A.D. would be the most appropriate age for this relevant event.

Unit D2 (Fig. 14b., sections 21-03 and 91-67) (~20 cm thick) corresponds to a pyroclastic deposit rich in lapilli and intermediate ash size fragments of white and orange colors. It lies below a paleosol dated to 1230±70 yr B.P. (780-883 A.D.), so an age of ~800 A.D. has been assigned to this eruption. Unit D3 (Fig. 14b and c., section 21-03), (45 and 55 cm thickness) corresponds to a gray to brown ash deposit, sometimes massive, with the presence of lapilli size fragments and hydrothermally altered blocks. It is underlain by a paleosol dated 1110±30 yr B.P. (895-990 A.D.), so an age of ~850 A.D. have been assigned to it. Overlying this paleosol is Unit D4 (Fig. 14b and c., section 21-03), composed of fine to very fine ash; its base (first 14 cm) is massive and has pink horizons, while the middle part (15 cm) is stratified and towards the top is deformed (9-23 cm thick). It is followed by a level rich in orange to white scoria lapilli fragments, poorly sorted in a red clay matrix (15-29 cm thick). According to each stratigraphic position, this event possibly took place around ~1000 A.D. (Table 9). These units are located in the proximal area: < 1 km SE from de Main crater).

Unit C1 (Fig. 14a., sections 21-10, 21-02), appears in the proximal area (< 1 km NW from de Main crater) and corresponds to a deposit of coarse-grained black ash to vesicular lapilli clasts. In the proximal area it can be correlated with a more than 1.8 m thick deposit of coarse lapilli to bomb scoria (sections 21-02 and 21-10) (see Fig. 8 for location and Fig. 13e). Unit C2 (Figs. 13e and 14a., section 21-02) (20-40 cm thick) is composed of a massive and poorly sorted hydrothermally altered deposit rich in lapilli fragments (orange, brown, gray), locally with block impacts. It is overlain by a discontinuous brown to orange paleosol with a maximum thickness of 4 cm (section 21- 02), which is dated to 510±30 yr B.P. (calibrated age 1409-1434 A.D.). By chronostratigraphic correlation, we have assigned ages of 1300 A.D. for Unit C1 and ~1420 A.D. for Unit C2. Using the thickness of the deposits in the proximal area, we can estimate that the eruptive focus of both events was located at the summit of the Irazú volcano (near the Main crater).

On top of Unit C2, there is a level of gray ash, with perturbation (physical and biological) and lateral wedging (10 cm thick); we have named this as Unit C3 (Figs. 13e and 14a, section 21-02) (age ~1460 A.D.) (Table 9). At the top, there is an erosional unconformity and a paleosol with hydrothermally altered tephras. Unit C4 (Figs. 13e and14a, section 21-02) (7 cm thick) is a phreatic ash level (brown to gray), with lapilli size fragments and non-juvenile blocks and desiccation cracks in the fine ash, with an age of ~1500 A.D. It may present black scoria, although hydrothermally altered fragments predominate. An erosional unconformity defines the top of the succession (Fig. 13e).

We dated a paleosol on a scoria layer (≥1 m thick) associated with the La Laguna cone (stratigraphic column 21-01) (intermediate area: ~1.5 Km E from de Main crater) (see Figs. 8 for location and Fig. 12c). The radiocarbon age provided was of 330±30 yr B.P. (1549-1598 A.D.), which is very close to that cited by Clark (1993) in 315±20 yr B.P. (1521-1577 A.D.). This paleosol separates two tephra levels B1 and B2 (Fig. 12c., section 21-01). Unit B1 (~1540 A.D.) corresponds a Strombolian deposit composed of lapilli scoria. In addition, near the summit of Irazú, there are stratified ash and lapilli scoria in the same deposit (55-100 cm thick) underlain by phreatic and phreatomagmatic layers, perhaps contemporaneous with the La Laguna cone. We also identified a lava flow (3 km long) to the N of La Laguna cone, which could be contemporaneous with the formation of this cone and (section 21-01), therefore, it could be one of the most recent lava flow in Irazú (≤1500 A.D.). Unit B2 (~1561 A.D.) has a more phreatic character as it is indicated by the presence of lapilli and ash size juvenile fragments with abundant lithic fragments of the same sizes and of different lithologies.

A paleosol dated in section 21-12 (Fig. 8 for location and Fig. 12a) with an age of 0±30 yr B.P. (calibrated age 1876 - 1916 A.D.) is located under a distinctive deposit with strong thickness variation (between 20 and 40 cm) even in the same outcrop (distal area: 3 km NE from the Main crater). This layer shows badly sorted white and orange angular clasts of various sizes and different degree of hydrothermal alteration, in an altered fine matrix. It is easily recognizable to the NE of the Main crater (on the road to San Gerardo Dairy), especially along the road cuts (sections 21-12 and 21-14) (Fig. 12a) near a landslide scarp associated with the

Toro Amarillo River canyon (Fig. 2 to location). This deposit is not characteristic of a primary volcanic tephra, instead resembles more an overbank avalanche or landslide deposit, event very frequent on the N flank of Irazú in historical and prehistorical times (Alvarado et al., 2021). This non-volcanic unit is an important guide layer for the stratigraphy at the NE sector, and for this reason we named it Tencha unit (Fig. 14b, sections 21-12 and 21-13) (~1900 A.D.). Clark (1993) identified this layer (unit Q of his study); however, he did not establish a possible origin or age for this deposit.

Regarding historical tephras, for the period comprised between 1723 and 1917, and despite there are some mentions in the written records to possible activity events at Irazú, the bibliographic review we conducted, as well as the field inspection, did not find historical and stratigraphic evidence to support them. We assumed that most of these supposed eruptive events were confused with fumarolic activity or strong earthquakes. A similar conclusion was reached by Tristán (1923) and Alvarado (1993). For this reason, only those events represented by specific tephra units, this is those corresponding to 1723-1724, 1917-1921, 1939-1940 and 1963-1965, were incorporated into the final stratigraphy. The deposits from the 1723–1724 and 1963–1965 eruptions have been extensively studied, perhaps the best and most reviewed pyroclastic deposits in Costa Rica (Alvarado, 1993; Clark et al., 1993; Benjamin et al., 2007; Boyce and Hervig, 2009; Alvarado and Schmincke, 2013; Brenes and Alvarado, 2013; Oeser et al., 2018). Unit A1 (Fig. 14b and c, sections 21-05, 91-54, 91-01, 91-44, 21-03, 21-14) (tephra from the 1723–1724 eruption) corresponds to black basaltic andesitic scoria with occasional andesitic white pumice (Alvarado, 1993) and phreatomagmatic ash layers and thick phreatomagmatic breccia deposits that are mainly recognizable at the summit of Irazú (Fig. 13d). The tephras from the 1917–1921 (unit A2) and 1939–1940 (unit A3) eruptions, are limited in the summit (Fig. 8 for location and Fig. 14c, section 21-14) and correspond to thin levels (0.5 to 4 cm thick) of ash fallout and dilute PDC deposits, with yellow to red coloration, being separated by local erosional unconformities (Alvarado, 1993). Finally, unit A4 (Fig. 14b and c, sections 91-01, 91-44, 21-03, 21-14, 21-09, 21-06, 91-40) (tephra from the 1963–1965 eruption) includes different deposits of dense and dilute ash-rich PDC deposits and ash-fall

layers, as well as phreatomagmatic and Strombolian deposits and rare thin (few centimeters), fine ash phreatic deposits (Fig. 13a). All the historical eruptive events had their origin in the Main crater and all these units have a distinctive geochemical composition (Alvarado et al. 2006).

Table 9. Upper Holocene tephrochronology of the Irazú volcano (stratigraphic units are indicated from the youngest to the oldest), PS: paleosol; Erosive contact: EC

Unit	Description and interpretation	Conventional age ^{14}C (B.P.)	Age*	Outcrop	Source
A4	Coarse to medium gray ash and lapilli. Phreatomagmatic and stratified andesitic strombolian deposits (fallout and PDCd).		1963-1965 A.D.	91-01, 91-44, 21-03, 21-14, 21-09, 21-06, 91-40	1,2
EC					
A3	Thin levels of medium-fine ash with yellow to red coloration. Stratified phreatomagmatic deposits (fallout and PCDd).		1939-1940 A.D.	21-14	2
EC					
A2	Thin levels of medium-fine ash with yellow to red coloration. Phreatomagmatic deposits (fallout, ballistic and PCDd).		1917-1921 A.D.	21-14	2
PS	Brown paleosol				
A1	Black scoria with occasional pumice and coarse black ash. It presents thick phreatomagmatic breccia deposits that are mainly recognizable at the summit of Irazú. Phreatomagmatic and stratified andesitic strombolian deposits (fallout and dilute PDCd).		1723-1724 A.D.	91-54, 91-01, 91-44, 21-03, 21-05	2
PS	Brown paleosol				
Tencha	Hydrothermalized blocks of different sizes and hydrothermalized ash matrix). Overbank avalanche deposits.		~1900 A.D.	91-63, 91-64, 91-65, 91-67, 21-12, 21-13	1
PS	Paleosol with charcoal	**0±30**	1876-1916 A.D.		
B2	Fine to coarse ash, lapilli, and juvenile fragments with abundant lithic fragments of the same sizes and of different lithologies. Phreatic deposits (fallout).		~1561 A.D.	21-01	1
PS	Brown paleosol with ash and organic material.	**330±30**	1549-1598 A.D.		
B1	Scoria (lapilli and bombs), non-juvenile blocks, orange ash, wedging. Bombs and blocks (La Laguna cone). Strombolian deposit (fallout).		~1540 A.D.	21-01	1
PS	Brown paleosol rich in altered ashes and charcoal.	**315±20**	1521-1577 A.D.		

C4	Brown ash, towards the top, there is a scoriaceous level with hydrothermalized lithics and towards the base blocks. Phreatic deposit (fallout).		~1500 A.D.	21-02	1
PS	Brown paleosol rich in ash and altered tephra.				
C3	Gray ash, coarse grain with wedging. Strombolian deposit (fallout).		~1460 A.D.	21-02	1
PS	Discontinuous brown to orange paleosol	**410±30**	1432-1520 A.D.		
C2	Orange to brown lapilli, poor selection. Phreatomagmatic deposit (fallout).		~1420 A.D.	21-02	1
PS	Paleosol	**510±30**	1409-1434 A.D.		
C1	Lapilli scoriaceous/ash, with scoriaceous bombs. The proximal area corresponds to a thick level of scoria. Strombolian deposit (fallout).		~1300 A.D.	21-02, 21-10	1
PS	Brown paleosol	**730±30**	1254-1302 A.D.		
PS	Brown paleosol	**920±60**	1040-1175 A.D.		
D4	Fine to a very fine ash, wavy to parallel, with pinkish layers. Towards the top lapilli with red clay, it is poorly sorted. Phreatomagmatic deposit (fallout).		~1000 A.D.	21-03	1
PS	Brown paleosol with charcoal and organic material	**1110±30**	895-990 A.D.		
D3	Coarse-grained brown ash, with lapilli and blocks. Predominantly phreatic deposit (fallout).		~850 A.D.	21-03	1
PS	Brown paleosol with charcoal and pre-Columbian pottery	**1230±70**	780-883 A.D.		
D2 (R Unit)	Lapilli (white and orange clasts) and intermediate coarse-grained brown to orange ash. Predominantly phreatic deposit (fallout).		~800 A.D.	91-63, 91-64, 91-65, 91-67, 21-03	1,4
PS	Brown paleosol with charcoal				
D1	Coarse-grained, dark gray ash, stratified with fine lapilli. Strombolian deposit (fallout).		~700 A.D.	91-54, 91-01, 91-44, 21-03, 21-06, 21-09, 21-08	1
PS	Brown paleosol with organic material	**1300±30**	740-773 A.D.		
PS	Paleosol with charcoal	**1325±35**	657-687 A.D.		
PS	Brown Paleosol	**1440±30**	604-643 A.D.		
E5	Fine to medium-grained ash, laminated with small orange layers. Strombolian deposit (fallout).		~540 A.D.	21-04	4
PS	Brown paleosol with hydrothermalized levels	**1610±30**	496-534 A.D.		
E4	Fine to medium-grained gray ash. Strombolian deposit (fallout).		~500 A.D.	21-04	4

PS	Brown to gray paleosol with charcoal fragments				
E3	Fine to medium-grained gray ash. Strombolian deposit (fallout).		~470 A.D.	21-04	4
PS	Organic Paleosol				
E2	Fine to medium-grained gray ash and white lapilli. Strombolian deposit (fallout).		~460 A.D.	21-04	4
PS	Brown paleosol				
E1	Medium-grain dark gray ash. Strombolian deposit (fallout).		~450 A.D.	21-04	4
PS	Dark paleosol with organic matter and charcoal	**1620±30**	415-533 A.D.		
PS	Paleosol with charcoal	**1600±180**	321-611 A.D.		
F	Very fine ash, to the base orange, wavy, lenticular. Phreatomagmatic deposit (fallout)		~400 A.D.	91-40, 91-53	1
PS	Brown Paleosol				
G	Fine to coarse-grained gray to orange ash with occasional weathered lapilli. Phreatomagmatic deposit (fallout)		~350 A.D.	91-33, 91-47	1
PS	Brown paleosol, occasionally rich in clay.				
H	Fine-grained gray ash, bioturbated. Strombolian deposit (fallout).		~300 A.D.	91-40	1
PS	Brown paleosol with altered pumice, occasionally with charcoal.				
I	Gray ash, medium to coarse grain, occasionally with accretionary lapilli and dispersed pumice. Phreatomagmatic deposit (fallout)		~250 A.D.	91-40, 91-53, 91-54	1
PS	Brown paleosol rich in ash				
J	A distal layer of very fine to coarse gray ash with lenticular levels. In the proximal facies, it appears to be represented by an agglutinated. Strombolian deposit (fallout and agglutinate).		~200 A.D.	21-05, 91-40	1,4
PS	Brown paleosol with charcoal	**1850 ± 30**	120-248 A.D.		
K	Very fine-grained orange ash. Phreatomagmatic deposit (fallout)		~100 A.D.	91-46, 91-47	1
PS	Charcoal fragment on the El Retiro layer (Turrialba Unit 4).	**2010 ± 60**	53 B. C. – 81 A.D.		3
4	Subplinian layer of the Turrialba volcano.		~25 A.D.	91-54, 91-64, 91-63, 21-04, 21-07, 21-12, 21-13	
PS	Brown soil, rich in ashes and charcoal.				
L	Medium to fine-grained gray ash with some discontinuous		~100 B. C.	91-40, 91-53, 91-54	1

	stratified horizons. Strombolian deposit (fallout).				
PS	Brown paleosol rich in ash				
M	Coarse grained gray ash with meteorized pumices. Phreatomagmatic deposit (fallout)		~200 B. C.	91-44, 91-47	1
PS	Brown paleosol occasionally with dispersed pumice and orange ashes and charcoal.				
N	Gray ash, medium to coarse grain and vesicular and scoriaceous lapilli (rare) with poor selection; accretionary lapilli. Phreatomagmatic deposit (fallout)		~300 B. C.	91-32, 91-40, 91-46, 91-53, 91-54	1
PS	Brown to orange paleosol, rich in clay and charcoal.	**2530±170**	1048-340 B. C.		
O	Very fine gray ash layer with occasional stratification. Strombolian deposit (fallout).		~800 B. C.	91-53	1
PS	Brown paleosol rich in ash				
P	Gray ash, very fine to coarse grain, with orange and pinkish levels with discontinuous wavy layers. Phreatomagmatic deposit (fallout)		~900 B. C.	91-54, 91-40	1
PS	Brown to black paleosol with charcoal		~1000 B. C.		

1. Clark (1993)
2. Alvarado (1993)
3. Reagan et al., (2006)
4. This work

**The age could be historical or calibrated age in case of ^{14}C or estimated age (~).*

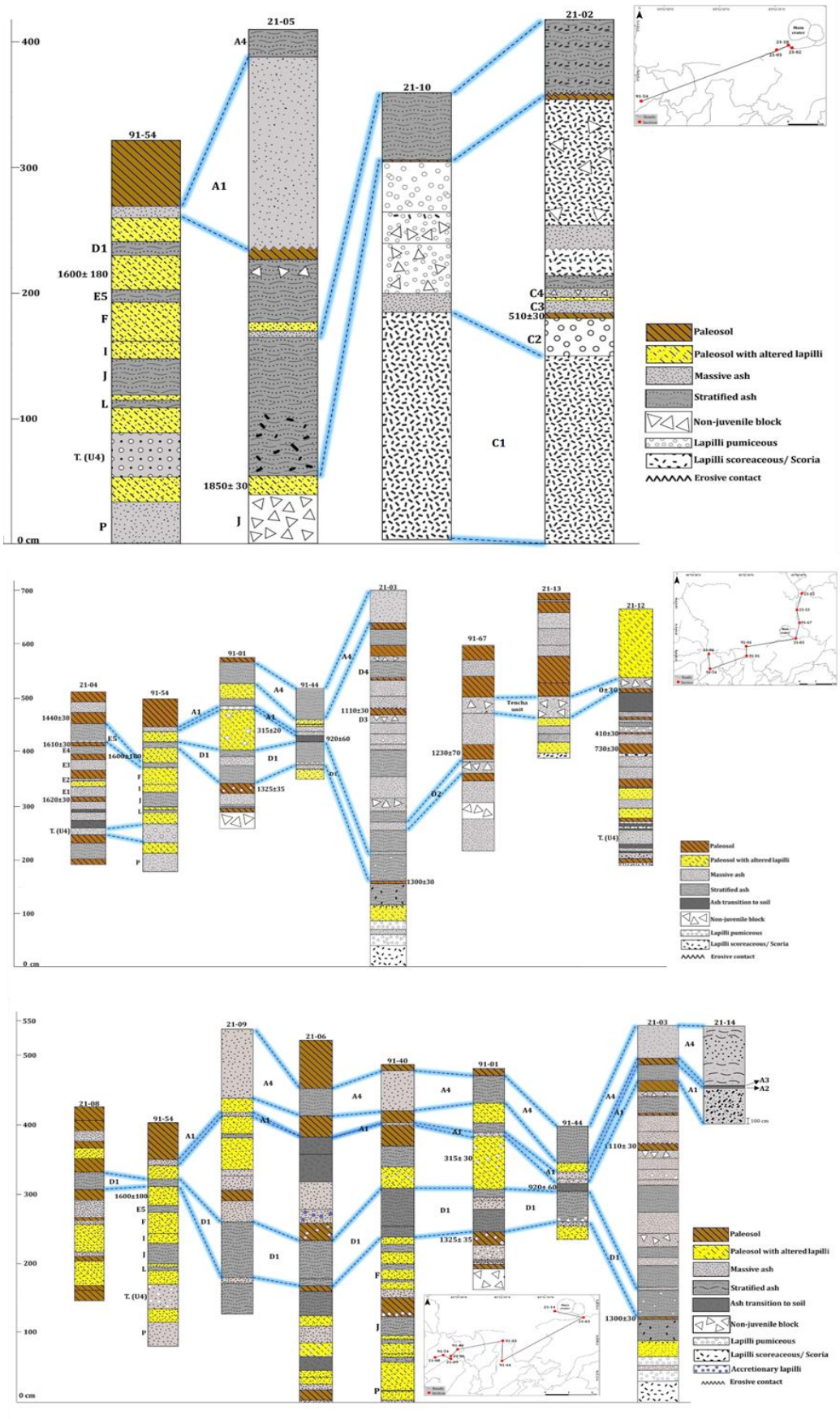

Figure 14. Stratigraphic correlation of the tephra deposits on the summit and SW and NE flanks of Irazú volcano (see text for more explanation).

3.1.3 Eruptive frequency of Irazú volcano

Considering together the prehistoric data analyzed in this study and the historical records, this provides an average of at least one eruption every 85 years. Moreover, the new data allow us to identify some important phases and quiescent periods where no activity has been registered (Fig. 15. From the data obtained, we have developed a diagram of eruptive frequency for the last 2.6 ka (following the methodology of Montero, 1986, Ryan et al.2022 and Benito et al. 2023), in which at least five main eruptive periods—with different phases in each and separated by a quiescent period—can be established (Fig. 15). The first eruptive period (I), with a recurrence of one eruption approximately every 100 years, was preceded by a period without an eruption (Q1) of apparently 500 years; however, this may be due to a data gap. This eruptive period was followed by a ~200 years quiescent period (Q2'), which was interrupted by an eruption, followed by 100 years of further quiescence (Q2'').

Probably due to better stratigraphic details and radiocarbon sampling, the second eruptive period (II) shows a higher eruptive frequency, with a recurrence of one eruption approximately every 33 years. In this sense, paleoclimatic studies in the sediments of Lago Chirripó, suggest intervals of lower lake level at about 1100 and 2500 yr B.P. (Horn, 1993) that may be associated with regional droughts in the Holocene (Hodell et al., 2000; Lane et al., 2014), which could be related to the preservation of tephras in this period. This period was followed by a quiescent period of 160 years (Q3'), which was interrupted by an eruption (Unit D1) that was succeeded by 100 years of quiescence (Q3'').

We identify a third eruptive period (III), which is represented by an event approximately every 100 years, followed by an important quiescent period of 300 years (Q4'). During this eruptive period, Wu et al. (2017) indicate evidence of a prolonged period of low lake levels at Laguna Zoncho in the southern Pacific region of Costa Rica between 1220 and 840 yr B.P. (730-1110 A.D.) possibly indicating the influence of the Terminal Classic Drought (TCD) in southern Costa Rica. Also, Hodell et al. (2000) point out that evidence of drying in Central America suggests that severe droughts between 1300 and 1100 yr B.P. may have been common and

widespread. Therefore, these climatic conditions may have favored the preservation of the tephra deposits of the units present in this eruptive period.

Between the Q4' (300 years of quiescence) and Q4'' (120 years of quiescence), we identified only one eruptive event (Unit C1). This last period without an eruption was interrupted by the fourth eruptive period (IV), which was characterized by one eruption every ~35 years. Subsequently, we have an important hiatus of approximately 160 years (Q5') that was succeeded by one important eruptive event (Unit A1). After these eruptive episodes, we have identified a final period without an eruption of 194 years (Q5'') that was followed by the fifth eruptive period (V), which registered one eruption every 23 years on average. It corresponds with the eruptions registered in historical time. The most important periods without eruptions are separated by only one event, which give rise to substantial eruptive events over time (Fig. 15). For example, periods Q3' – Q3" and Q4' – Q4" separated by significant eruptions such as those represented in Units D1 and C1, respectively.

Concerning the nature of volcanic eruptions, the lithological and sedimentological characteristics of tephra deposits provide the clues to identify corresponding eruption styles (Tables 2 and 4). In this sense, we have identified 30 tephrostratigraphic units in the last 2.6 ka, where 11 of them correspond to phreatomagmatic eruptions, 13 to magmatic (Strombolian) eruptions, two combined (phreatomagmatic and magmatic) and four phreatic (Fig. 15). It is notable the lack of lava flows during this period. Alvarado (1993) indicated that many eruptive episodes of the Holocene at the summit of Irazú began with magmatic or "dry" eruptions and culminated with phreatic and phreatomagmatic eruptions, such as the case of the 1963–1965 eruption. Consequently, if the eruptive pattern and frequency are maintained, Irazú should be considered an active volcano that may erupt again in a few years or tens of years.

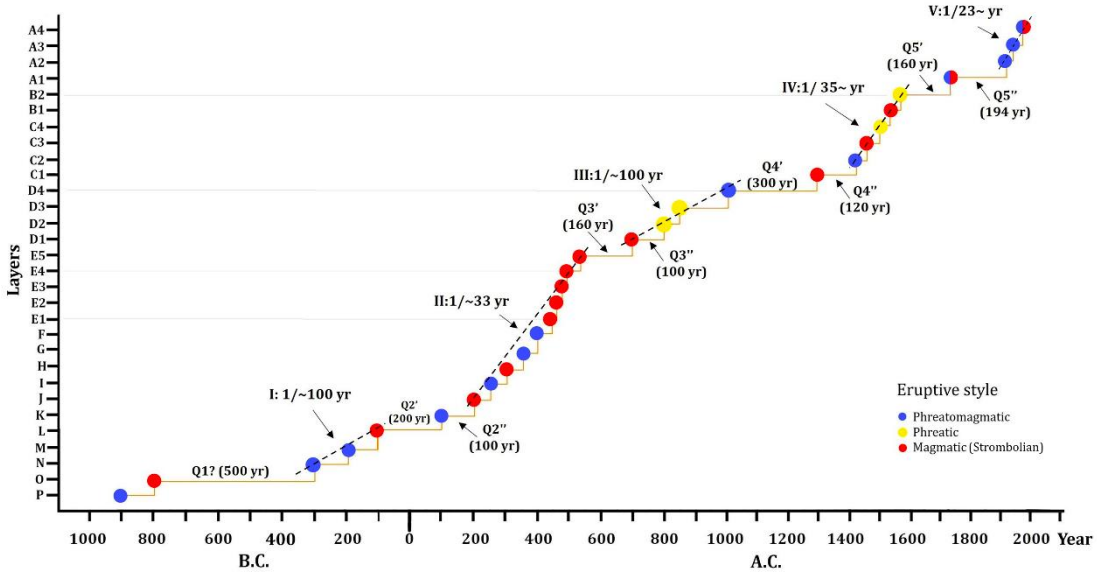

Figure 15. Eruptive frequency of the main units given in the literature and the new data provided in the present study. The eruptive frequency has been higher in the last 2.6 ka due to improved chronostratigraphic sampling. Some quiescent periods are also distinguished. Also, the eruptive styles of the eruptions registered in the last 2.6 ka are showed.

3.2 Spatial (volcanic susceptibility) analysis

To obtain the spatial analysis (i.e.: volcanic susceptibility map), we estimated the spatial density of volcano- structural elements based on their distribution and distance (Figure 9). In the case of the vents, we distinguished between the monogenetic scoria cones formed on the volcano flanks and the main craters located at the summit of the volcano. For the scoria cones, we obtained ages ranging from 330 ± 35 yr B.P. to 10390 ± 30 yr B.P. (Table 10). The craters, however, can be related to all historical eruptions (from 1723). Based on these data, we were able to divide the vents into three groups: a) historic craters, b) scoria cones younger than 2000 B.C. and c) scoria cones older than 2000 B.C.

Table 10. ^{14}C ages of the scoria cones at west of the summit and in the south flank

Name	Coordenates		Conventional age (yr B.P.)	Calibrated age
	Latitud	Longitud		
La Laguna cone	9,9307946	-83,8441156	330 +/- 30 BP	1549-1598 A.D.
Cazuelas 1 Cone	9,9333418	-83,8544112	1890 +/- 30 BP	77 - 232 A.D.
Cazuelas 2 cone	9,9326108	-83,8549251	2890 +/- 30 BP	1210 - 980 B.C.
Santa Rosa cone	9,912747	-83,8387706	7620 +/- 30 BP	6510 - 6410 B.C.
South tower cone	9,9430462	-83,8541176	7097+/- 20 BP	6024 - 5912 B.C.
Pasquí cone	9,9287294	-83,839393	8180 +/- 30 BP	7198 - 7068 B.C.
East Tower cone	9,9768857	-83,8271126	10390 +/- 30 BP	10530 - 10100 B.C.

After classifying the volcano-structural elements, their distribution, and the distance between them, we apply the bandwidth (parameter h) for each of them according to the methos of Capello et al. (2012). In the case of Irazú, the larger values of h correspond to fissures, scoria cones (≤ 2 ka B.C.), and faults, while fumaroles and historical craters represent the lowest values of the bandwidth. Therefore, these data indicate a lower dispersion of fumaroles and craters and a higher dispersion of faults or fissures (Table 11).

Regarding volcanic susceptibility (Fig. 16), the highest values correspond to the area of the Main crater (3427 m a.s.l.), from which all historical eruptions have been vented. Another zone that shows a high susceptibility value is the northern flank of the volcano. The south flank corresponds to a zone of medium susceptibility values because of the presence of fissures and scoria cones that were active during the Holocene. Therefore, we cannot rule out possible future eruptive vents on this flank. The western and eastern flanks have much lower susceptibility values due to the absence of recent structural features.

Table 11. Bandwidth parameter (h) and weights obtained for all the volcano-structural datasets defined on Irazú volcano.

Dataset	h (m)	Weight
Historical crater	195	0.4
Scoria cone (≤ 2 ka B.C)	2898	0.25
Scoria cone (≥2 ka B.C)	1845	0.2
Fumaroles	906	0.08
Fissures	5016	0.05
Faults	2746	0.01
Dikes	1526	0.01

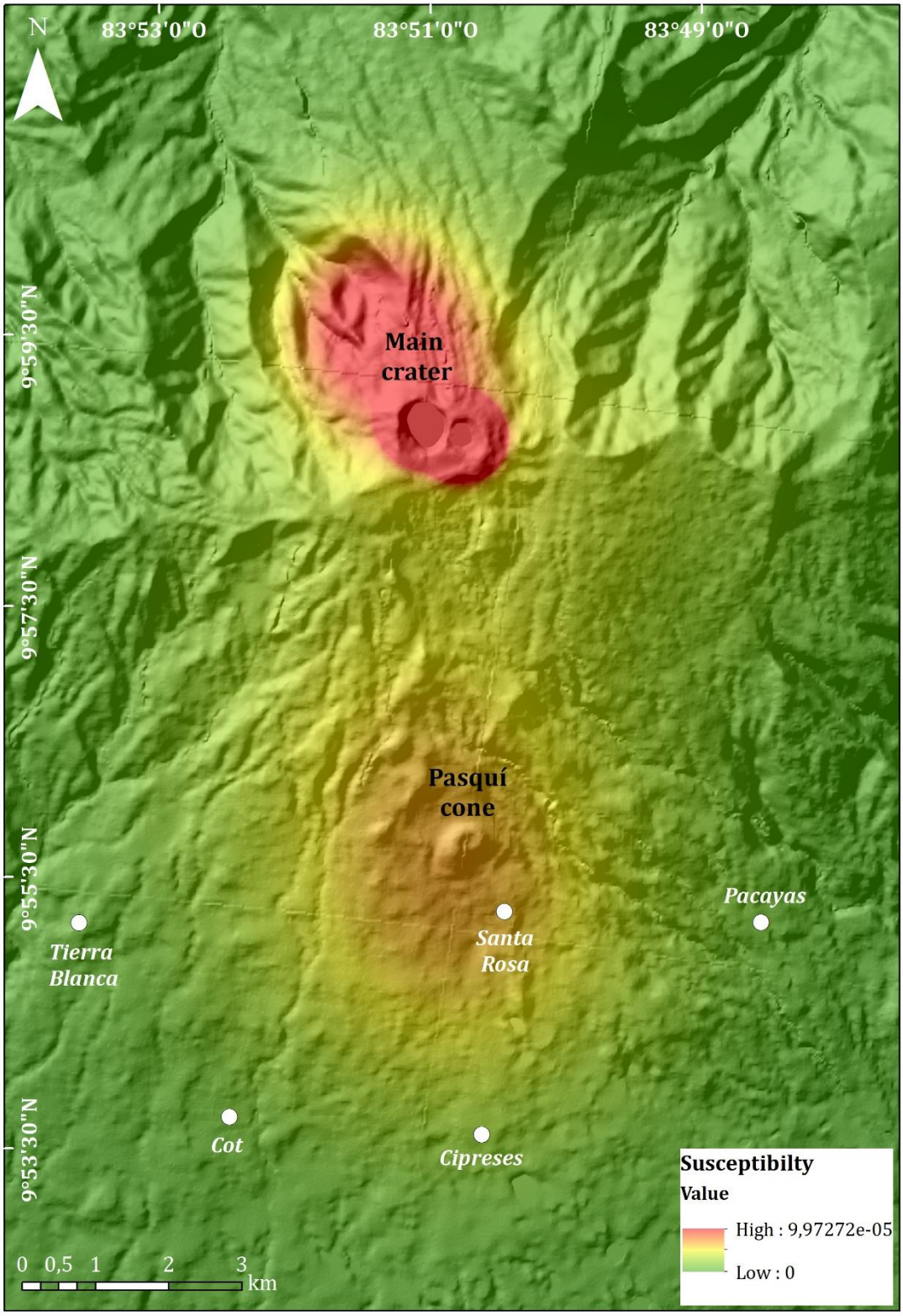

Figure 16. Susceptibility map of Irazú volcano obtained using QVAST

3.3 Temporal probability analysis

3.3.1 Temporal probability analysis for the geological and historical time

The first node (unrest) gives a total of 33 unrest and 552 no-unrest episodes. Concerning the origin, we assumed that magmatic eruptions were preceded by a magmatic unrest (i.e., arrival of fresh magma into the system), while phreatic explosion where just associated with a geothermal unrest. Therefore, the second node (origin) shows that most of these unrest episodes were of magmatic origin (29 in total), followed by four geothermal unrest episodes. At the third node (outcome), there are 33 eruptive events, of which 29 are magmatic and 4 are phreatic explosion (Tables 12 and 13).

Table 12. Principal characteristics of the volcanic events and unrest episodes recorded over the past 2.6 ka (900 B.C –2023 A.D.). Only eruptions of known age or estimated age are included.

Unrest	Origin	Outcome	Location	Composition	VEI	Hazard group	Date
Yes	Magmatic	Magmatic eruption	Central	Mafic	≥1	2	900 B.C
Yes	Magmatic	Magmatic eruption	Central	Mafic	≥1	2	800 B.C
Yes	Magmatic	Magmatic eruption	Central	Mafic	≥1	2	300 B.C
Yes	Magmatic	Magmatic eruption	Central	Mafic	≥1	2	200 B.C
Yes	Magmatic	Magmatic eruption	Central	Mafic	≥1	2	100 B.C
Yes	Magmatic	Magmatic eruption	Central	Mafic	≥1	2	100 A.D.
Yes	Magmatic	Magmatic eruption	Central	Mafic	≥1	2	200 A.D.
Yes	Magmatic	Magmatic eruption	Central	Mafic	≥1	2	250 A.D.
Yes	Magmatic	Magmatic eruption	Central	Mafic	≥1	2	300 A.D.
Yes	Magmatic	Magmatic eruption	Central	Mafic	≥1	2	350 A.D.
Yes	Magmatic	Magmatic eruption	Central	Mafic	≥1	2	400 A.D.
Yes	Magmatic	Magmatic eruption	Central	Mafic	≥1	2	450 A.D.
Yes	Magmatic	Magmatic eruption	Central	Mafic	≥1	2	460 A.D.
Yes	Magmatic	Magmatic eruption	Central	Mafic	≥1	2	470 A.D.
Yes	Magmatic	Magmatic eruption	Central	Mafic	≥1	2	500 A.D.
Yes	Magmatic	Magmatic eruption	Central	Mafic	≥1	2	540 A.D.
Yes	Magmatic	Magmatic eruption	Central	Mafic	≥1	2	700 A.D.
Yes	Geothermal	Phreatic eruption	Central	Mafic	≥1	2	800 A.D.
Yes	Geothermal	Phreatic eruption	Central	Mafic	≥1	2	850 A.D.
Yes	Magmatic	Magmatic eruption	Central	Mafic	≥1	2	1000 A.D.
Yes	Magmatic	Magmatic eruption	Central	Mafic	≥1	2	1300 A.D.
Yes	Magmatic	Magmatic eruption	Central	Mafic	≥1	2	1420 A.D.
Yes	Magmatic	Magmatic eruption	Central	Mafic	≥1	2	1460 A.D.

Unrest	Origin	Outcome	Location	Composition	VEI	Hazard group	Date
Yes	Geothermal	Phreatic eruption	Central	Mafic	≥1	2	1500 A.D.
Yes	Magmatic	Magmatic eruption	Central	Mafic	≥1	2	1540 A.D.
Yes	Geothermal	Phreatic eruption	Central	Mafic	≥1	2	1561 A.D.
Yes	Magmatic	Magmatic eruption	Central	Mafic	3	1	1723 A.D.
Yes	Magmatic	Magmatic eruption	Central	Mafic	2	1	1917 A.D.
Yes	Magmatic	Magmatic eruption	Central	Mafic	1	3	1924 A.D.
Yes	Magmatic	Magmatic eruption	Central	Mafic	1	3	1928 A.D.
Yes	Seismic	Magmatic eruption	Central	Mafic	1	4	1933 A.D.
Yes	Magmatic	Magmatic eruption	Central	Mafic	1	3	1939 A.D.
Yes	Magmatic	Magmatic eruption	Central	Mafic	3	5	1963 A.D.

From the Experts Elicitation Process mentioned in the methods section, we assigned in the node outcome values of prior weights of 0.5 for magmatic eruption, 0.3 for phreatic explosion, 0.1 for no eruption, and 0.1 in the case of sector failure, despite this event did not occur in the time period considered but has been common in the older history of Irazú. Considering epistemic uncertainty and based on the existing information, we assigned a data weight of 40 for magmatic eruption and phreatic explosion, and 30 for sector failure and no eruption, respectively (Table 13).

The eruptions of Irazú in historical times were documented at the summit, specifically in the Main crater, in the prehistoric time we determined (in previous sections) that for the last 2.6 ka the eruptive foci of the deposits study were located at the summit. Therefore, node 4 (location) has 33 registers at the summit (Central location, see Tables12). In contrast, there are no geological or historical records of eruptions on the north, south, east, and west flanks. Therefore, the Prior weight assigned for the Central location was 0.96 and a data weight of 50, indicating that there is reduced epistemic uncertainty in the data. However, following the logic of the event tree we have assigned Prior weight of 0.01 to its flanks (north south, east, and west locations) (Table 13). For the node Composition, all available analyses of products (magmas and pyroclastic) from Irazú correspond to eruptions of basaltic, andesitic and andesite -basaltic composition (Krushensky, 1972; Allegre and Condomines, 1976; Alvarado, 1993; Alvarado et al., 2006; Carr et al., 2007; Alvarado and Gans., 2012), for this reason the 33 events were considered of mafic composition and we assigned a Prior weight of 0.099 and a data weight of 50 to each of them. Concerning VEI, the 1917-1921, 1928-1930, 1933, and 1939 eruptions

were of VEI 2, the 1723-1724 and 1963-1965 eruptions were of VEI 3, and 1924 eruption was of VEI 1 (Alvarado, 1993; Clark et al., 2006) (Table 3).

With respect to the prehistoric eruptions, it was not possible to determine a precise VEI because their deposits are not well-preserved and only some fallout tephra layers were identified. However, if we compare the historical eruptions with the prehistoric ones, we cannot exclude some of the last ones could have had a VEI of at most 3. In this sense, Alvarado et al. (2006) pointed out that the Holocene eruptions of Irazú produced mainly basaltic andesites and had a low volcanic explosivity index (VEI ≤ 3), and Alvarado and Schmincke (2013) emphasized that Plinian phases were not identified in the past geologic record of Irazú (VEI ≤6). Therefore, we assigned a data weight of 10 to the prehistoric eruptions (VEI ≥1) because of the epistemic uncertainty of the data (Table 13).

For node 7 (hazard group) we identified which hazards accompanied each event and which was their extent (in km) in each case. Comparing among all the events, we obtained a total of five hazard groups. (Tables 4 and 5). The Bayesian event tree structure for our initial analysis and the input parameters for each branch are shown in Table 10.

Table 13. Input data for HASSET temporal analysis of Irazú volcano considering the geological and historical time. The total time period was divided into 585-time windows of five years in which a total of 33 unrest episodes have been identified.

Node number	Node name	Event	Past data	Prior weight	Data weight
1	Unrest	Yes	33	0.7	30
1	Unrest	No	552	0.3	10
2	Origin	Magmatic	29	0.5	40
2	Origin	Geothermal	4	0.3	30
2	Origin	Seismic	0	0.1	20
2	Origin	Other	0	0.1	20
3	Outcome	Magmatic eruption	29	0.5	40
3	Outcome	Phreatic explosion	4	0.3	40
3	Outcome	Sector failure	0	0.1	30
3	Outcome	No eruption	0	0.1	30
4	Location 1	Central	33	0.96	50
4	Location 2	North	0	0.01	50
4	Location 3	South	0	0.01	50

Node number	Node name	Event	Past data	Prior weight	Data weight
4	Location 4	East	0	0.01	50
4	Location 5	West	0	0.01	50
5	Composition	Mafic	33	0.99	50
5	Composition	Felsic	0	0.01	50
6	VEI	0	0	0.05	40
6	VEI	1	1	0.2	40
6	VEI	2	4	0.2	40
6	VEI	3	2	0.31	50
6	VEI	4	0	0.01	50
6	VEI	5	0	0.01	50
6	VEI	6	0	0.01	50
6	VEI	7	0	0.01	50
6	VEI	≥1	26	0.2	10
7	Hazard group	1	2	0.3	45
7	Hazard group	2	26	0.1	10
7	Hazard group	3	3	0.2	20
7	Hazard group	4	1	0.1	20
7	Hazard group	5	1	0.3	50

This allowed us to calculate the probability for each tree branch for each five-years period (Fig. 17). For each node, we assigned the Experts Elicitation Process the prior weights and data weights required by the Bayesian inference used by HASSET to calculate the posterior probabilities (Sobradelo and Martí, 2010; Sobradelo et al., 2014; Jimenez et al., 2018).

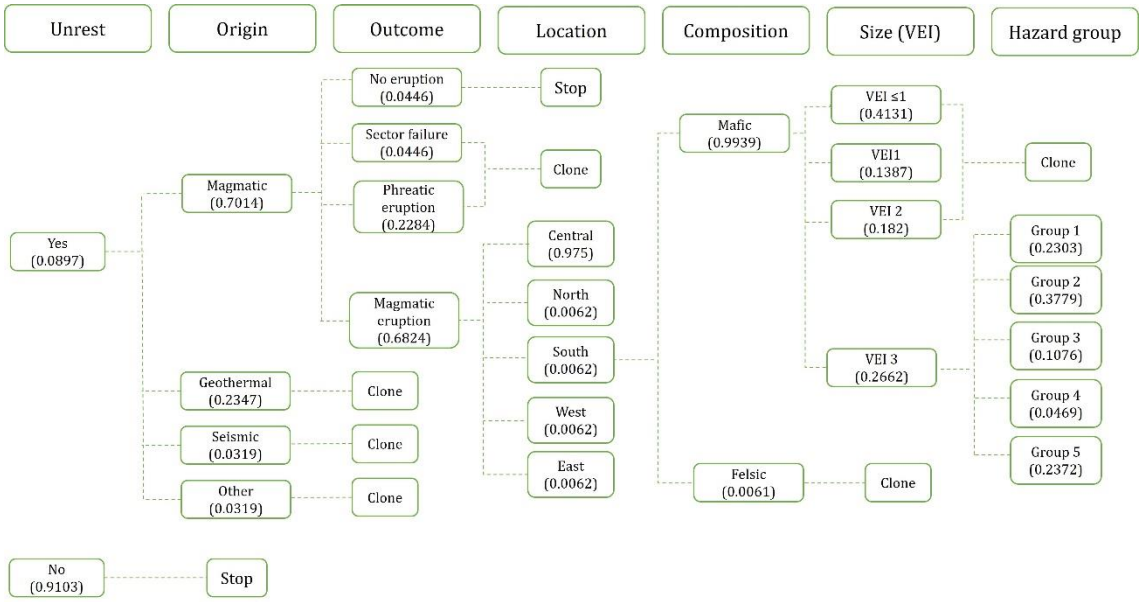

Figure 17. Bayesian event tree of Irazú for the geological and historical period including results for the probability estimate using HASSET.

The results obtained (Table 14) indicate that the probability of having an event (magmatic eruption or phreatic explosion) in the next five years is 0.0564. The most probable scenario for this forecasting period is a magmatic unrest with a magmatic eruption from the Main cater with VEI ≥1 (i.e., VEI between 1 and 3) mostly generating fallout. The second most probable scenario corresponds to a magmatic unrest, with magmatic eruption of VEI =3 from the Main Crater, generating fallout, short PDCs, ballistic and lahars (mainly affecting the southern and northern flanks). This scenario is similar to the eruptions of 1723-1724, 1939-1940, or 1963-1965.

As a third scenario but with a lower probability, a geothermal unrest culminating in phreatic explosion is also conceivable. As mentioned before, the inclusion in the analyzed period of prehistoric events, makes that the identification of the events occurred is much less complete than only considering the historical period. This means that events that have occurred in the historical period, such as earthquakes or landslides not related to eruptive events, cannot be considered here, as there is not prove that they occurred. This implies that the scenarios considered in the forecasting window are restricted to volcanic eruptions, not considering other hazards also common in the history of Irazú volcano.

Table 14. Most likely five-year scenarios considering unrest events with eruption

	Scenario	Probability estimate	Standard desviation
1.	Yes- Magmatic- Magmatic Eruption- Central- Mafic- VEI ≥1- Group 2	0.0065	0.00481
2.	Yes- Magmatic- Magmatic Eruption- Central- Mafic- VEI 3- Group 5	0.00263	0.00176
3.	Yes- Magmatic- Magmatic Eruption- Central- Mafic- VEI 3- Group 1	0.00255	0.00172
4.	Yes- Magmatic- Magmatic eruption- Central- Mafic- VEI 2- Group 1	0.00174	0.00124
5.	Yes- Magmatic- Magmatic Eruption- Central- Mafic- VEI 2- Group 3	0.00081	0.00072
6.	Yes- Geothermal- Phreatic explosion- Central- Mafic- VEI ≥1- Group 2	0.00073	0.0006

3.3.2 Temporal probability analysis for historical time

As the data set corresponding to the historical period (last 300 years) includes more types of events of activity at Irazu, which have been recorded in the written chronicles, the construction of the probabilistic event tree considered other events than only magmatic eruptions or phreatic explosions. So, the first node (unrest) gave a total of 15 unrest and 85 no-unrest episodes. The second node (origin) showed that most of these unrest episodes were of magmatic origin (7 in total), followed by six geothermal and two seismic unrest episodes. At the third node (outcome), there were only 7 eruptive events, and eight registers that did not end in an eruption (all these data are included in the event tree). Therefore, we assigned in the node outcome values of prior weights of 0.4 for magmatic eruption and no eruption, respectively; in the case of phreatic explosion and sector failure the values were 0.1, respectively. Considering epistemic uncertainty and based on the information available, we assigned a data weight of 40 for magmatic eruption, and 30 for phreatic explosion, sector failure, and no eruption (Tables 15 and 16).

Table 15. Principal characteristics of the volcanic events with and without unrest in the historical time

Unrest	Origin	Outcome	Location	Composition	VEI	Hazard group	Date
Yes	Magmatic	Magmatic eruption	Central	Mafic	3	1	1723 A.D.
Yes	Geotermal	No eruption	____	____	____	2	1825 A.D.
Yes	Geotermal	No eruption	____	____	____	2	1844 A.D.
Yes	Geotermal	No eruption	____	____	____	2	1859 A.D.
Yes	Geotermal	No eruption	____	____	____	2	1870 A.D.
Yes	Geotermal	No eruption	____	____	____	2	1888 A.D.
Yes	Geotermal	No eruption	____	____	____	2	1910 A.D.
Yes	Magmatic	Magmatic eruption	Central	Mafic	2	1	1917-1921 A.D.
Yes	Magmatic	Magmatic eruption	Central	Mafic	1	3	1924 A.D.
Yes	Magmatic	Magmatic eruption	Central	Mafic	1	3	1928 -1930 A.D.
Yes	Seismic	Magmatic eruption	Central	Mafic	1	4	1933 A.D.
Yes	Magmatic	Magmatic eruption	Central	Mafic	1	3	1939 -1940 A.D.
Yes	Magmatic	Magmatic eruption	Central	Mafic	3	5	1963 -1965 A.D.
Yes	Seismic	No eruption	____	____	____	2	1984 A.D.
Yes	Seismic	No eruption	____	____	____	6	1991 A.D.

Table 16. Input data for HASSET temporal analysis of Irazú volcano considering the historical time. The total time period was divided into 100-time windows of tree years in which a total of 15 unrest episodes have been identified.

Node number	Node name	Event	Past data	Prior weight	Data weight
1	Unrest	Yes	15	0.8	40
1	Unrest	No	85	0.2	30
2	Origin	Magmatic	7	0.4	30
2	Origin	Geothermal	6	0.2	20
2	Origin	Seismic	2	0.2	30
2	Origin	Other	0	0.1	20
3	Outcome	Magmatic eruption	7	0.4	40
3	Outcome	Phreatic explosion	0	0.1	30
3	Outcome	Sector failure	0	0.1	30
3	Outcome	No eruption	8	0.4	30
4	Location 1	Central	7	0.96	50
4	Location 2	North	0	0.01	50
4	Location 3	South	0	0.01	50
4	Location 4	East	0	0.01	50
4	Location 5	West	0	0.01	50
5	Composition	Mafic	7	0.99	40
5	Composition	Felsic	0	0.01	40
6	VEI	0	0	0.01	30
6	VEI	1	1	0.22	40
6	VEI	2	4	0.22	40
6	VEI	3	2	0.42	40
6	VEI	4	0	0.01	20
6	VEI	5	0	0.01	20
6	VEI	6	0	0.01	20
6	VEI	7	0	0.01	20
7	Hazard group	1	2	0.2	40
7	Hazard group	2	7	0.1	30
7	Hazard group	3	3	0.1	40
7	Hazard group	4	1	0.1	20
7	Hazard group	5	1	0.3	50
7	Hazard group	6	1	0.2	50

Since these data are consistent with historical data, it is proven that the location of these events was the Main crater (central location) and that in all cases the composition of the eruptions was mafic, therefore they were assigned a prior weight of 0.96 and 0.99, respectively. As for VEI, the values vary between 1 and 3, so VEI 1, 2 and 3 received the highest prior weight (Table 16). In the case of the hazard group (node 7) we defined six hazard groups according to the information on hazard types and corresponding extend occurred in each event (see Table 5). This allowed us to calculate the probability for each tree branch for each tree-years period (Fig. 18).

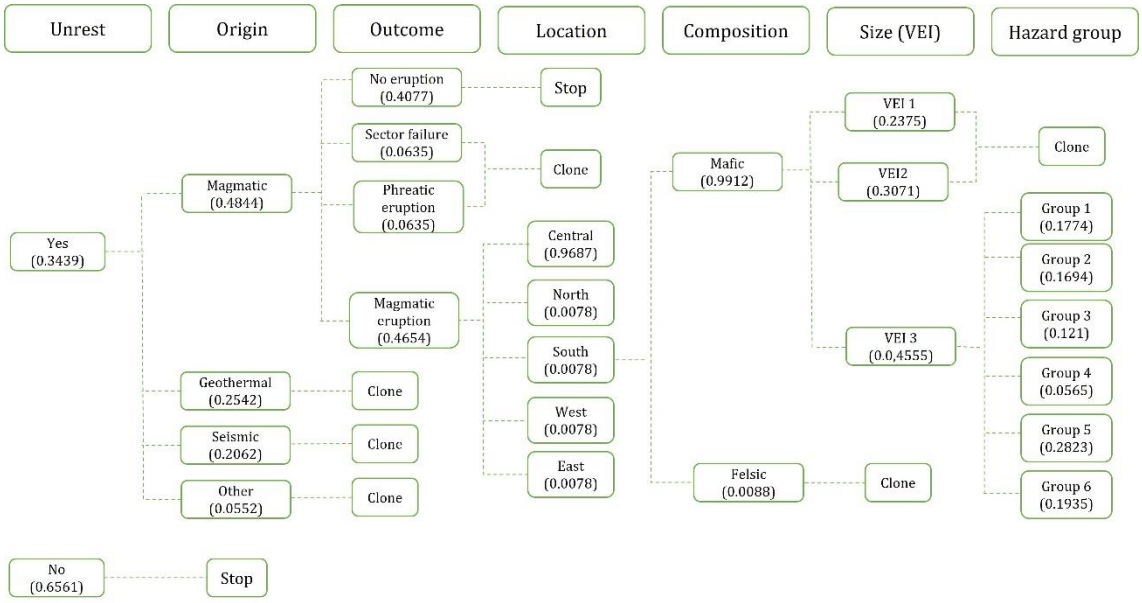

Figure 18. Bayesian event tree of Irazú for the historical period including results for the probability estimate using HASSET.

In the case of historical data, we identified 8 unrest events that did not culminate in an eruption. For this reason, we elaborated the event tree at two different levels of progression: a) From node one to node 3, considering all events, and b) the full event tree but just considering the events that culminated in an eruption. This procedure is important in order to separate those unrest events that may leave to an eruption from those other that will not, assigning to each of them the corresponding probabilities. In the first case we obtained the 5 most probable scenarios (Table 17), the most probable being a magmatic unrest culminating in magmatic eruption (0.07752 estimated probability). The second was a magmatic

unrest not culminating in eruption. Also, a geothermal or seismic unrest that does not culminate in eruption was also possible, such as the events of the 19th century that were characterized for the presence of intense fumarolic activity (Table 15).

Regarding unrest culminating in eruption, we obtained six possible scenarios (Table 17), being the most likely (0.00953 probability estimate) a VEI=3 eruption with fallout, lahars, PDCd and ballistics, all of large extension, similar to the 1963-1965 eruptive episode. The other likely scenarios (VEI between 1 and 3) could range from medium-to-large fallout and lahars, as well as small ballistic and medium earthquake (between 3.1- 5.0 Mw). It is important to emphasize that for all probable scenarios, fallout, especially ashfall, would mainly affect the southwest flank, while in the case of lahars it would affect the south and southwest flank. Regarding the PDCd and ballistics, they would be restricted to the area of the Main Crater.

Table 17. (a) Most likely five-year scenarios considering unrest events with and without eruption. (b) Most likely five-year scenarios considering unrest events with eruption only.

Scenario	Probability estimate	Standard desviation
(a)		
1. Yes- Magmatic- Magmatic Eruption	0.07752	0.02486
2. Yes- Magmatic- No Eruption	0.06791	0.02347
3. Yes- Geothermal- No eruption	0.03564	0.01635
4. Yes- Seismic- Magmatic Eruption	0.03301	0.01419
5. Yes- Seismic- No Eruption	0.02891	0.01297
(b)		
1. Yes- Magmatic- Magmatic Eruption- Central- Mafic- VEI 3- Group 5	0.00953	0.0041
2. Yes- Magmatic- Magmatic Eruption- Central- Mafic- VEI 3- Group 1	0.00599	0.00289
3. Yes- Magmatic- Magmatic Eruption- Central- Mafic- VEI 2- Group 1	0.00404	0.00205
4. Yes- Magmatic- Magmatic Eruption - Central- Mafic- VEI 2- Group 3	0.00275	0.00154
5. Yes- Magmatic- Magmatic Eruption- Central- Mafic- VEI 1- Group 3	0.00213	0.00123
6. Yes- Seismic- Magmatic Eruption- Central- Mafic- VEI 2- Group 4	0.00055	0.00051

3.4 Hazard maps of Irazú volcano

3.4.1 Ashfall hazard

The 1963-1965 proximal tephra deposits were rapidly channeled in several areas by erosion, while more distal ash was removed by runoff and mass wasting in several sectors. A few studies reported the ash thickness in several localities shortly during and after the eruption (Murata et al. 1966; Parsons, 1967; Barquero, 1976). The first isopach map (27 stations) was carried out in 1993, 26 years after the

eruption (Clark, 1993; Clark et al. 2006). It represents minimum values in several places, because the mapped and measured sections are often thinner than reported at the eruption time due erosion and compaction. There are also several contradictions in the few data; for example, in San José, Waldron (1967) reported 2.1 cm, Gawarechki et al. (1980) about 8 cm, instead Clark et al. (2006) report an isopach thickness of less than 5 cm for the same eruption. We complemented this information 48-56 years after the eruption with 62 new stations (Fig. 10) and corrected the isopach curves for the few measurements taken at the time of the eruption.

With this information we obtained 11 isopachs, with values ranging from 2000 cm (in the summit area) to 1 cm in localities 40 km to the W, such as Santa Ana, San Rafael de Alajuela or Escazú. The ashfall mainly affected a perimeter between 5 and 7 km and the W and SW flank of Irazú, particularly the GMA (Fig. 19), this is since in the Irazú, the trade winds enter from the Caribbean coast towards the Pacific mainly between December and April with predominant directions coming from the E and NE (Zárate, 1988). On the Pacific slope, at lower altitudes, there are some variations in the rainy season (Pacific storms), where at the level above the Irazú crater the wind comes from the SW and W for several consecutive days. This suggests that at 3400 m the SW and W winds coming from the Pacific Ocean could drive the ash clouds towards the Caribbean slope in a E-NE direction (Zárate, 1988; Alvarado, 2001). This explains that ash reached sectors as far away as Limón, Nicoya, San Isidro de El General, and Nicaragua, which did not report significant impacts (Fig. 20).

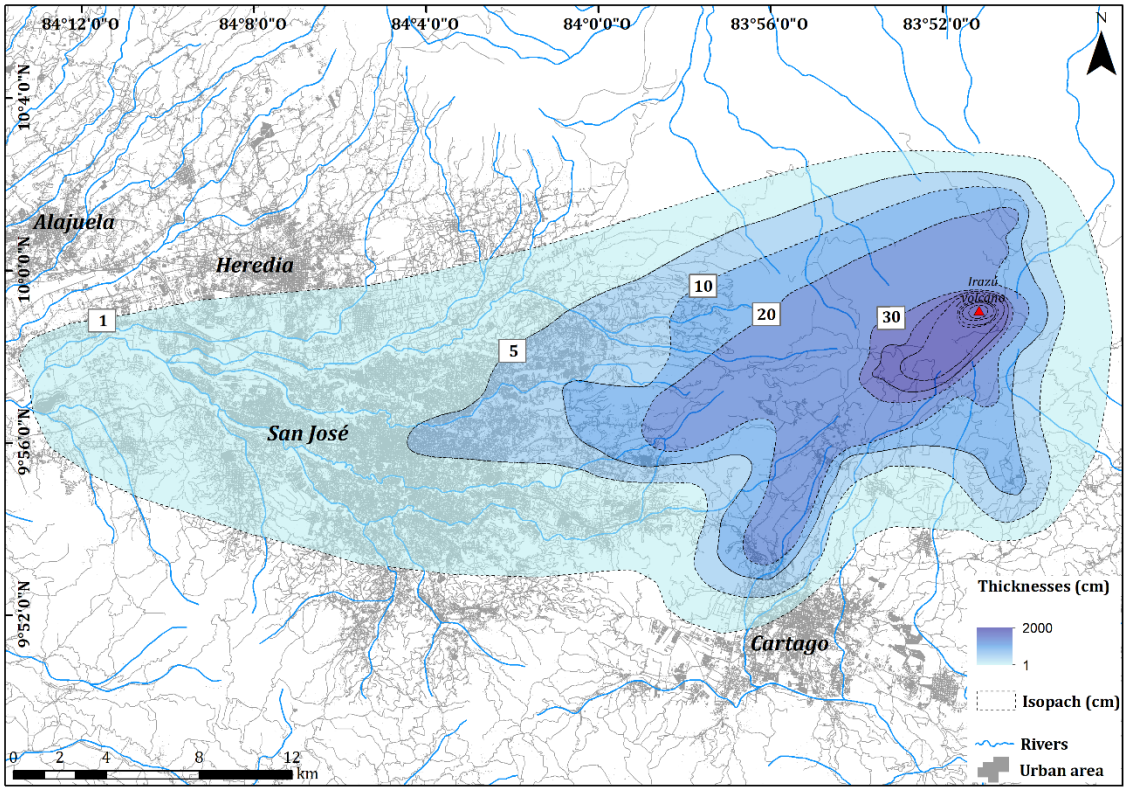

Figure 19. A) Isopach map (in cm) of the eruption of 1963-1965. B) It shows a detail of the thickness of the deposit in the proximal area.

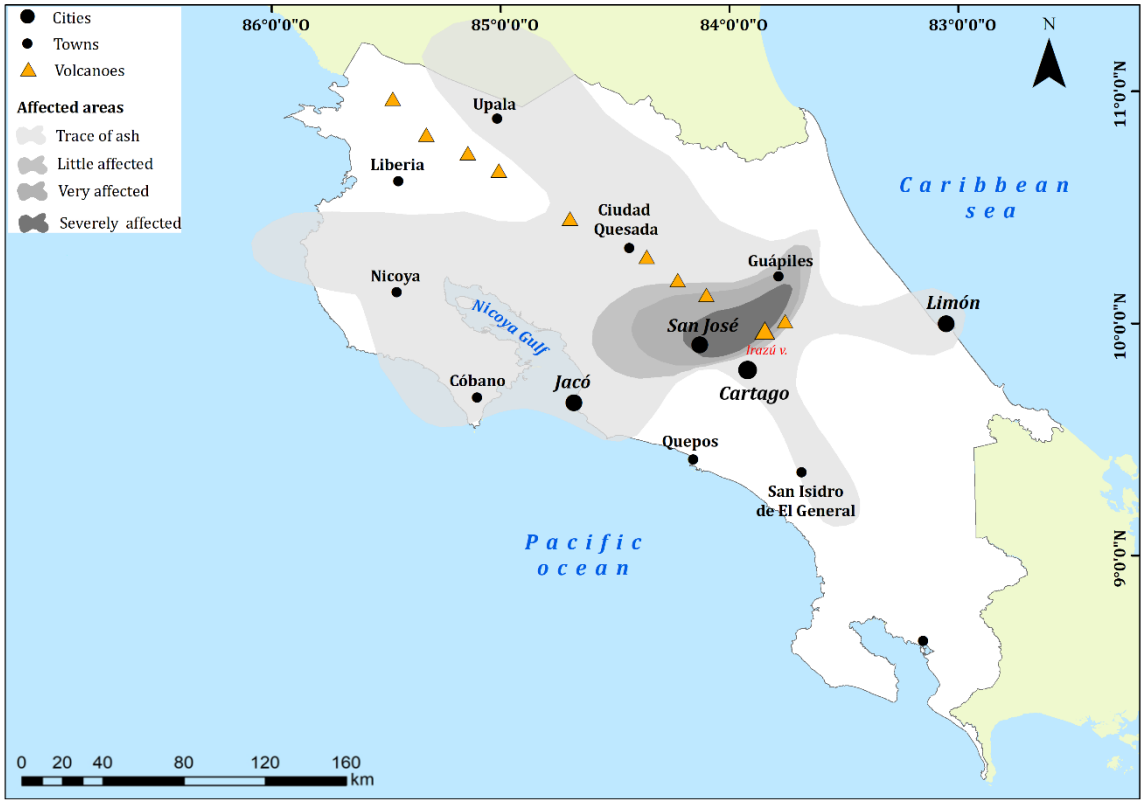

Figure 20. Distribution of volcanic ash from Irazú (1963-1965) and its grade of affectation in the main cities and towns.

3.4.2 Lahars hazard

According to historical data, the rivers through which lahars have flown are located to the south, southeast and west of the volcano, mainly the Reventado, Virilla, Tiribí, Torres, Pacayas, Toyogres, Paéz and Birrís rivers (Figure 21). Thus, in our simulations of lahars invasion, made using LaharZ (Schilling 1998), we established three categories of hazard: low (1 000 000 m^3), medium (3 000 000 m^3), and high (5 000 000 m^3). It is important to emphasize that between 1963 and 1965 the Virilla, Tiribí and Torres rivers registered lahars, where some people are said to have perished (Vargas, 1967). Regarding the South flank on the Reventado river about 40 lahars were estimated between 1963 and 1965 (ICE, 1965; Ulate and Corrales, 1966; Alvarado and Schimcke, 1994). This scenario, according to the results obtained in the previous section, could be repeated, so that the current implications would be greater, due to the urban development that has taken place in the GAM.

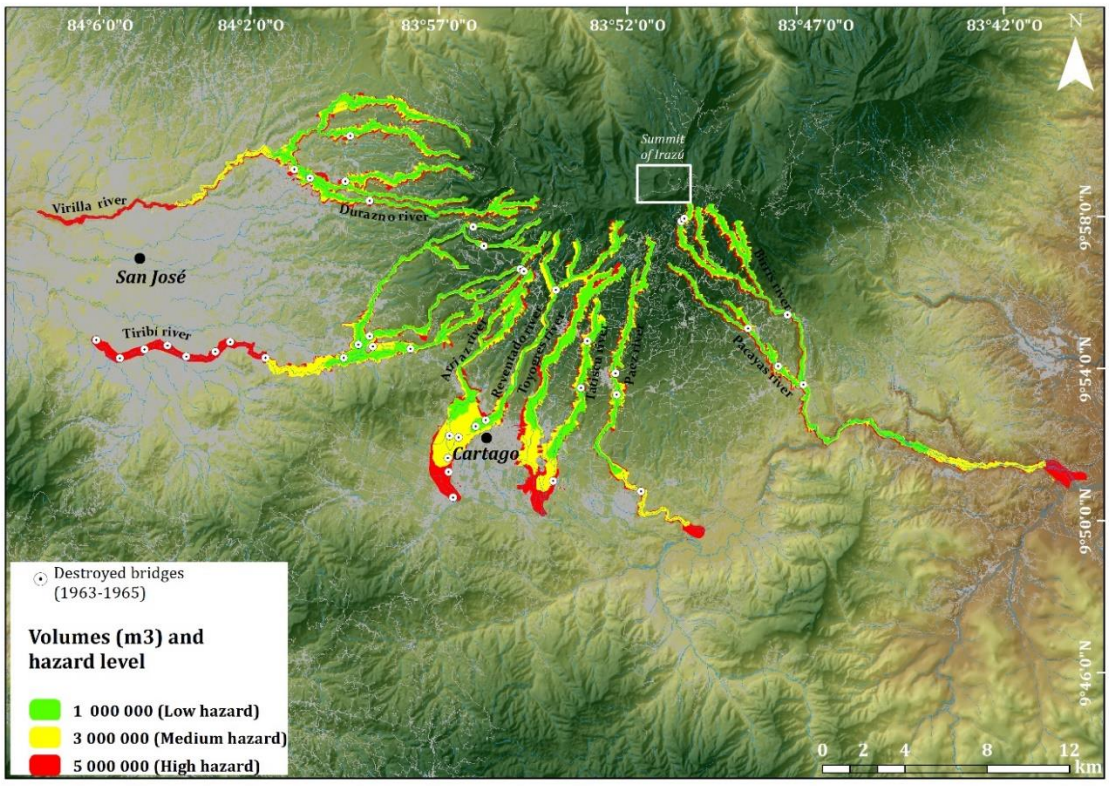

Figure 21. Rivers that could be affected by lahars associated with an eruption similar to that of 1963-1965, with estimated volumes of 1 000 000, 3 000 000 and 5 000 000 m^3. Simulations have been made using LaharZ (Schilling, 1998).

3.4.3 Ballistic hazard

Figure 22 show the ballistic hazard map, considering historical data and information collected in the field. We established three hazard categories, from highest to lowest probability (high, medium, low): a) 0 km to 2 km, b) 2 km to 4 km and c) 4 km to 6 km. The first two kilometres (high hazard) coincide with the limits of the Irazú Volcano National Park, so in case of an eventual eruption this would be a restricted area free of human settlements. However, in the medium and low hazard areas there are some exposed communities, such as Pastora, San Juan de Chicúa, and San Rafael de Irazú (Fig. 22).

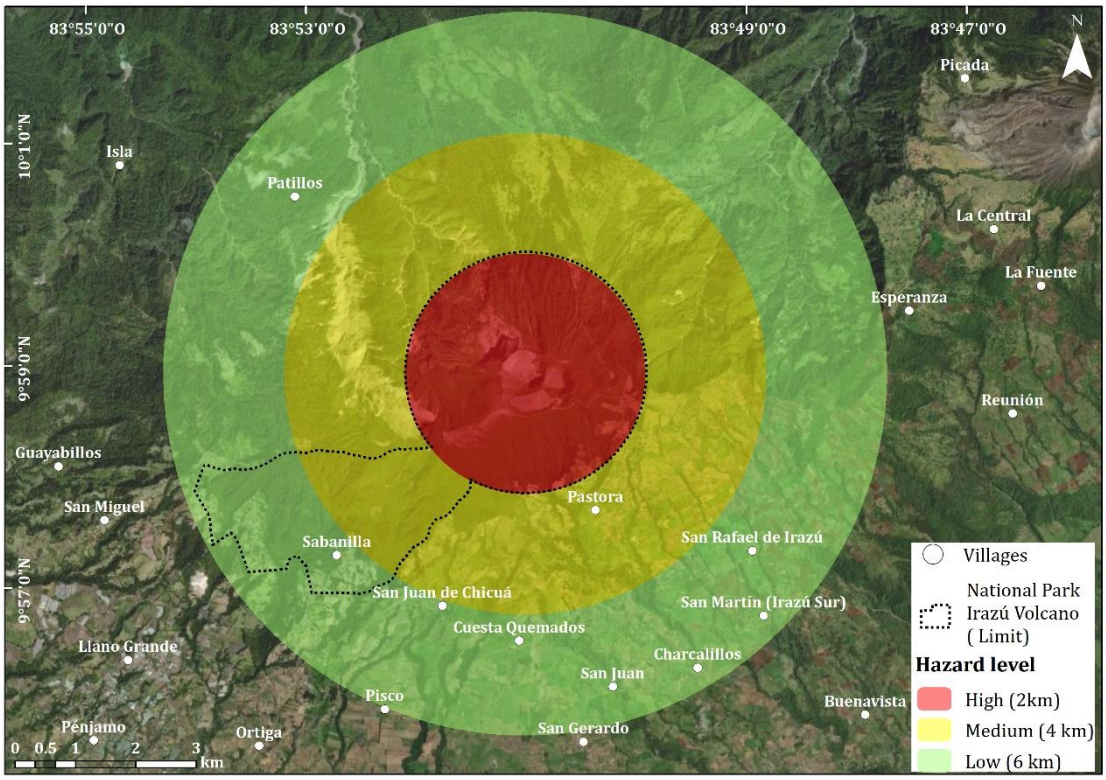

Figure 22. Ballistic Hazard Map associated with an eruption of 1963-1965.

3.4.4 Pyroclastic Density Current (PDC) hazard

Considering the historical records and the field data, we simulated the emplacement of PDCs using the tool VORIS 2.0.1 (Felpeto et al., 2007). We considered a column collapse of 10 km, which fits with the deposition of ashes with inclined lamination and lateral wedging, indicative of PDCd in sites such as Laguna,

Finca Retes, and San Gerardo (10, 5 and 3 km from the Main crater, respectively) (Figure 23).

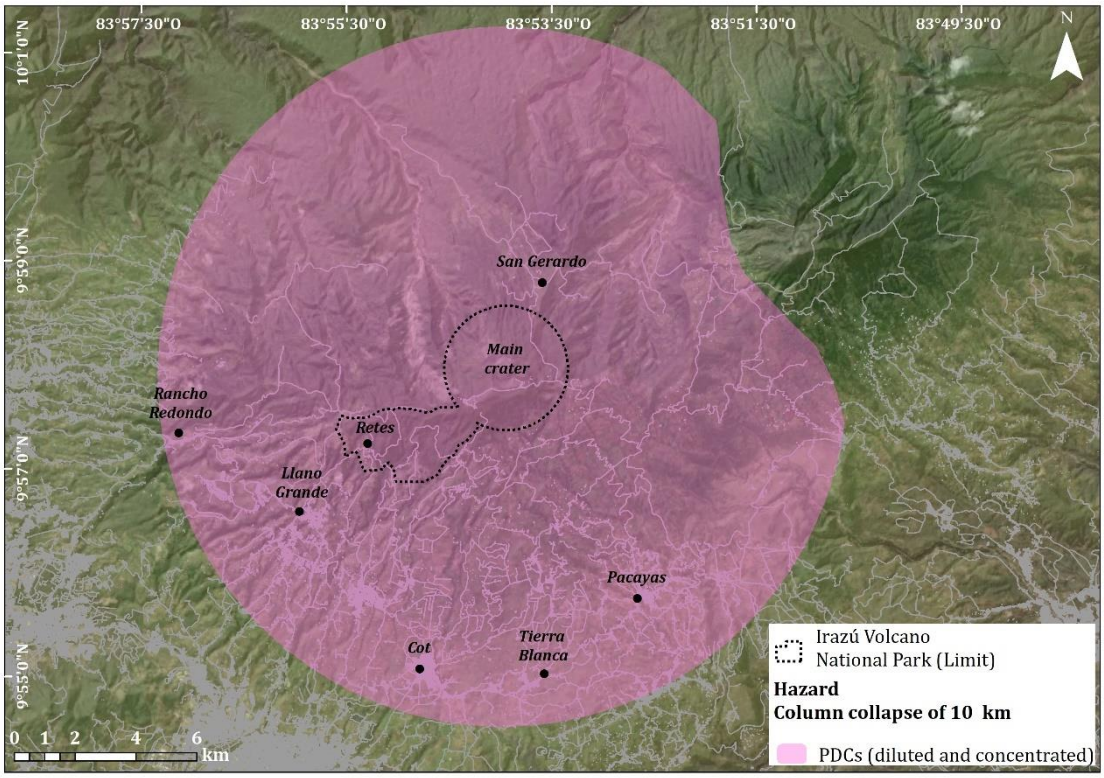

Figure 23. Simulation de PDC hazard with column collapse of 10 km, using VORIS 2.0.1 (Felpeto et al., 2007).

3.4.5 Qualitative map of volcanic hazard

By combining the modelled scenarios, we obtained one qualitative map with three levels of hazard: area 1 (high hazard), area 2 (medium hazard), and area 3 (low hazard). We established these levels based on an overlay of layers of the hazards registered (ashfall, lahars, PDC, and ballistics) in the 1963-1965 eruptive scenario. The high-hazard area corresponds to those areas that could be impacted by ashfall, lahars, PDC, and ballistics. The medium hazard area could be impacted by two hazards: lahars and PDC (S and SE flanks of the volcano) or lahars and ashfall (W and SW flanks of the volcano). The low-hazard area is only expected to be affected by ash fall (mainly towards the GAM) or lahars on the southern flank of the volcano (Figure 24). This is a qualitative ranking of hazard zones not considering the physical characteristics of each hazard, only the number of hazards that may affect simultaneously a particular area during an eruption of the characterizes of the one considered here. It is obvious that the impact of a lahar or a distal fall out may

be (or is) not the same, but in terms of the initial information to be transmitted to Civil Protection, it is crucial to identify first the areas that may be affected by any hazard derived from an eruption. Later, it will be considered the potential impact caused that may be caused by each hazard but is a subject that is beyond the objectives of this PhD Thesis.

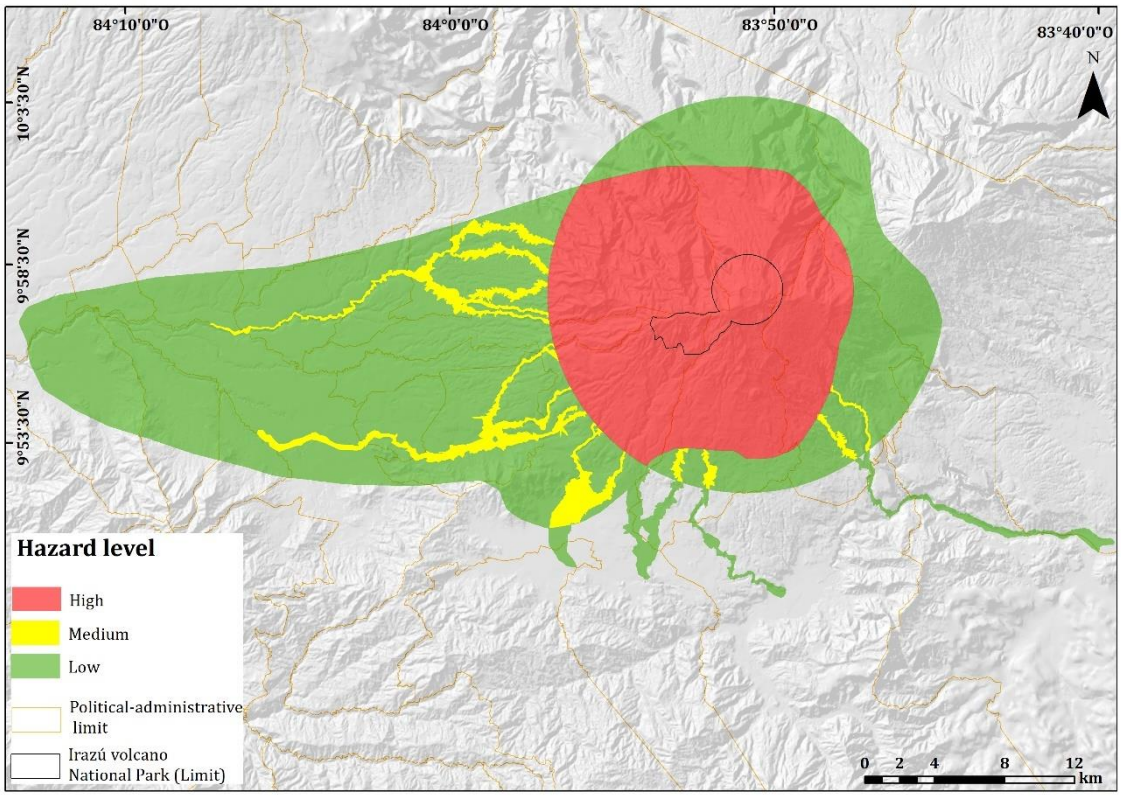

Figure 24. Qualitative hazard map integrating the most hazardous expected scenarios for ashfall, lahars, ballistic, and PDC. This map is based on the eruption of 1963-1965.

3.5 Estimation of the exposure of critical infrastructure, economic systems, and the population to volcanic hazards

3.5.1 Population exposure analysis

In the high hazard area, there are a total of 104 rural villages distributed in five cantons: Alvarado, Oreamuno, Cartago, Goicoechea and Vázquez de Coronado. In the medium hazard area are located 207 villages, exposed to ashfall and lahars, located in the cantons of Oreamuno, Cartago, Vázquez de Coronado, La Unión, Curridabat, Desamparados, San José, Moravia, Santo Domingo and Tibás, the last seven correspond to urban areas. The area of low hazard concentrated 2048 towns exposed basically to ashfall, the majority of them are located in cantons of the GAM

(W and SW flank), such as San José, Tibás, Montes de Oca, Desamparados, Moravia, Escazú or La Unión, and correspond to urban areas. On the E and SE flanks are located hamlets in the upper parts of rural cantons, such as Paraiso, Turrialba, Jimenez, and Alvarado (Figure 25). In terms of population, there are at least 2 173 775 people exposed, mostly in 16 urban cantons (Table 18), which will be mainly affected by ashfall.

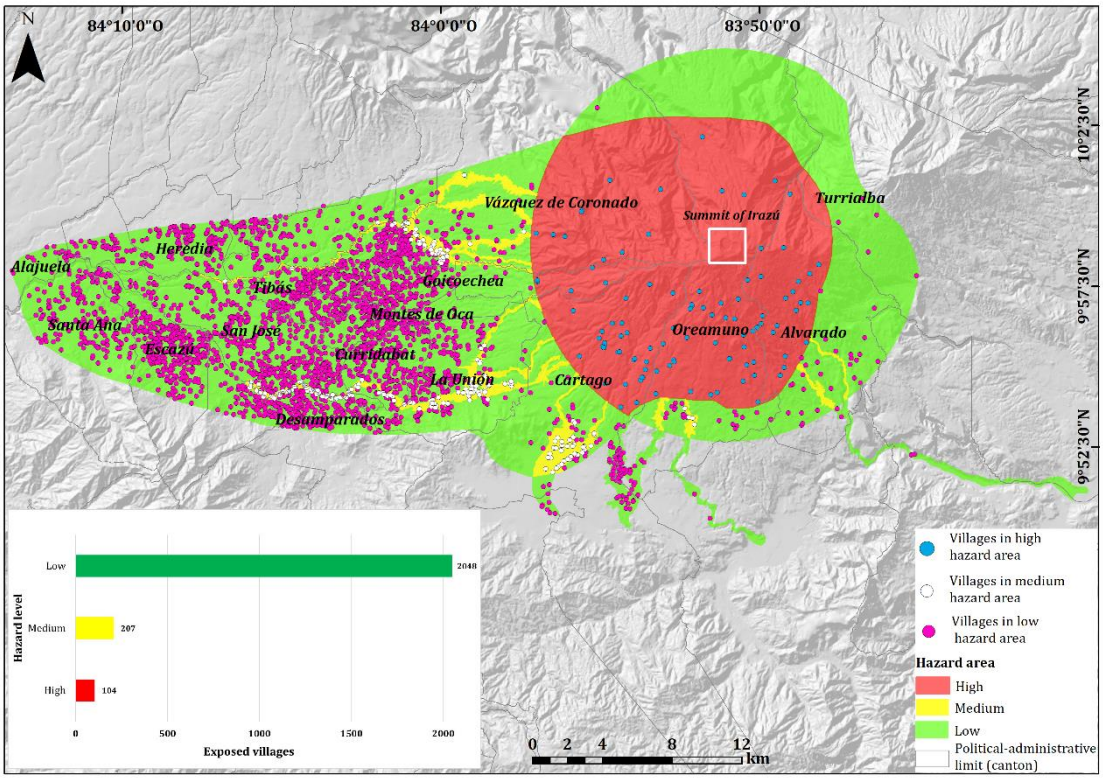

Figure 25. Villages and cantons exposed to hazard areas

Table 18. Population exposed to volcanic hazards by canton.

Canton	Area km²	Total of population (2022)	Canton	Area km²	Total of population (2022)
Alajuela*	192	322 143	La Unión*	44	99 539
Alajuelita*	21	81 012	Montes de Oca*	16	53 862
Alvarado	79	17 134	Moravia*	29	59 546
Belén*	12	23 759	Oreamuno	203	48 911
Cartago	147	165 417	San Isidro*	27	22 806
Curridabat*	16	71 026	San José*	45	352 381
Desamparados*	59	223 226	San Pablo*	8	29 860
Escazú*	35	71 500	Santa Ana*	61	58 020
Flores*	7	22 026	Santo Domingo	25	45 932
Goicoechea	32	132 104	Tibás*	8	74 592
Heredia*	25	131 901	Vázquez de Coronado	224	67 078
***Urban cantons**					

3.5.2 Land use exposure analysis

We identified 142 km^2 of pasture, 93 km^2 of crops and 74 km^2 of urban area, the distribution of them varying for each of the hazard areas. In the high hazard area, there are 2 km^2 of urban area, 42 km^2 of crops and 54 km^2 of pasture (Fig. 26), the last two represent the use land with major exposition and they are distributed in 5 cantons (Cartago, Oreamuno, Alvarado, Vázquez de Coronado and Goicoechea). According to the Ministerio de Agricultura y Ganaderia (MAG) these administrative units are part of the Eastern Central Region, which is characterized by the development of crops, such as potatoes, onions, cabbage, carrots, and cauliflower; in the case of the pastures are destined for dairy cattle, dual-purpose cattle, and cattle bovines (Flores, 2020). Crops (distributed mostly in the S, SW, and SE flanks of volcano) are located in the villages of Santa Rosa, Cipreses, Cot, Potrero Cerrado Pacayas, Capellades, Cervantes, Tierra Blanca, and Llano Grande, regarding the pastures (distributed mostly in the NW and SE flanks of volcano) are located in villlages of Cascajal, San Rafael, Rancho Redondo, Santa Rosa, and Cipreses (Fig. 26). Obviously, these economic activities are highly vulnerable to volcanic hazards, mainly ash.

The low hazard area is located mainly toward the W and SW flanks of the volcano, when the 92% of the urban area is located (it is exposed at the ashfall mainly). This area corresponds to the GAM, which corresponds to the main urban agglomerate of the country and includes the conurbations of the four largest cities (San José, Alajuela, Cartago and Heredia) (Fig. 26); it covers 3.84% of the national territory and is home to 94% of the country's urban population, and is also the area where 76% of exports are produced and 70% of the gross domestic product (GDP) is generated (Martínez Baldares, 2013; Segovia-Fuentes, 2019).

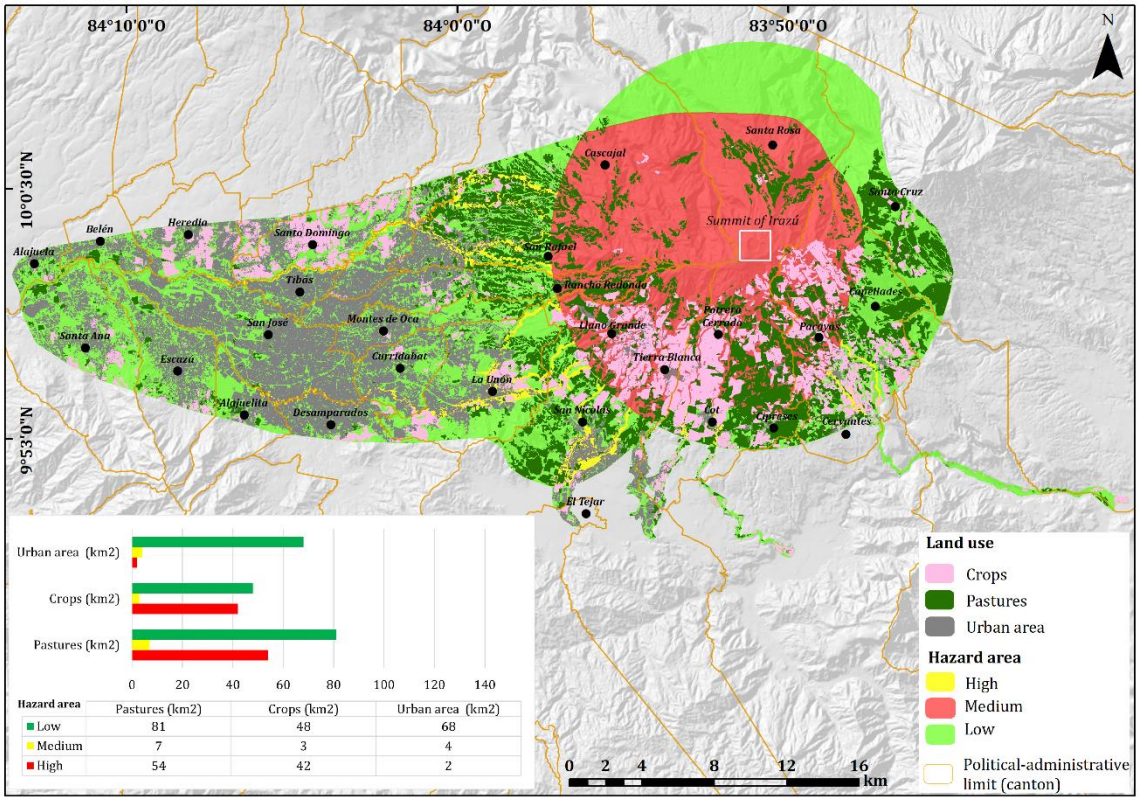

Figure 26. Exposure and distribution of the land use in the volcanic hazard areas

3.5.3 Critical infrastructure exposure analysis

The number of schools and high schools exposed in the hazard areas are 326 in total. In the high hazard area, there are 2 high schools (Liceo de Tierra Blanca in Cartago and the Liceo Rural Santa Rosa in Oreamuno) and 19 schools (7 in Oreamuno, 6 in Alvarado, 4 en Cartago, and 1 in Vázquez de Coronado and Goicoechea, respectively). The medium hazard area concentrates only 5.5% of the educational centers, with a total of 14 schools and 4 high schools distributed in 5 cantons (Curridabat, La Unión, Vázquez de Coronado, Cartago and Oreamuno) and they are located in areas that could be impacted for ashfall and lahars, mainly in the proximal area of the Tiribí, Virilla, Durazno, Taras, Reventado and Paéz rivers. Finally in the low hazard area we identified the 88% of the educative centers (97 high schools and 190 schools), distributed mainly in urban cantons, such as San José (63), Desamparados (24), Goicoechea (20), La Unión (19), Montes de Oca (14) and Cartago (12) (Fig. 27).

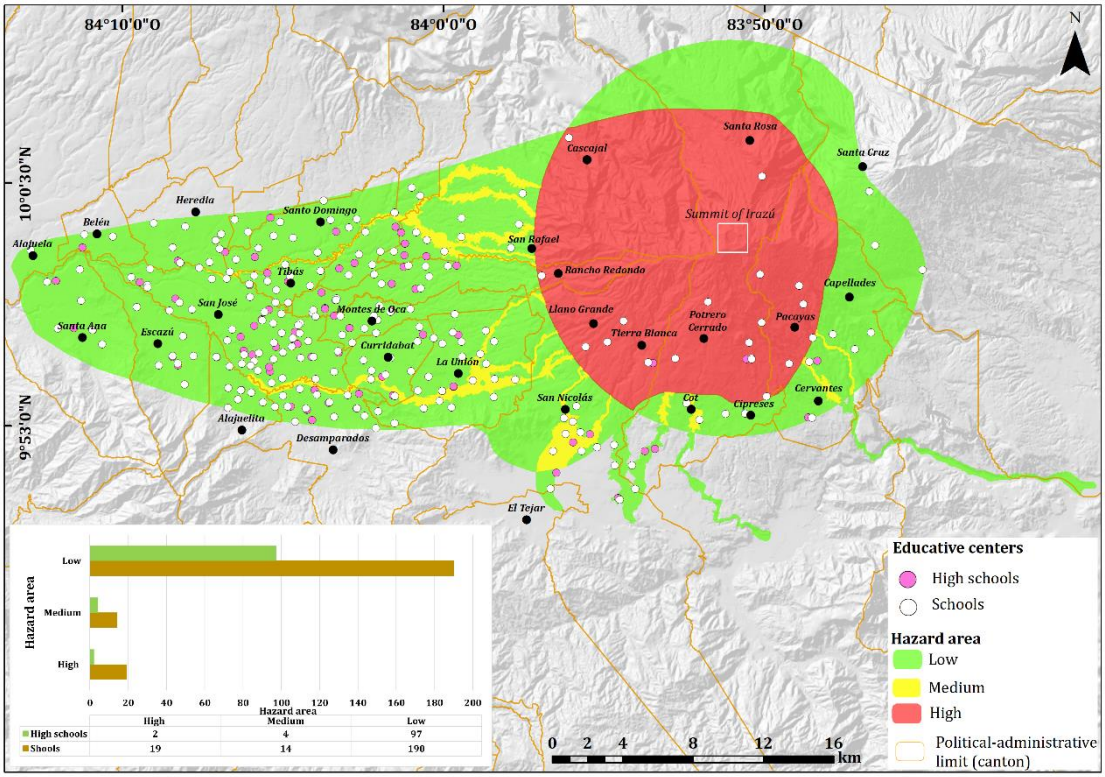

Figure 27. Exposure and distribution of the educative centers in the volcanic hazard areas

Figure 28 shows the distribution and category of the 237 health centers distributed in the hazard areas. The high hazard area concentrates three EBAIS located in Llano Grande, Tierra Blanca, and Santa Rosa. In the medium hazard area are located 11 EBAIS distributed in Moravia, La Unión, Curridabat and Cartago cantons.

The low hazard area concentrated the 93.6% of these health centers, which are exposed mainly to ashfall; we accounted 222 EBAIS, 9 hospitals of which 3 are National General Hospitals (México, Rafael Ángel Calderón Guardia and San Juan de Dios) and 6 are National Specialized Hospitals (Humberto Araya Rojas National Rehabilitation Center, Raúl Blanco Cervantes Geriatrics and Gerontology Hospital, Manuel Antonio Chapuí Psychiatric Hospital and Roberto Chacón Paut Psychiatric Hospital; finally there are 6 specialized centers (National Blood Bank, National Centre for Pain Management and Palliative Care, National Centre for Medical Imaging, Ophthalmology Clinic, Laboratory of Molecular Human Genetics, and National Cytology Laboratory) (Figure 28).

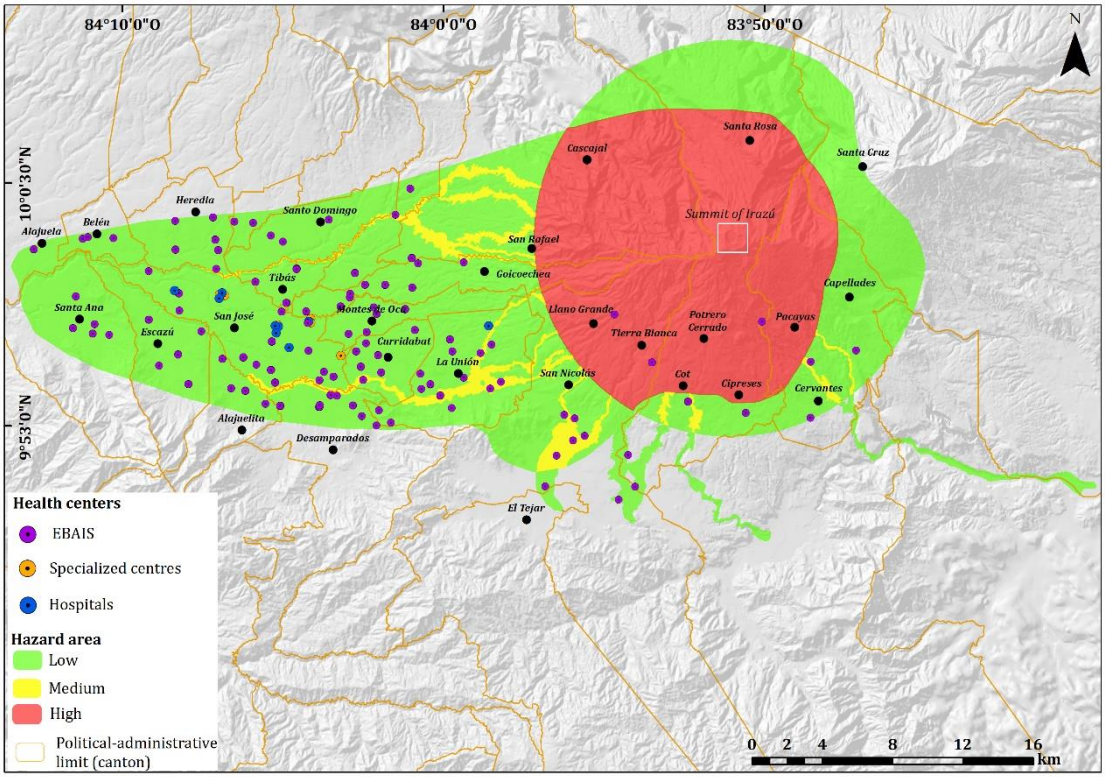

Figure 28. Exposure and distribution of the health centers in the volcanic hazard areas

In terms of roads, we counted 8875 kilometres of roads (between primary, secondary, and tertiary categories). In the high hazard area, tertiary roads are prominent (883 km), due to the fact that in this sector are located the majorly of crops and pastures; followed by 369 km of primary roads that connected the main towns, such as Tierra Blanca, Pacayas, Potrero Cerrado, Rancho Redondo and Llano Grande with other urban areas of higher hierarchy, for example Cartago and San José cities. The medium hazard area registers 396 km of primary roads, highlighting the roads in the urban areas of La Unión and San Nicolás. The low hazard area has the highest number of primary roads (5357 km) as it corresponds to the urban area, where cities such as San José, Escazú, Montes de Oca or Curridabat are located (Figure 29).

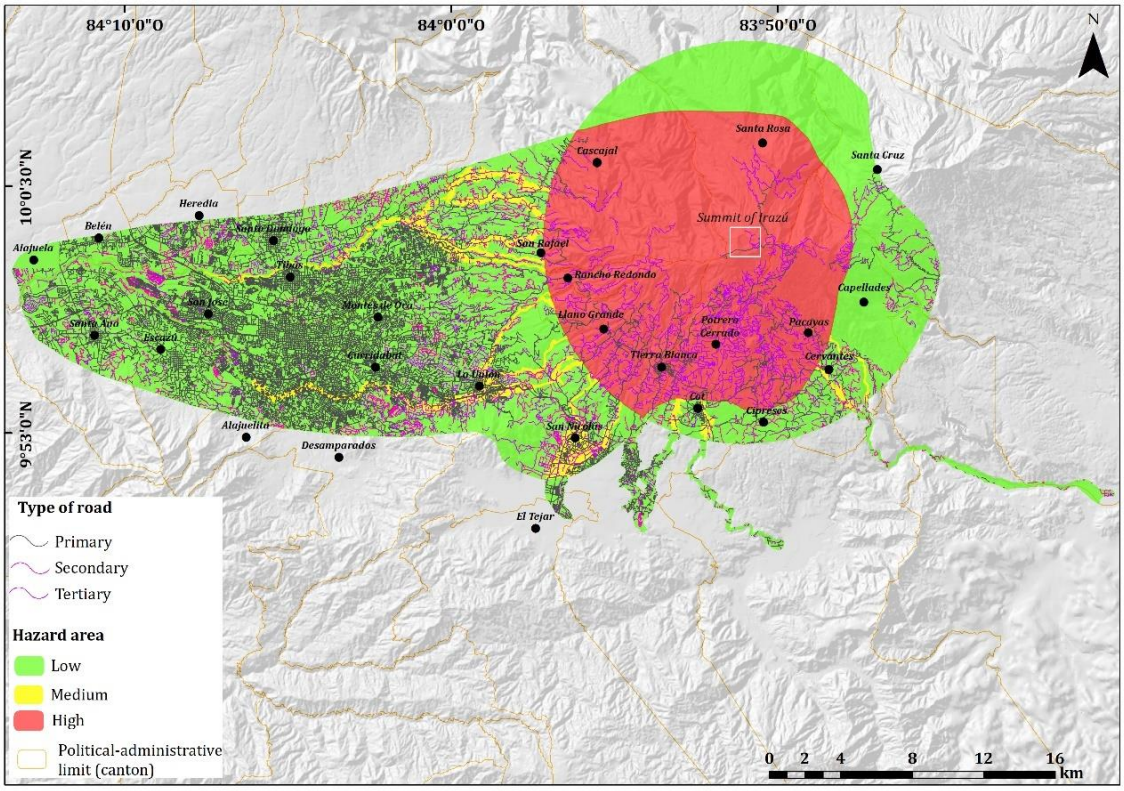

Figure 29. Exposure and distribution of the roads in the volcanic hazard areas

3.5.4 Informal settlements exposure analysis

We identified 151 informal settlements (NW and SW flanks of volcano) in the medium and low hazard areas, distributed in 17 urban cantons. In the case of the low hazard area 116 informal settlements are exposed to ashfall, mainly en San José (31), La Unión (14), Tibás (13), Curridabat and Alajuelita (8) (Table 19). Medium hazard area registered 35 informal settlements exposed to lahars (partially or totally), mainly in the Virilla, Tiribí, Reventado, Taras and Arriaz rivers, located in Cartago, La Unión, Curridabat, Tibás, and Vázquez de Coronado cantons (Figure 30, Table 19), we emphasize settlements located in lahar hazard areas, present higher exposure conditions due to their location.

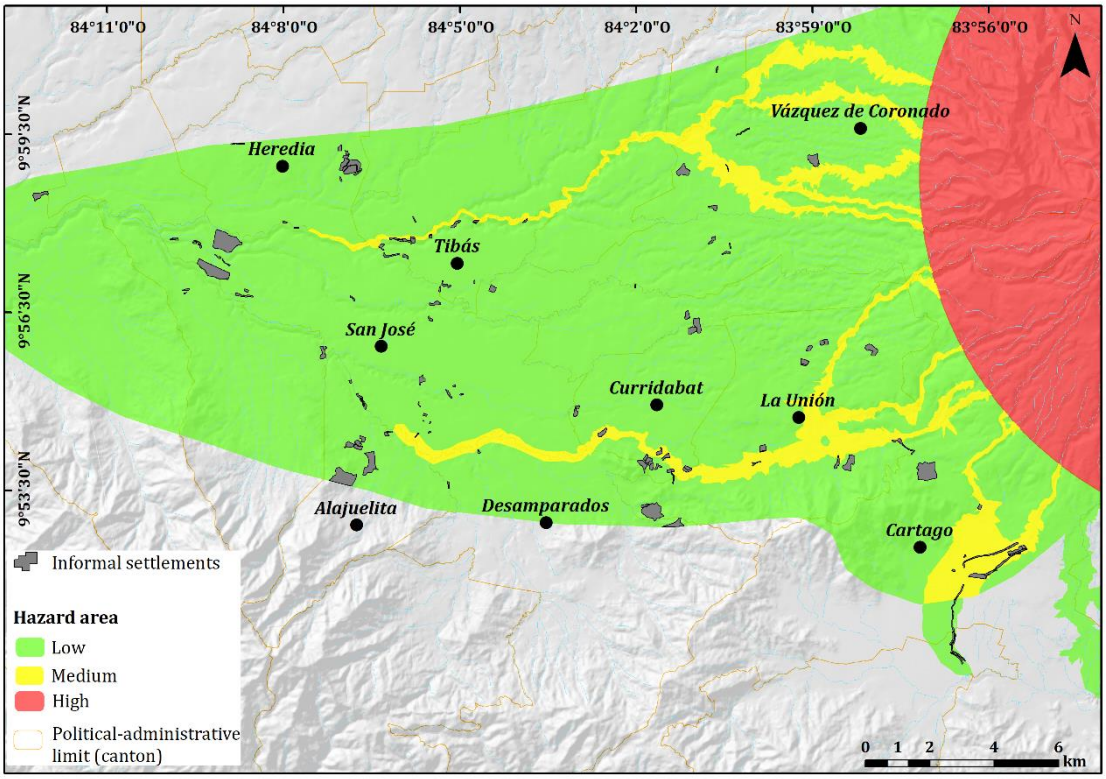

Figure 30. Exposure and distribution of informal settlements in the volcanic hazard areas

Table 19. Informal settlements exposed to lahars and ashfall

Hazard	Canton	Informal settlements
Ashfall	Alajuela	Urbanización El Futuro
	Alajuelita	Juan Pablo II, La Deportiva, El Jazmín, Proyecto La Paz, El Muro, Asociación Pro-Vivienda Los Pinos, Bajo Las Gavetas, La Aurora Precario III, La Plaza, Los Chorros, Vendedores Ambulantes.
	Cartago	Alto Ochomogo, Cristo Rey, La Cruz Diques Sur, Guadalupe Diques Sur, La Mora Diques Sur, La Mora Diques Sur, Los Ángeles Diques Sur, Nazareth Diques Sur.
	Curridabat	Las Luisas, U Europa Junta Progresista Barrio Lujan, Barrio Corazón De Jesús, El Mirador, Gloria Calderón, Kira De Castillo, Llanos De Gloria, Miravalles, Ponderosa I, Ponderosa II, Ponderosa III.
	Desamparados	Pueblo Nuevo La Paz, Proyecto Los Ángeles.
	El Guarco	Santa Gertrudis Diques Sur
	Escazú	Barrio La Pista Norte Guachipelín, Barrio La Pista Sur Guachipelín, La Quebrada Calle Los Mangos.
	Goicoechea	Las 85 -Sector 1, Las Amelias, Luchando Por Un Futuro
	Heredia	La Cuenca Este, La Cuenca Los Negritos Sur, La Cuenca Oeste, La Milpa Segunda Etapa, La Milpa Tercera Etapa, La Victoria La Radial, Palacios Universitarios, Villa Paola, La Unión.
	La Unión	Concepción, Las Luisas, Buena Vista, La Cima 2, San Vicente, La Arboleda, Calle Garita, Linda Vista, Asentamiento Las Brisas, Calle Garita, Quebrada El Fierro, Asentamiento San Martin, Clima 1 San Valentín, Pueblo Nuevo.
	Montes de Oca	Calle La Mora, Barrio Sinaí
	Moravia	Calle Torre Molina
	Oreamuno	El Crematorio Calle Molina
	San José	Barrio Los Alamos, Premio Nobel De La Paz, Gracias A Dios, Hogar Propio, Monseñor Arrieta, La Frontera, La Nueva Juventud De Pavas, Loma Linda, Calderón Fournier, Lomas Barracones De Luna Park, Florida Sur, La Esperanza, Las Brisas De Rossiter Carballo, Bella Vista, Finca San Juan, Metrópoli 2 Anexo Zonas Verdes, Nueva Esperanza, Condominio Cipreses, Once De Abril El Pochote, Metrópoli 1 Precario Tarzán, El Play, Barrio Nuevo, Bajo Los Ledezma Barrio El Jardín, La Ladrillera, Asprovicruz, Ranchos Ina, La Carpio, Asentamiento Corporación Maya, Santa Lucia, La Línea Del Tren, Bajos De Hatillo 5 Las Gavetas.
	Santo Domingo	Santa Rosa
	Tibás	Barrio San Judas Tadeo, Manolo Rodríguez II, La Esperanza, El Progreso, Precario Norte A Y B, Triangulo De Solidaridad II, Los Manolos Bajo Cuesta Colima, Nuevos Horizontes, El Plantel, Precario La Unión, Garabito, Hacia El Siglo XXI, Bajos Manolo Rodríguez.
	Vázquez de Coronado	Urbanización Los Cipreses, Las Lomas, San Martin II Rosarito Fournier, Finca Omega El Rodeo.
Lahars	Cartago	Barrio Nuevo Diques Norte, María Auxiliadora Diques Norte, Sagrado Corazón De Jesús Diques Norte, Santa Eduviges Diques Norte, Santa Elena Diques Norte, Linda Vista Diques Norte, Santa Teresita Diques Norte, Alto Ochomogo, Barrio Fátima Diques Norte, Barrio La Unión, La Cruz Diques Sur, La Lima, Las Azucenas Las Rosas, Miguel Trejos Diques Norte, Miraflores El Higuerón Diques Norte, Guadalupe Diques Sur, Nazareth Diques Sur.
	Curridabat	15 De Agosto, El Mirador, Kira De Castillo, Miravalles, Ponderosa III, Santa Cecilia
	La Unión	La Arboleda, San Diego, Quebrada El Fierro, Asentamiento San Martin.
	San José	Monseñor Arrieta
	Tibás	Barrio San Judas Tadeo, La Esperanza, El Progreso, Precario Norte A y B, Hacia El Siglo XXI.
	Vázquez de Coronado	Las Lomas, El Carmen

CHAPTER 4: DISCUSSION

4.1 Stratigraphy, vents location, and distribution of deposits

The Irazú volcano is one of the most active volcanoes in Costa Rica, its last eruptive period between 1963 and 1965 (VEI = 3) was characterized by Vulcanian, Strombolian, and phreatomagmatic eruptions. Around Irazú, important crops and livestock activities are developed, and toward the SW flank is located the GAM, where approximately 50% of the country's population lives. Considering the previous, we carried out a detailed tephro-chronostratigraphy to subsequently construct a spatial and temporal analysis for hazard assessment, which was the basis for constructing hazard scenarios to estimate the social, economic, and critical infrastructure exposure to volcanic hazards.

The eruptive record of the Irazú volcano has been poorly studied, only 19 tephrostratigraphic units from the last 2.6 ka, located at intermediate distances (up to 6 km) from the summit of the Irazú volcano were proposed by Clark (1993). For this reason, we conducted a detailed reconstruction of the tephro-chronostratigraphy of the Irazú volcano for the Upper Holocene. In addition, we also correlated these volcanic deposits with their possible vents, thus considering this region for future eruptive sites.

Tephra deposits corresponding to the units P to A4 (Table 9) appear in sections that are located about 6 km SW and 3 km NE of summit (see Fig. 8). The recognizable volcanic morphologies (pyroclastic cones and craters), the existence of proximal coarse tephra deposits (deposits of bombs, agglutinates, and agglomerates), and their areal distribution and thickness variations in the columns and outcrops (see Fig. 8 and 14a, b, and c), provide information on the most probable location of the source vents of the different eruptions, in addition to the preferential emplacement directions followed by the corresponding deposits. Thus, the position of cones and craters, the distribution of the deposits, and their ages, allow to infer the existence of a E-W fissure at the summit of Irazú on which different eruptive foci that have been active over the last 2.6 ka (Figure. 31). This fissure was already

suggested by Hudnut (1983) who indicated that craters at the summit of Irazú were aligned from east to west striking N80°W. Moreover, Alvarado (1989, 1993) suggested that this alignment of cones and craters corresponded to a migration of the eruptive focus in an E-W direction, lying the oldest cone to the east, near Finca Liebres (Fig. 31) and becoming successively younger towards the west.

According with the ages of these proximal deposits, it is interesting to observe that the eruptive activity in this fissure have not presented a specific pattern in the last 2600 years (Fig. 15 and Table 4). The eruptive foci (called Sapper) of the oldest eruptions, from 1000 A.D., i.e., units P to D4, would have been located near the present position of the Sapper hill (W of the fissure), as suggested by the areal extent toward the SW flank and thickness variations of the deposits, which widen and get thinner, respectively, from that point. Alvarado et al. (2006) proposed that the Tristán Unit (Unit J in Fig. 14c, sections 21-05, 91-40) may indicate that the source was located adjacent to the Sapper hill at the summit of Irazú (Fig. 31). Unit C1 allows to estimate another possible eruptive focus due to the fact that, near the summit, this deposit presents a thickness greater than 1.8 m and is composed of coarse lapilli scoria and bombs (sections 21-02 and 21-10) (Fig. 13e). Consequently, we can estimate that the vent of this tephra layer was located near the summit. The paleosol dated on this deposit (510±30 yr B.P.) permits us to place this event at ~1300 A.D. (Table 9).

Unit B2 is located above a paleosol in La Laguna cone at E of the fissure (Fig. 12c) dated at 330±30 yr B.P. (1549–1598 A.D.). This event could be the origin of the lahars mentioned in the legend of Irazú associated with a possible eruption of ~1561 A.D. (Alvarado, 2000). Clark et al. (2006) dated a paleosol to 315±20 yr B.P. (1521–1577 A.D.) and related it to the event recorded in 1561; however, both ages and the stratigraphic record (section 21-01) indicate that these are two different events (B1 and B2 Units) separated by thin paleosols, but which occurred very close in time (B1: ~1540 A.D., and B2: ~1561 A.D.) (Fig. 12c). In addition, near the summit of Irazú, there are a stratified level of ash fallout and lapilli scoriaceous (55–100 cm thick) underlain by phreatic and phreatomagmatic layers, perhaps contemporaneous with the La Laguna cone. It is possible that several contemporaneous active vents (Strombolian fissures) coexisted. In such a case, the

La Laguna cone was formed around 1540 A.D., while the overlying tephra level was from 1561. A prehistoric scoria cone and two tuff rings are located further to the east. Another composite crater is represented by prominent cliffs immediately to the south of the Main and Diego de La Haya vents (Fig. 31) (Alvarado et al., 2006).

Alvarado et al. (2006) identified a phreatic/phreatomagmatic breccia (Alfaro unit) with a thickness of ~4 m at the SE of Main Crater with a stratigraphic position pre-1723. If this correlation is accurate, we can propose that these units correspond to the same event, which could have been the one that gave rise to Main crater around XVI or XVII centuries., i.e., before the eruption of 1723, the first historical eruption registered at Irazú. Therefore, this crater is recent, and its formation corresponds to one of the most important phreatomagmatic events at Irazú over the last 2 ka.

In historical times, Elizondo et al. (2019) point out that the first documentary record indicates that between 1899 and 1916, at least 12 small vents (intracrater foci) were present in the sector where the current Main Crater is now located, which merged in subsequent eruptive periods (e.g., 1917-1921, 1924,1928, 1930, 1939-1940 and 1963–1965) to form the current Main Crater. All this evidence allows us to conclude that the E-W fissure has been active and presents an important geomorphologic evolution for both prehistoric and historic times (Fig. 31).

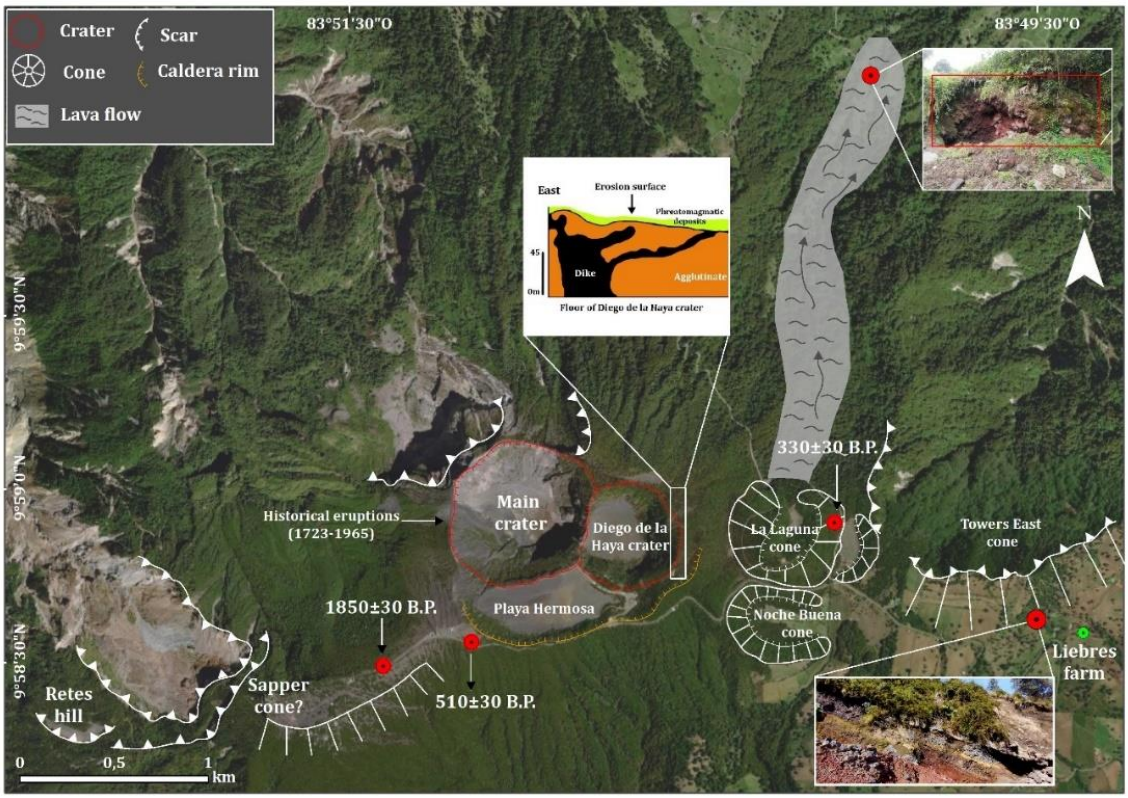

Figure 31. Detail of the E-W fissure, showing the geoforms (craters and pyroclastic cones) and their associated ages. To the north of the pyroclastic cone La Laguna is probably the most recent lava flow identified in this investigation and at the east end is the avalanche scar of the pyroclastic cone East Towers (so called in this investigation).

The tephrostratigraphy and tephrochronology of Irazú volcano presented in this study reveal that it has not shown a uniform eruption frequency during its most recent period (2.6 ka), however, we were able to establish an average of at least one important eruption every 85 years (at least VEI ≥1) (Fig. 15), it indicates the eruptive potential of this volcano.

4.2 Long-term hazard assessment

Considering the eruptive history and the socio-economic development around Irazú, we conducted a long-term hazard assessment. Our results from the spatial analysis show that areas with greatest susceptibility are located at the summit (mainly in the Main crater, Fig. 16), where the pre-historical and historical eruptions have been vented. It is important to indicate that this area coincides with the Irazú Volcano National Park. However, the southern flank of the volcano presents a considerable probability too, due to the presence of scoria cones that

were active during the Holocene (Table 10). Moreover, it is important to point out the presence of two lava flows: a) on the western side, of basaltic to andesitic-basaltic composition, and b) on the eastern side, of andesitic-basaltic composition (Thomas, 1983; Tournon, 1984; Alvarado, 1993). 40Ar/39Ar dating indicates an age of 20 000 ± 12 000 years for the eastern lava flow and 57000± 13 000 years for the western basaltic lava flow (Alvarado et al., 2006). Despite, these ages are much older than the periods considered in our analysis, future eruptive activity in these sectors cannot be ruled out.

The results from the temporal analysis, based on geological and historical data, let us to determine that the Irazú has mostly registered events that have culminated in a magmatic eruption, which suggests the entry of fresh magma into the system. Therefore, a magmatic unrest with a magmatic eruption of VEI between 1 and 3 could occur in the future, with ashfall, ballistics, PDCd as well as lahars, particularly if we only take into account historical data. For the same period (1723 A.D. - 1991 A.D.) there have been episodes of unrest that did not culminate in an eruption, but which were characterized by the presence of fumaroles (i.e., 19th century activity), suggesting a reactivation (pressurization) of the hydrothermal system, with or without presence of fresh magma into the system, so we cannot rule out this type of activity in the future.

4.3 Impact and vulnerability implications

In this sense, the temporal analysis indicates that an eruptive scenario such as that of 1963-1965 has a considerable probability of occurrence (see Tables 14 and 17), although this eruption was of relative low magnitude (VEI=3) had a significant impact on the population and the economy (dairy farming and crops, mainly vegetables and coffee), on civil works (collapse of roofs, damage to the railway line to the Caribbean, collapse of bridges, water collection systems), in addition, two people were killed by ballistics and up to 20 by lahars in the Taras sector, Cartago (Murata et al., 1966; Waldron, 1967). Considering the impact of the eruptive activity of 1963-1965, in this research we have simulated and reconstructed all hazards registered in this eruption (ashfall, lahars, PDC and ballistics). These results allowed us to identify how many population, villages,

crops, pastures, urban areas, critical infrastructure (roads, educative and health centers) and informal settlements are currently exposed and could be affected by new eruptive activity at Irazú volcano.

Some of the main highlights of this research are that there are an estimated 2 173 775 inhabitants exposed to volcanic hazards, with the majority concentrated in the GAM, which represents the 92% of the urban area located in the low hazard area and could be affected by ashfall. This population boom that GAM has experienced is related to the industrial development (industrial jobs) that has taken place in this region, as Costa Rica's economic policies have favored the development of industrial parks in San José, Heredia, Alajuela, and Cartago, which can be noted in the levels of concentration and centralization of these activities in the GAM. This industrial development has generated that the GAM concentrates most of the housing construction in the country, for example, between 2013 and 2016 Alajuela and Cartago were the cantons (at national level) with the highest number of houses built (Ramírez and Sánchez, 2012; Informe Estado de la Nación, 2018).

Concerning crops and pastures, most of them are located in the high hazard area (98% of the surface area) (Fig. 26), in rural villages in the Central Eastern Region, where 80% of Costa Rica's vegetable production is grown; 90% of the potatoes consumed in the country are produced, while onions represent 80% of the economic income of farmers; for example, the communities of Llano Grande and Tierra Blanca are eminently agricultural, since 80% of the land is dedicated to agriculture and the remaining 20% to livestock (Ramírez et al, 2008; MAG, 2018). Therefore, there is a significant exposure of these economic systems to volcanic hazards; for this reason, the expansion of the agricultural frontier should be regulated and contingency plans for emergency management should be promoted by the State, as well as financial protection mechanisms in the agricultural sector. This situation could be compared to the effects of the eruption of the Turrialba volcano between 2010 and 2017, where ash affected crops and pastures; between May and October 2016, a weekly loss of ₡21 000 000 in milk was estimated; moreover, between 2010 and 2016, agricultural producers were benefited with subsidies, it represented a cost for the State of approximately ₡ 79 008 915 (Campos-Durán and Barrantes-Castillo, 2020).

Despite the vulnerability of the agricultural sector, no detailed risk studies have been conducted in Costa Rica to estimate the possible economic losses that an eruption (such as the one in 1963-1965) could generate in this sector. In this same sense, there are not studies about the degree of tolerance of crops and grasses to possible ash thicknesses. Therefore, detailed studies are needed for making such types of estimations. However, the results from this research constitutes the basis for further, more detailed studies and it should be considered by the agricultural authorities in order to generate public policies that promote financial protection mechanisms such as crop insurance against volcanic eruptions.

The analysis of the road network shows a total of 8875 kilometers of roads exposed to volcanic hazards. These elements are vital for commercial development, since they are communication routes that facilitate the transport of products. If we look at the case of the GAM, industrial development depends on the state of the roads to transport their products for export. For example, in the first half of 2023, exports from the medical sector reached $3,656 million, positioning itself as the main export sector of Costa Rica (PROCOMER, 2023). If an eruption similar to that of 1963-1965 would occur, it is important for private industry to have insurance and business continuity plans. In the case of agricultural areas, roads are vital for the transport of products such as vegetables and dairy products that are consumed in the national market. In addition, roads that could serve as evacuation routes should be considered within the emergency plans.

Regarding of the exposure of health centers, the National General Hospitals and National Specialized Hospitals are located in San José, i.e., patient care is centralized, so that an eruptive event similar to that of 1963-1965 would affect patient care, making it necessary for health centers to have operational plans and procedures to guide their response to emergencies. Furthermore, if we consider the exposed population, the ashfall would generate health problems in the population. Despite these data, research conducted in Costa Rica on the effects of ash on human health is scarce. The first scientific studies were carried out during the Irazú eruption between 1963 and 1965, where it was determined that the main epidemiological effects on the population were acute conjunctivitis, laryngitis, bronchitis, and asthma (Horton and McCaldin, 1964; Solano, 1964).

A relevant result of this research is the number of informal settlements located in lahar hazard areas; although in 1963-1965, the main affected areas were in the sector of Taras, Cartago, there are currently approximately 151 settlements of this type exposed to this hazard. The only existing studies on lahar risk perception and modeling of lahar flows have focused on Los Diques, Cartago (Alvarado and Boschini, 1988; Campos, 1988; Alvarado and Schmincke, 1994; Salgado, 2002; Solano, 2003; Barrantes et al. 2008; Amador et al., 2018; Granados-Bolaños et al., 2021), so it is necessary to conduct research in these other exposed settlements (Table 19).

4.4 Risk management implications

Despite the fact that Costa Rica has a rigorous regulatory framework for risk management (Law 8488 -National Law on Emergencies and Risk Prevention-, the National Risk Management Policy 2016-2030 and the National Risk Management Plan 2021-2025.), being the Comisión Nacional de Prevención de Riesgos y Atención de Emergencias (CNE) the authority in charge, and two institutes dedicated to volcanic monitoring (OVSICORI-UNA and the National Seismological Network - UCR), detailed studies are needed to update the eruptive recurrence of those volcanoes that represent the greatest hazard to the population and the economy. In this sense, in this research, we present an update and reconstruction of the tephrostratigraphy of Irazú and its eruptive recurrence in the last 2.6 ka, which has allowed us to carry out a long-term temporal and spatial analysis of the eruptive scenarios that could be expected in Irazú. Based on these data we determined that an eruption similar to that of 1963-1965 (VEI=3) has a considerable probability of occurrence, so we have simulated/reconstructed this eruptive scenario, which was the basis for carrying out the exposure analysis of the population, land use and critical infrastructure.

Based on the previous, this research provides valuable contributions in two ways: a) input for territorial planning processes, b) to update emergency plans at the local level. In the case of land-use planning, our results (mainly hazard maps) should be considered within the territorial planning process, as volcanic hazards must be incorporated into land-use planning processes (Decreto Nº 32967-MINAE,

2006). Regarding the Emergency Plans, the data we have presented in this research should be considered to update the "Volcanic Emergency Plan: Irazú-Cartago Volcano", which dates to 1991 (CNE, 1991) and strengthen aspects such as evacuation routes, drills in vulnerable populations and in educational and health centers.

CHAPTER 5: CONCLUSIONS

New radiocarbon ages and an updated stratigraphy of Irazú's summit and its SW and NE flanks have allowed us to define at least 30 major tephrostratigraphic units for the last 2.6 ka and to update the eruptive recurrence for this period. According to its geomorphological, stratigraphical, and radiometric ages, we suggest that the La Laguna cone and Main Crater formed in recent times (between ~1500 and ~1600 A.D.) and that Sapper hill was the source area of eruptions older than ~200 A.D. Therefore, volcanism has moved along a fissure zone with a E-W direction in the uppermost part of the volcano, which has been active during the Upper Holocene. Before this research, there was some debate about possible eruptions in the 19th century, however, none of the radiocarbon ages had dated any eruptive event close to this period, and the review of historical documents and field records does not support the occurrence of any eruption between 1724 and 1917. These results are supported by historical data indicating a quiescent period between 1723-1724 and 1917 (193 years). Therefore, our results confirm the rigor of our data and their interpretations. The data presented shows that Irazú volcano has significant eruptions between every 23 and 100 years.

The volcano is currently in a state of potential activation, but activity could increase progressively tending to a new eruptive stage in the next few years or tens of years. In this sense, our results allowed us to estimate from the spatial analysis, based on volcano structural elements, that an eventual eruption of Irazú could occur mainly at the summit (in the Main Crater) and in less probability in the South Flank, where we identified some fissures and pyroclastic cones that registered activity during the Upper Holocene. This is particularly relevant for the areas surrounding the volcano, where there are high-vulnerable population centers which may be severely affected by volcanic hazards (e.g., ashfall, lahars).

Concerning the methodology used in the temporal probability analysis, it is important to remark that the probabilities obtained using only historical data present less uncertainty since that data used are more reliable, as they are based on direct observations and also monitoring for the last years (e.g., 1984 A.D. and 1991

A.D.). This results in a shorter observational period but with more precise data. However, this has the inconvenient that some scenarios with larger frequencies of occurrence may be not considered, so biasing the resulting analysis. On the other side, considering a longer period that includes geological data may incorporate these scenarios not included in the historical period but may discard possible scenarios from which there is not a prove of their occurrence (e.g., seismic shocks, lahars not related to eruptive events, unrest that have not culminated with an eruption, etc.). Therefore, in long term volcanic hazard assessment it is crucial to determine the time period that may be considered depending on the availability and quality of data, always identifying the restrictions imposed by this selection.

Although the scarcity of data (mainly prehistoric) represents a limitation to the methodology used, it allowed us to define eruptive scenarios with varying probabilities of occurrence; this information was the basis for the elaboration of hazard maps of 1963-1965 eruption. This is of extreme importance considering that the main hazards of Irazú (ash fall and lahars of medium to large extension) could eventually affect agricultural and urban areas, mainly in the cities of San José and Cartago, as has already happened, for example, in the eruptions of 1723-1724, 1939-1940 and 1963-1965.

Although Irazú eruptions could be characterized by a relatively low VEI (up to 3), they represent a high hazard for the area of potential impact, since more than 2 000 000 of people and industrial centers located in the GAM are exposed at the ashfall. Crops and pastures represent the economic activity with the greatest exposure, as their location could be affected by considerable ash thicknesses (greater than 30 cm). If we analyzed the emergency at the Turrialba volcano (between 2010 and 2017), we can conclude that given the current socioeconomic conditions, the country does not have the financial response capacity to face an emergency equal or similar to that of 1963-1965.

The results obtained in this study should be considered for contributing to the design of emergency plans that allow an adequate response to future eruptions. Likewise, these results should be included in the territorial planning processes where regulations are established to manage land use in volcanic hazard areas, as

well as public politics in risk management based on educational processes and social sensibilization.

Despite the fact that there is monitoring of volcanic activity by the competent entities and a policy that states that community actors must participate actively in risk management to guarantee social development, risk studies have not yet been carried out to estimate the possible economic losses and the conditions of vulnerability of the population. For example, we have identified that there are about 151 informal settlements in areas at risk from Lahar, where only one of them has been the subject of risk perception studies and flood modeling, so it is necessary to develop research in these most vulnerable communities.

In summary, this PhD Thesis constitutes a necessary step in the promotion of hazard studies to contribute to risk reduction in are such the one potential affected by the Irazú volcano. Despite significant efforts have done and currently ongoing in Costa Rica to be alert about natural hazard that may impact the country, in particular in relation to the high number of active volcanoes that it hosts, there is still significant effort that should be done to conduct systematic hazard assessment and promotion of educational programs to contribute to risk reduction in this country. Is with this aim that this PhD Thesis has been carried out and we hope that it will contribute to such purpose.

References

Allegre, C., Condomines, M. 1976. Fine chronology of volcanic processes using ^{238}U-^{230}Th systematics. Earth and Planetary Sci. Letters, 28: 395-406. https://doi.org/10.1016/0012-821X(76)90201-6

Alvarado, G. E. 1989. Los volcanes de Costa Rica. San José: EUNED.

Alvarado, G. E. 1993. Volcanology and Petrology of Irazú Volcano, Costa Rica. (Ph.D. Thesis). Univ. Kiel, Alemania.

Alvarado, G. E., Schmincke, H.-U. 1994. Stratigraphic and sedimentological aspects of the rain triggered lahars of the 1963-1965 Irazú eruption, Costa Rica. Zbl. Geol. Paläont. Teil, 1(H. 1/2), 513-530.

Alvarado, G. E., Boschini, I. 1988. Evaluación preliminar de las amenazas geológicas y periodos de recurrencia en el Valle del Guarco, Cartago: Su eventual incidencia en el deslizamiento de San Blas. 4 Sem. Nac. Geotecnia. 14-15 abril, San José.

Alvarado, G. E., Vega, E., Chaves, J., Vázquez, M. 2004. Los grandes deslizamientos (volcánicos y no volcánicos) de tipo debris avalanche en Costa Rica. Rev. Geol. Amér. Central, 30, 83-99. https://doi.org/10.15517/RGAC.V0I30.7260

Alvarado, G. E., Carr, M. J., Turrin, B. D., Swiher, C., Schmincke, H.-U., Hudnut, K. W. 2006. Recent volcanic history of Irazú volcano, Costa Rica: alternation and mixing of two magma batches, implying at least two intracrustal chambers. En Rose, W. I., Bluth, G. J. S. Carr, M. J., 27 580 Ewert, J. W., Patino, L. C. y Vallance, J. W. (Eds.), Volcanic Hazards in Central America (Geol. 581 Soc. Amer., Sp. Paper, 412, 259-276). Boulder: Geol. Soc. Amer. Inc. https://doi.org/10.1130/2006.2412(14)

Alvarado, G. E., Gans, P. B. 2012. Síntesis geocronológica del magmatismo, metamorfismo y metalogenia de Costa Rica, América Central. Rev. Geol. Amér. Central, 46, 7-122. https://revistas.ucr.ac.cr/index.php/geologica/article/view/1836/1804

Alvarado, G.E., Schmincke, H.-U. 2013. The 1723 A.D. Violent Strombolian and Phreatomagmatic Eruption at Irazú Volcano, Costa Rica. Rev. Geol. Amér. Central, 48, 41-61. https://doi.org/10.15517/RGAC.V0I48.12212

Alvarado, G. E., Mora, M. M., Ulloa, A. 2013. La caída de "ceniza" proveniente del volcán Irazú (Costa Rica) el 8 de diciembre de 1994: ¿una explosión freática? Rev. Geol. Amér. Central, 48, 159-168. https://doi.org/10.15517/RGAC.V0I48.12241

Alvarado, G. E., Campos-Durán, D., Brenes-André, J., Alpízar, Y., Núñez, S., Esquivel, L., Sibaja, J., Fallas, B. 2021. Peligros volcánicos del Irazú, Costa Rica. Comisión Nacional de Prevención de Riesgos y Atención de Emergencias [Inter. Report].

Alvarado, L. F. 2001. Climatología de la atmósfera libre sobre Costa Rica. Top. Meteor. Oceanog. 8(2), 89-115.

Amador, J.A., Anderson, M. J., Calderón, B., Pribyl, K. 2018. The October 1891 Cartago (Costa Rica) floods from documentary sources and 20CR data. Int. J. Climatol. 38, 4830- 4845. https://doi.org/10.1002/joc.5701

Armbrister, T. 1964. The sky is falling. A volcano blows its top, smothering a nation with ash. The Saturday Evening Post, 14, 20-25.

Aspinall, W.P. 2006. Structured elicitation of expert judgment for probabilistic hazard and risk assessment in volcanic eruptions. In: Mader, H.M., Coles, S.G., Connor, C.B., Connor, L.J. (Eds.), Statistics in Volcanology, Special Publication of IAVCEI, vol. 1. Geological Society of London, London, pp. 15–30.

Barckhausen, U., Ranero, C., von Huene, R., Cande, S., Roeser, H. 2001. Revised tectonic boundaries in the Cocos Plate off Costa Rica: Implications for the segmentation of the convergent margin and for plate tectonic models. J. Geophys. Res., 106, 207-220. https://doi.org/10.1029/2001JB000238

Barquero, J. 1976. El volcán Irazú y su actividad (Tesis Lic.). Esc. Ciencias Geográficas, Univ. Nacional.

Barquero, R. y Alvarado, G. E. 1989. Los enjambres de temblores en el arco volcánico de Costa Rica. Bol. Obs. Vulc. Arenal, 2(3), 1-5.

Barquero, R., Montero, W. y Rojas, W. 1991. Actividad sísmica relacionada con el sismo de Cóbano. La Crisis Sísmica del Golfo de Nicoya y eventos sísmicos relacionados, Costa Rica, 1990. ICE, 4, 45-73 [Int. Report].

Barquero, R., Lesage, P., Metaxian, J. P., Creusot, A., Fernández, M. 1995. La crisis sísmica en el volcán Irazú en 1991 (Costa Rica). Rev. Geol. Amér. Central, 18, 5-18. https://doi.org/10.15517/RGAC.V0I18.13494

Barrantes, G., Segura, A., Walcott, K. 2008. Percepción y prevención del riesgo por lahar en los diques de Cartago. Rev. Geográfica de América Central, 42, 83-96. https://www.revistas.una.ac.cr/index.php/geografica/article/view/307

Bartolini, S., Capello. A., Martí, J., Del Negro, C. 2013. QVAST: a new Quantum GIS plugin for estimating volcanic susceptibility. Nat. Hazards Earth Syst. Sci. 13, 3031-3042. https://doi.org/10.5194/nhess-13-3031-2013

Bartolini, S., Geyer, A., Martí, J., Pedrazzi, D., Aguirre-Díaz, G. 2014. Volcanic hazard on Deception Island (South Shetland Islands, Antarctica). J. Volcanol. Geotherm. Res. 150-168. https://doi.org/10.1016/j.jvolgeores.2014.08.009

Becerril, L., Cappello, A., Galindo, I., Neri, M., Del Negro, C. 2013. Spatial probability distribution of future volcanic eruptions at El Hierro Island (Canary Islands, Spain). J. Volcanol. Geotherm. Res. 257, 21-30. https://doi.org/10.1016/j.jvolgeores.2013.03.005

Benjamin, E. R., Plank, T., Wade, J. A., Kelley, K. A., Hauri, E., Alvarardo, G. E. 2007. High water content in basaltic magmas from Irazú Volcano, Costa Rica. J. Volcanol. Geotherm. Res., 168 (1-4), 68-92. https://doi.org/10.1016/j.jvolgeores.2007.08.008

Benito, B., Alvarado, G.E., Marchamalo, M., Rejas, J.G., Murphy, P., Franco, R., Castro, D., Gacia-Lanchares., Sánchez, J. 2023. Temporal and spatial evolution of the 2011 eruption in the Cumbre Vieja rift zone (Tajogaite volcano, La Palma, Canary Islands) from geophysical and geodetic parameter analyses. Natural Hazards, 118, 2245–2284. https://doi.org/10.1007/s11069-023-06090-y

Bergoeing, J. P. 1978. La fotografía aérea y su aplicación a la geomorfología de Costa Rica. San Jose: Ministerio de Obras Públicas y Transportes, IGN.

Bergoeing, J. P. 1979. Geomorfología del sector volcánico Las Nubes-Cabeza de Vaca. Informe semestral IGN (enero-junio), 136-146.

Bergoeing, J. P. 1998. Geomorfología de Costa Rica. Inst. Geográf. Nacional, San José.

Bergoeing, J. P. 2007. Geomorfología de Costa Rica. (2 ed.). Librería Francesa.

Bergoeing, J. P. 2009. Costa Rica, paisajes volcánicos. San Jose: Ediciones Jadine.

BGVN. 1993. Global Volcanism Program-Report on Irazu (Costa Rica) (Venzke, E., ed.). Bulletin of the Global Volcanism Network, 18:10. Smithsonian Institution. https://doi.org/10.5479/si.GVP.BGVN199310-345060

BGVN. 1994a. Global Volcanism Program-Report on Irazu (Costa Rica) (Wunderman, R., ed.). Bulletin of the Global Volcanism Network, 19:10. Smithsonian Institution. https://doi.org/10.5479/si.GVP.BGVN199410-345060

BGVN. 1994b. Report on Irazu (Costa Rica) (Wunderman, R., ed.). Bulletin of the Global Volcanism Network, 19:11. Smithsonian Institution. https://doi.org/10.5479/si.GVP.BGVN199411-345060

BGVN. 1996a. Report on Irazu (Costa Rica) (Wunderman, R., ed.). Bulletin of the Global Volcanism Network, 21:5. Smithsonian Institution. https://doi.org/10.5479/si.GVP.BGVN199605-345060

BGVN. 1996b. Report on Irazu (Costa Rica) (Wunderman, R., ed.). Bulletin of the Global Volcanism Network, 21:8. Smithsonian Institution. https://doi.org/10.5479/si.GVP.BGVN199608-345060

BGVN. 1997a. Report on Irazu (Costa Rica) (Wunderman, R., ed.). Bulletin of the Global Volcanism Network, 22:5. Smithsonian Institution. https://doi.org/10.5479/si.GVP.BGVN199705-345060

BGVN. 1997b. Report on Irazu (Costa Rica) (Wunderman, R., ed.). Bulletin of the Global Volcanism Network, 22:9. Smithsonian Institution. https://doi.org/10.5479/si.GVP.BGVN199709-345060

Blong, R. 2000. Volcanic hazards and risk management. In Sigurdsson, H. (ed.), Encyclopedia of Volcanoes. San Diego: Academic, 1215–1228.

Bonilla, M. 2020. Estudio de Tomografía Eléctrica (ERT), en tres Sitios de Torres ubicadas en el sector del Volcán Irazú. ICE, Ing. y Construcción. [Inter. Report].

Boschini, I. 1998. Los temblores sentidos en Costa Rica durante el año 1987: Enfoque hacia las grandes obras del ICE. ICE [Int. Report].

Boyce, J. W., Hervig, R. L. 2009. Apatite as a monitor of late-stage magmatic processes at Volcán Irazú, Costa Rica. Contributions to Mineralogy and Petrology. 157, 135-145. https://doi.org/10.1007/s00410-008-0325-x

Brenes, J., Alvarado, G. E. 2013. Aplicación de la teoría de fragmentación/transporte secuencial a los depósitos de las erupciones de 1723 y 1963-65 del volcán Irazú, Costa Rica. Caso de dispersión positiva y modelo fractal. Revista Geológica de América Central. 48, 87-98. https://revistas.ucr.ac.cr/index.php/geologica/article/view/12237/11506

Calder, E. S., Wagner, K., Ogburn, S. E. 2015. Volcanic Hazard Maps. In Brown, K., Loughlin, S. C., Sparks, R. S. J., Vye-Brown, C., et al. Global Volcanic Hazards and Risk: Technical Background Paper for the Global Assessment Report on Disaster Risk Reduction 2015. Global Volcano Model and IAVCEI. pp. 335–342.

Campos, I. 1988. Deslizamiento de San Blas. ICE, Depto. Cómputo Electrónico, Sección Aplicaciones Científicas. [Inter. Report].

Campos-Durán, D., Barrantes-Castillo, G. 2020. Evaluación de la vulnerabilidad asociada a la actividad del volcán Turrialba (2010-2017) en el distrito de Santa Cruz de Turrialba, Costa Rica. Rev. Geol. de América Central, 63, 1-19. doi: 10.15517/rgac.v63i0.43404

Campos-Durán, D., Quintero-Quintero, R. 2020. Intensidades macrosísmicas del sismo de Capellades del 30 de noviembre de 2016 (Mw = 5,4) y el contexto sísmico de la región central de Costa Rica. Boletín de Geología, 42(1), 57-68. https://doi.org/10.18273/revbol.v42n1-2020003

Cappello, A., Neri, M., Acocella, V., Gallo, G., Vicari, A., Del Negro, C. 2012. Spatial vent opening probability map of Etna volcano (Sicily, Italy). Bull Volcanol 74:2083–2094. doi:10.1007/s00445-012-0647-4

Carr, M. J., Saginor, I., Alvarado, G. E., Bolge, L. I., Lindsay, F. N., Mildkakis, K., Turrin, B., Feigenson, M. D. y Swisher, C. 2007. Element Fluxes from the Volcanic Front of Nicaragua and Costa Rica. Geochem. Geophys. Geosyst. 8(6). 1-22. https://doi.org/10.1029/2006GC001396

Cascante-Matamoros, M., Porras-Espinoza, H. 2017. Interpretación de los sismos pequeños y moderados bajo el volcán Irazú. Rev. Geográf. Amér. Central, 1(58), 181 - 194. https://doi.org/10.15359/rgac.58-1.7

Clark, S. K. 1993. The recent eruptive history of Irazú volcano, Costa Rica: A study of the tephra deposits of the last 2500 years with geochemical and isotopic analysis of the 1963-1965 eruption. (M.Sc. Thesis). Univ. Iowa.

Clark, S. K., Reagan, M. K., Trimble, D. A. 2006. Tephra deposits for the past 2600 years from Irazú Volcano, Costa Rica. In Rose, W. I., Bluth, G. J. S., Carr, M. J., Ewert, L. C., Patino, L. C., Vallance, J. W. (Eds.), Volcanic Hazards in Central America (Geol. Soc. Amer., Sp. Paper: 412, 225-234). Boulder: Geol. Soc. Amer. Inc. https://doi.org/10.1130/2006.2412(12)

Coen, E. 1964. An Introduction to the Study of Volcano Irazu. Geophys. Magazine, 32(2), 131-152.

Connor, C.B., Hill, B.E.1995. Three nonhomogeneous Poisson models for the probability of basaltic volcanism: application to the Yucca Mountain region, Nevada. J. Geophys. Res. Solid Earth. 100:10107–10125. https://doi.org/10.1029/95JB01055

Comisión Nacional de Prevención de Riesgos y Atención de Emergencias. 1991. Plan de emergencia volcánica: Volcán Irazú-Cartago. https://www.cne.go.cr/CEDO-CRID/pdf/spa/doc4/doc4.htm

Crandell, D.R., Miller, C.D., Glicken, H. X., Christiansen, R. L., Newhall, C. G. 1984. Catastrophic debris avalanche from ancestral Mount Shasta volcano, California. Geology, 12 (3): 143–146. https://doi.org/10.1130/0091-7613(1984)12<143:CDAFAM>2.0.CO;2

Cutter, S. L., Ismail-Zadeh, A., Alcántara-Ayala, I., Altan, O., Baker, D. N., Briceño, S. 2015. Global risks: Pool knowledge to stem losses from disasters. Nature, 522, 277–279. https://doi.org/10.1038/522277a

Decreto Nº 32967-MINAE.2006. Manual de Instrumentos Técnicos para el proceso de Evaluación de Impacto Ambiental (Manual de EIA). https://www.imprentanacional.go.cr/pub/2006/05/04/COMP_04_05_2006.html

DeMets, C., Gordon, R.G., Argus, D.F., Stein, S. 1990. Current plate motions. Geophysical Journal International. 101 (2), 425 – 478. https://doi.org/10.1111/j.1365-246X.1990.tb06579.x

De la Haya, D. 1852. La actividad del Volcän Irazü en 1723. La Gaceta, 175-177, San José.

Dzierma, Y., Thorwart, M. M., Rabbel, W., Flueh, E. R., Alvarado, G. E., Mora, M. M. 2010. Imaging crustal structure in south central Costa Rica with receiver functions. Geochemistry, Geophysics, Geosystems, 11, 1-21. https://doi.org/10.1029/2009GC002936

Elizondo, V., Alvarado, G. E., Soto, D. 2019. Evolución espaciotemporal de las bocas eruptivas de los volcanes Irazú, Arenal, Turrialba y Poás en tiempo histórico (Costa Rica). Rev. Geol. Amér. Central, 61, 35-55. https://revistas.ucr.ac.cr/index.php/geologica/article/view/40087/41126

Fallas, M., Prado, A., Mora, M. M., Ruiz, P., Alfaro, E. J., Soto, G. J. 2018. El deslizamiento del 8 de diciembre de 1994 en el volcán Irazú (Costa Rica): aspectos históricos y geomorfología con base en fotografías aéreas históricas y recientes. Rev. Geol. Amér. Central, 58, 55-84. https://doi.org/10.15517/rgac.v58i0.32844

Fernández, M., Mora, M., Barquero, R. 1998. Los procesos sísmicos del volcán Irazú. Rev. Geol. de Amér. Central, 21, 47-59. https://doi.org/10.15517/RGAC.V0I21.8600

Felpeto, A., Martí, J., Ortiz, R. 2007. Automatic GIS-based system for volcanic hazard assessment. J. Volcanol. Geotherm. Res. 166, 106–116. https://doi.org/10.1016/j.jvolgeores.2007.07.008

Felpeto, A., Martí, J., Ortiz, R. 2007. Automatic GIS-based system for volcanic hazard assessment. J. Volcanol. Geotherm. Res. 166, 106–116. https://doi.org/10.1016/j.jvolgeores.2007.07.008

Flores, G. 2020. Plan Operativo Institucional Caracterización del área de Influencia Región de Desarrollo Central Oriental. Ministerio de Agricultura y Ganadería. https://www.mag.go.cr/regiones/central_oriental/CARACTERIZACION-RDCO.pdf

Floris, M., Pavanelli, N., Capaccioni, B., Tonelli, G., Vaselli, O., Duarte E. 2005. Studio delle condizioni di instabilità del versante meridionale del Vulcano Irazu (Costa Rica, America Centrale). Giornale di Geologia Applicata, 2, 75–79. https://doi.org/10.1474/GGA.2005–02.0–10.0036

Fournier d'Albe, E. M. 1979. Objectives of volcanic monitoring and prediction. Journal of the Geological Society, 136, 321-326. https://doi.org/10.1144/gsjgs.136.3.0321

Galve, J. P., Alvarado, G. E., Pérez-Peña, J. V., Mora, M. M., Booth-Rea, G., Azañón, J. M. 2016. Megafan formation driven by explosive volcanism and active tectonic processes in a humid tropical environment. Terra Nova, 28(6), 427–433. https://doi.org/10.1111/ter.12236

Galve, J.P., Alvarado, G.E., Pérez-Peña, J.V., Pérez-Consuegra, N., Ruano, P., Becerril, L., Devoto, S., Reyes-Carmona, C., Azañón., J.M. 2022. River avulsions and megafan development triggered by high recurrent explosive volcanism. Geomorphology. https://doi.org/10.1016/j.geomorph.2022.108466

Gawarecki, S. J., Moxham, R. M., Morgan, J. O., Parker, D. C. 1980. An infrared survey of Irazú volcano and vicinity, Costa Rica. Proceeding of the Fourteenth International Symposium of Remote Sensing of Environment, 23-30 April 1980, San José. Environmental Institute of Michigan.

Granados-Bolaños, S., Quesada-Román, A., Alvarado, G. E. 2021. Low-cost UAV applications in dynamic tropical volcanic landforms. J. Volcanol. Geotherm. Res., 410, 107143. https://doi.org/10.1016/j.jvolgeores.2020.107143

Guellert, G. 2012. El cambio de paradigma: de la atención de desastres a la gestión del riesgo. Boletín Científico Sapiens Research, 2: 13-17. https://www.srg.com.co/bcsr/index.php/bcsr/article/view/8

Gutiérrez, F. 1963. Actividad del volcán Irazú. Inf. Semestral enero-junio: 33-38, IGN, San José.

Güendel, F. 1985. Enjambres sísmicos en el Volcán Irazú. Catálogo de temblores 1984. Observatorio Vulcanológico y Sismológico de Costa Rica.

Güendel, F. 1987. Actividad reciente en el macizo del volcán Irazú. En Guila, L. E. (ed.): Mesa de Trabajo sobre el Deslizamiento de San Blas. CNE, San José, pp. 66-73.

Hayes, J. L., Holbrook, W. S., Lizarralde, D., Avendonk, H. J. A., Bullock, A. D., Mora, M., Ramírez, C., Alvarado, G. E. 2013. Crustal structure across the Costa Rican Volcanic Arc. Geochem. Geophys. Geosyst., 14(4), 1087-1103. https://doi.org/10.1002/ggge.20079

Hidalgo, P.J., Alvarado, G.E.; Linkimer, L. 2004. La lavina del Valle Central (Costa Rica): ¿lahar o debris avalanche? Rev. Geol. Amér. Central, 30, 101-109. https://doi.org/10.15517/RGAC.V0I30.7261

Hodell, D.A., Brenner, M., Curtis, J.H. 2000. Climate change in the northern America tropics and subtropics since the last ice age: Implications for Environment and Culture. Imperfect Balance: Landscape Transformations in the Pre-Columbian Americas, edited by David L. Lentz, New York Chichester, West Sussex: Columbia University Press, 2000, pp. 13-38. https://doi.org/10.7312/lent11156-005

Horn, S.P. 1993. Postglacial vegetation and fire history of the Chirrup Paramo of Costa Rica. Quaternary Research. 40, 107–116. doi:10.1006/qres.1993.1061

Horton, R. J. M., Mccaldin, R. O. 1964. Observations on air pollution aspects of Irazu volcano, Costa Rica. Public Health Rep., 79, 925-929.

Hudnut, K. 1983. Geophysical Survey of Irazú Volcano. (Bachelor Thesis). Dartmouth College, Hanover, EE. UU.

ICE. 1965. Informe sobre el problema del Río Reventado. ICE, San José. [Inter. Report].

Informe Estado de la Nación. 2018. Tendencias y patrones del crecimiento urbano en la GAM, implicaciones sociales, económicas y ambientales y desafíos desde el Ordenamiento territorial. https://repositorio.conare.ac.cr/bitstream/handle/20.500.12337/2982/Tendencias_patrones_crecimiento_urbano_GAM.pdf?sequence=1&isAllowed=y

Jiménez, D., Becerril, L., Bartolini, S., Martí, J. 2018. Spatio-temporal hazard estimation in San Miguel volcano, El Salvador. J Volcanol. Geotherm. Res. 358, 171-183. https://doi.org/10.1016/j.jvolgeores.2018.04.003

Kornhuber, K., Mahecha, M., Mechler, R., Reichstein, M., Ruane, A.C., Schweizer, P.-J. and Williams, S. 2022. ISC-UNDRR-RISK *KAN* Briefing note on systemic risk*, Paris,* France, International Science Council. https://doi.org/10.24948/2022.01

Kruschensky, R. D., Escalante, G. 1967. Activity of Irazú and Poás Volcanoes, Costa Rica, November 1964-July 1965. Bull. Volcanol., 31, 75-94.

Krushensky, R. D. 1972. Geology of Istarú Quadrangle. USGS Bull. 1358; Washington, 46 pp. https://doi.org/10.3133/b1358

Kutterolf, S., Freundt, A., Pérez, W. 2008. Pacific offshore record of plinian arc volcanism in Central America: 2. Tephra volumes and erupted masses. Geochemistry, Geophysics, Geosystems. 9(2), 1-19. https://doi.org/10.1029/2007GC001791

Lane, C.S., Horn, S.P., Kerr, M.T. 2014. Beyond the Mayan lowlands: Impacts of the terminal classic drought in the Caribbean Antilles. Quaternary Science Reviews. 86, 89–98. https://doi.org/10.1016/j.quascirev.2013.12.017

Linkimer, L. 2003. Neotectónica del extremo oriental del cinturón deformado del centro de Costa Rica. Tesis de Licenciatura, Escuela Centroamericana de Geología, Universidad de Costa Rica, Costa Rica.

Linkimer, L., Arroyo, I. G., Soto, G. J., Porras, J. L., Araya, M. C., Mora, M. M., Taylor, M. 2018. El sismo de Capellades del 2016 y su secuencia sísmica: Manifestación de fallamiento de rumbo en el arco volcánico de Costa Rica. Boletín de Geología, 40(2), 35-53. https://doi.org/10.18273/revbol.v40n2-2018002

López, A. 1999. Neo- and Paleostress partitioning in the SW corner of the Caribbean plate and its fault reactivation potential (Tesis Ph.D.). Tübinger Geoswissenschaftliche Arb., A (53).

Lücke, O. H. 2012. Moho structure of Central America based on three-dimensional lithospheric density modelling of satellite derived gravity data. Int. J. Earth Sci., 103, 1733-1745, https://doi.org/10.1007/s00531-012-0787-y

Lücke, O. H., Arroyo, I. G. 2015. Density structure and geometry of the Costa Rican subduction 684 zoned from 3-D gravity modeling and local earthquake data. Solid Earth, 6, 1169-1183. https://doi.org/10.5194/se-6-1169-2015

Martí, J. 2017. Assessing Volcanic Hazard: A Review. Oxford Handbook Topics in Physical Sciences. https://doi.org/10.1093/oxfordhb/9780190699420.013.32

Martí, J., Felpeto, A. 2010. Methodology for the computation of volcanic susceptibility an example for mafic and felsic eruptions on Tenerife (Canary Islands). J. Volcanol. Geotherm. Res. 195, 69-77. https://doi.org/10.1016/j.jvolgeores.2010.06.008

Martí, J., Gropelli, G., Brum da Silveira, A. 2018. Volcanic stratigraphy: A review. Journal of Volcanology and Geothermal Research. 357, 68-91. https://doi.org/10.1016/j.jvolgeores.2018.04.006

Martí, J., Becerril. L., Rodríguez, A. 2022. How long-term hazard assessment may help to anticipate volcanic eruptions: The case of La Palma eruption 2021 (Canary

Islands). J Volcanol. Geotherm. Res. 431. https://doi.org/10.1016/j.jvolgeores.2022.107669

Maskrey, A. 1998. La aplicación de los sistemas de información geográfica al análisis de riesgo en América Latina. ITDG/La Red, 334 pag.

Martínez Baldares, T. 2013. Plan Regional Urbano de la Gran Área Metropolitana de Costa Rica: avances y desafíos. Cuadernos de vivienda y urbanismo. 5 (9), 70-87. https://doi.org/10.11144/Javeriana.cvu5-9.prug

Marzocchi, W., Sandri, L., and Selva, J. 2008. "BET_EF: A Probabilistic Tool for Long- and Short-Term Eruption Forecasting." Bull Volcanol, 70:623–632. DOI 10.1007/s00445-007-0157-y

Marzocchi, W., Sandri, L., Selva, J. 2010. "BET_VH: A Probabilistic Tool for Long-Term Volcanic Hazard Assessment." Bull Volcanol, 72: 705–716. https://doi.org/10.1007/s00445-010-0357-8

Miller, C. F. 1966. Operation ceniza-arena: The retention of fallout particle from volcan Irazú (Costa Rica) by plants and people. Stanford Res. Inst., Merlo Park. https://apps.dtic.mil/sti/pdfs/AD0673202.pdf

Ministerio de Agricultura y Ganaderia. 2016. Informe de Gestión del Sector Agropecuario y Rural. Secretaría Ejecutiva de Planificación Sectorial Agropecuaria (Sepsa). https://www.mag.go.cr/bibliotecavirtual/D10-10967.pdf

Ministerio de Vivienda y Asentamientos Humanos. 2022. Distribución Geográfica de Asentamientos Informales en Costa Rica. https://www.mivah.go.cr/Informacion_Geo_Espacial_General.shtml

Montero, W., Dewey, J. W. 1982. Shallow focus seismicity, composite focal mechanism and tectonics of the Valle Central of Costa Rica. Bull. Seism. Soc. Amer. 72 (5), 1611-1626. https://doi.org/10.1785/BSSA0720051611

Montero, W. 1986. Periodos de recurrencia y tipos de secuencias sísmicas de los temblores interplaca e intraplaca en la región de Costa Rica. Revista Geológica de América Central. 5, 35-72.

Montero, W. 1994. Neotectonic and related stress distribution in a subduction-collisional zone: Costa Rica, in Geology of an Evolving Island Arc: The Isthmus of Southern Nicaragua, Costa Rica, and Western Panama, Profil, Vol. 7, 126-141, eds Seyfried H. Hellmann W., Universität Stuttgart.

Montero, W., Alvarado, G.E. 1995. El terremoto de Patillos del 30 de diciembre de 1952 (Ms = 5,9) y el contexto neotectónico de la región del volcán Irazú, Costa Rica. Rev. Geol. Amér. Central, 18, 25-39. https://doi.org/10.15517/RGAC.V0I18.13522

Montero, W. 2001. Neotectónica de la región central de Costa Rica: Frontera oeste de la Microplaca de Panamá. Revista Geol. Amér. Central, 24, 29-56. https://doi.org/10.15517/RGAC.V0I24.8551

Montessus de Ballore, F. 1884. Temblores y erupciones volcánicas en Centro-América con un apéndice meteorológico. Imprenta del Dr. Francesco Sagrini, San Salvador.

Mora, M., Taylor, W., y Soto, G. 2012. Sismicidad inducida y otros efectos causados en el arco magmático. En: L. Linkimer, y G. Soto (Ed.). El Terremoto de Sámara del 5 de septiembre de 2012 (pp. 62-78). Red Sismológica Nacional (ICEUCR). [Inter. Report]. https://rsn.ucr.ac.cr/images/Sismologia/sismosHistoricos/33_samara_2012.pdf.pdf

Morales, L., Montero, W. 1984. Los temblores sentidos en Costa Rica durante: 1973-1983, y su relación con la sismicidad del país. Rev. Geol. Amér. Central, 1, 29-56. https://doi.org/10.15517/RGAC.V0I01.10468

Muller, C., Hernández, E., Chavarría, F., Gervaix, F., Pacheco, J., Protti, M., Vega, F. 2020. Deslizamiento del sector oeste del Volcán Irazú. Con datos fotogramétricos y geodésicos al 20 de mayo 2015. OVSICORI-UNA. [Inter. Report].

Murata, K. J., Dondoli, C., Sáenz, R. 1966. The 1963-65 Eruption of Irazu Volcano, Costa Rica (The period of March 1963 to October 1964). Bulletin Volcanologique, 29: 765-796. https://doi.org/10.1007/BF02597194

Neri, A., Aspinall, WP., Cioni, R., Bertagnini, A., Baxter, PJ. 2008. Developing an event tree for probabilistic hazard and risk assessment at Vesuvius. J. Volcanol. Geotherm. Res., 178(3): 397–415. https://doi.org/10.1016/j.jvolgeores.2008.05.014

Oeser, M., Ruprecht, P., Weyer, S. 2018. Combined Fe-Mg chemical and isotopic zoning in olivine constraining magma mixing-to-eruption timescales for the continental arc volcano Irazú (Costa Rica) and Cr diffusion in olivine. American Mineralogist. 103 (4), 582-599. https://doi.org/10.2138/am-2018-6258

Pacheco, J., Avard, G., Martínez, M., De Moor, M., Vega, F., Chavarría, F. 2015. Volcán Irazú: deslizamiento en la parte alta del flanco norte. OVSICORI-UNA [Inter. Report].

Paniagua, S., Soto, G. 1988. Peligros volcánicos en el Valle Central de Costa Rica. Ciencia y Tecnología, 12(1-2), 145-156.

Parsons, W. H. 1967. Irazú Volcano. Cranbrook Inst. Science, News Letters, 36 (6), 70- 79.

Pavanelli, N., Capaccioni, B., Sarocchi, D., Calderoni, G., Vaselli, O., Tassi, F., Duarte, E. 2004. Geology and stability of the southern flank of Irazu volcano, Costa Rica. Acta Vulcanológica, *16*(1), 1-7. https://doi.org/10.1400/19096

PROCOMER. 2023. Nueva empresa de manufactura de dispositivos médicos se instalará en Costa Rica y llevará empleo a Región Occidente. https://www.procomer.com/noticia/nueva-empresa-de-manufactura-de-dispositivos-medicos-se-instalara-en-costa-rica-y-llevara-empleo-a-region-occidente/

Ryan, P.C., Alvarado, G.E., McCanta, M., Barca, M.K., Davis, G., Hurtado de Mendoza, L. 2022. The importance of overbank deposits and paleosol analyses for comprehensive volcanic hazard evaluation: the case of Holocene volcanism at Miravalles Volcano, Costa Rica. Natural Hazards. 1-37. https://doi.org/10.1007/s11069-021-05187-6

Rouwet, D., Mora-Amador, R., Ramírez, C., González, G., Baldoni, E., Pecoraino, G., Inguaggiato, S., Capaccioni, B., Lucchi, F., Tranne, C. A. 2021. Response of a hydrothermal system to escalating phreatic unrest: the case of Turrialba and Irazú in Costa Rica (2007-2012). Earth, Planets and Space, 73:142, https://doi.org/10.1186/s40623-021-01471-8

Ruiz, P., Turrin, B. D., Soto, G. J., Del Potro, R., Gagnevin, D., Gazel, E., Swisher, C. C. 2010. Unveiling Turrialba (Costa Rica) volcano's latest geological evolution through new 40Ar/39Ar, 741 ages. In AGU Fall Meeting Abstracts. https://ui.adsabs.harvard.edu/abs/2010AGUFM.V23B2437R

Quintero-Quintero, R., Porras-Hernández, H. 2018. Sismo de Capellades 01 diciembre 2016, Cartago, Costa Rica. Rev. Geográf. Amér. Central. 61E, 4, Especial. http://dx.doi.org/10.15359/rgac.61-4.6

Ramírez, R., Sánchez, L. 2012. Patrones de localización, concentración y evolución del empleo industrial en la Gran Área Metropolitana (GAM) de Costa Rica. Ciencias Económicas. 30 (2), 131-154. https://doi.org/10.15517/rce.v30i2.8011

Ramírez, L., Alvarado, A., Pujol, R., MacHugh, A., Brenes, L. G. 2008. Indicadores para estimar la sostenibilidad agrícola de la cuenca media del río Reventado, Cartago, Costa Rica. Agronomía Costarricense, 32(2). https://revistas.ucr.ac.cr/index.php/agrocost/article/view/6758

Reagan, M, Duarte, E., Soto, G. J., Fernández, E. 2006. The eruptive history of Turrialba volcano, Costa Rica, and potential hazards from future eruptions. In W. I. Rose, G. J. S. Bluth, M. J. Carr, J. W. Ewert, L. C. Patino, J. W. Vallance (eds.): Volcanic Hazards in Central America, Special Paper. 412, 235-257. doi: 10.1130/2006.2412(13)

Rougier, J., Sparks, R.S.J., Hill. L. 2013. Risk and Uncertainty Assessment for Natural Hazards, Cambridge University Press, Cambridge, pp. 588

S. A. 1964. Mapas Istarú y Abra (con los puentes y ríos afectados). Presidencia de la República. [Inf. Interno].

Salgado, D. 2002. Problemática de la cuenca del río Reventado-Cartago: Los aspectos de ocupación en área de amenaza natural múltiple y los conflictos de uso del suelo en áreas con regulaciones preventivas. CNE. [Inf. Interno].

Sapper, K. 1925. Los volcanes de la América Central. Estudios sobre América Central y España, Max Niemayer, Extra-Serie 1, Halle (Staale).

Schaufelberger, P., Jiménez, E. 1933. Apuntes de Geología 7. Algunas nociones sobre Terremotos y Temblores en Costa Rica. San José: Imprenta La Tribuna.

Schilling, S. P. 1998. LAHARZ; GIS programs for automated mapping of lahars inundation hazard zones. US Geological Survey Open-File Report, pp 98–638, Geological Survey. https://doi.org/10.3133/ofr98638

Segovia-Fuentes, M. 2019. Crecimiento urbano: enfoque territorial fuera de la Gran Área Metropolitana y la provincia de Limón. Acta Académica. 63, 43-64. http://revista.uaca.ac.cr/index.php/actas/article/view/32

Sheridan, M.F., Malin, M.C. 1983. Application of computer-assisted mapping to volcanic hazard evaluation of surge eruption: Vulcano, Lipari, Vesuvius, explosive volcanism. J. Volcanol. Geotherm. Res. 17, 187–202. https://doi.org/10.1016/0377-0273(83)90067-7

Siebert, L., Sinkin, T., Kimberly, P. 2010. Volcanoes of the World. ix + 551 pp. Smithsonian Institution, Univ. California Press, Londres.

Sillmann, J., Christensen, I., Hochrainer-Stigler, S., Huang-Lachmann, J., Juhola, S., Simkin, T., Siebet, L., McClell, L., Bridge, D., Newhall, C. & Latter, J.M. 1981. Volcanoes of the world, (Smithsonian Institutions) Dowden, Hutchinson and Ross, Strondsburg, PA. Soulas, J.P., 1981. Recent changes in the Quaternary stress field of the Venezuelan Andes, EOS, 62, 1026

Silverman, B.W., 1986. Density Estimation for Statistics and Data Analysis. Chapman & Hall, London.

Sistema Nacional de Información Territorial. 2022. Servicios OGC. https://www.snitcr.go.cr/ico_servicios_ogc

Sojo, D. 2018. Geología de la hoja Paraíso (1:10 000), Costa Rica. Rev. Geol. Amér. Central, 59, 101-124. https://doi.org/10.15517/rgac.v59i0.34161

Sobradelo, R., Martí, J. 2010. Bayesian event tree for long-term volcanic hazard assessment: Application to Teide-Pico Viejo stratovolcanoes, Tenerife, Canary Islands, J. Geophys. Res., 115, B05206. https://doi.org/10.1029/2009JB006566

Sobradelo, R., Bartolini, S., Martí, J. 2014. HASSET: a probability event tree tool to valuate future volcanic scenarios using Bayesian inference Presented as a plugin for QGIS, Bull. Volcanol., 76, 770-785. https://doi.org/10.1007/s00445-013-0770-x

Solano, E. 1964. Dermatología y Ceniza. XXXII Congreso Médico Nacional, pp. 51-55.

Solano, C. 2003. El ordenamiento territorial y la percepción del riesgo en el segmento inferior de la subcuenca del río Reventado, provincia de Cartago, Costa Rica (Tesis Maestría en Geografía). UCR, Sistema de estudios de Posgrado.

Soto, G.J., Sjöbohm, L. 2015. Escenarios de amenaza del volcán Irazú, Costa Rica, aproximación preliminar, informe final, 2015-12. https://doi.org/10.13140/RG.2.2.22061.54240

Tristán, JF. 1922. La actividad del volcän Irazü. Publ Coleg Superior de Senoritas, Costa Rica, Ser A. 7 (18): 1-18

Tristán, JF. 1923. The activity of the volcano Irazü in Costa Rica. Zeitschr Vulkanologie, 7 (2), 93-104.

Ulate, C. A., Corrales, M. F. 1966. Mud floods related to the Irazu volcano eruptions. J. Hydraulics Division, HY 6, Bd. 92, 117-129.

Ulloa, A., Rodríguez, E., Zúñiga, Y., Picado, C. 2016. Actualización geológica de la mina Llano Grande. Grupo Pangeas, S. A. [Inter. Report].

United Nations Office for Disaster Risk Reduction. 2009. Terminology on disaster risk reduction, 30 pag. https://www.undrr.org/publication/2009-unisdr-terminology-disaster-risk-reduction

Thomas, K.E. 1983. An investigation of the Cervantes Formation of Irazü Volcano, Costa Rica. Ba-thesis, Dept Earth Sei, Dartmouth College; Hanover, 29 pp

Tournon, J. 1984. Magmatismes du mesozoique ä 1' actuel en Amerique Centrale: L'exemple de Costa Rica, des ophiolites aux andesites. Phd-thesis, Mem Sc Terre, Univ Curie; Paris, 84-49, iix + 335.

Vargas, J. M. 1967. Belleza y Amenaza del volcán Irazú. Efemérides Costarricenses, 1(3), 1-17.

Vargas, A. 2001. Contribución a la geología y geomorfología de una parte del cantón de Coronado; Costa Rica. Rev. Geol. Amér. Central, 24, 67-78. https://doi.org/10.15517/RGAC.V0I24.8553

Waldron, H.H., 1967. Debris flow and erosion control problems caused by the ash eruptions of Irazu Volcano, Costa Rica. USGS Bull. 1241; Washington, 35 pp. https://doi.org/10.3133/b1241I

Wu, J., Porinchu, D. F., Horn, S. P. 2017. A chironomid-based reconstruction of late-Holocene climate and environmental change for southern Pacific Costa Rica. The Holocene, 27(1), 73–84. https://doi.org/10.1177/0959683616652702

Young, S. R, Baxter, P. J, Pomonis, A, Ernst, G. G. J., Benson, C. 1998. Volcanic hazards and community preparedness at Volcán Irazú, Costa Rica. British Geol. Surv. Technical Report, WC/98/16R: 1-120.

Zárate, E. 1988. Factores meteorológicos asociados a desastres causados por erupciones volcánicas en Costa Rica. Ciencia y Tecnología, 12(1-2), 41-52.